ANALYSIS AND DESIGN OF SPECIAL ANTENNA CONFIGURATIONS

G. A. Richards, et al

Ohio State University

Prepared for:

Ballistic Research Laboratories

November 1972

BRL CR 81

BRL

AD

CONTRACT REPORT NO. 81

DAAD05-69-C-0031

ANALYSIS AND DESIGN OF SPECIAL ANTENNA CONFIGURATIONS

Prepared by

ElectroScience Laboratory
The Ohio State University
Columbus, Ohio 43212

November 1972

USA BALLISTIC RESEARCH LABORATORIES
ABERDEEN PROVING GROUND, MARYLAND

Destroy this report when it is no longer needed.
Do not return it to the originator.

Secondary distribution of this report by originating or sponsoring activity is prohibited.

Additional copies of this report may be purchased from the U.S. Department of Commerce, National Technical Information Service, Springfield, Virginia 22151

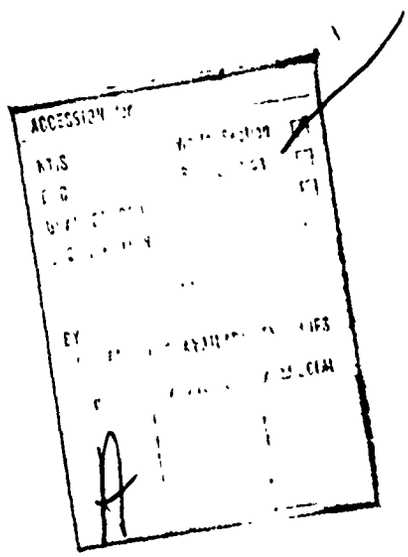

The findings in this report are not to be construed as an official Department of the Army position, unless so designated by other authorized documents.

The use of trade names or manufacturers' names in this report does not constitute indorsement of any commercial product.

Unclassified
Security Classification

DOCUMENT CONTROL DATA - R & D

(Security classification of title, body of abstract and indexing annotation must be entered when the overall report is classified)

1. ORIGINATING ACTIVITY (Corporate author) The Ohio State University Columbus, Ohio 43212	2a. REPORT SECURITY CLASSIFICATION Unclassified 2b. GROUP

3. REPORT TITLE

ANALYSIS AND DESIGN OF SPECIAL ANTENNA CONFIGURATIONS

4. DESCRIPTIVE NOTES (Type of report and inclusive dates)

5. AUTHOR(S) (First name, middle initial, last name)

G. A. Richards, J. H. Richmond, and N. H. Geary

6. REPORT DATE NOVEMBER 1972	7a. TOTAL NO. OF PAGES ~~137~~ 130	7b. NO. OF REFS
8a. CONTRACT OR GRANT NO. DAAD 05-69-C-0031 b. PROJECT NO. c. d.	9a. ORIGINATOR'S REPORT NUMBER(S) 9b. OTHER REPORT NO(S) (Any other numbers that may be assigned this report) BRL Contract Report No. 81	

10 DISTRIBUTION STATEMENT

Approved for public release; distribution unlimited.

11. SUPPLEMENTARY NOTES Details of illustrations in this document may be better studied on microfiche.	12. SPONSORING MILITARY ACTIVITY Ballistic Research Laboratories Aberdeen Proving Ground, Maryland

13 ABSTRACT

A new reaction solution has been formulated for three-dimensional wire antennas located in free space or over a ground plane, using a piecewise-sinusoidal expansion for the unknown current distribution on the antenna. A set of linear equations has been developed for solution by a digital computer. Impedance, radiation efficiency, field patterns, gain, and directivity can be calculated.

Computer programs based on this new formulation were used to determine the impedance versus frequency for various loop antennas. Verification of the calculations with experimental results showed that the technique is highly accurate not only for the impedance but also for the current distribution. Calculated and measured results for several three-dimensional dipoles and a square halo antenna are also given.

/

DD FORM 1 NOV 68 1473 REPLACES DD FORM 1473, 1 JAN 64, WHICH IS OBSOLETE FOR ARMY USE.

Unclassified
Security Classification

14 KEY WORDS	LINK A		LINK B		LINK C	
	ROLE	WT	ROLE	WT	ROLE	WT

BALLISTIC RESEARCH LABORATORIES

CONTRACT REPORT NO. 81

NOVEMBER 1972

ANALYSIS AND DESIGN OF SPECIAL ANTENNA CONFIGURATIONS

Principal Investigator

ElectroScience Laboratory
The Ohio State University
Columbus, Ohio 43212

Contract No. DAAD 05-69-C-0031

ABERDEEN PROVING GROUND, MARYLAND

2

BALLISTIC RESEARCH LABORATORIES

CONTRACT REPORT NO. 81

ANALYSIS AND DESIGN OF SPECIAL ANTENNA CONFIGURATIONS

ABSTRACT

A new reaction solution has been formulated for three-dimensional wire antennas located in free space or over a ground plane, using a piecewise-sinusoidal expansion for the unknown current distribution on the antenna. A set of linear equations has been developed for solution by a digital computer. Impedance, radiation efficiency, field patterns, gain, and directivity can be calculated.

Computer programs based on this new formulation were used to determine the impedance versus frequency for various loop antennas. Verification of the calculations with experimental results showed that the technique is highly accurate not only for the impedance but also for the current distribution. Calculated and measured results for several three-dimensional dipoles and a square halo antenna are also given.

FINAL REPORT

ANALYSIS AND DESIGN OF SPECIAL ANTENNA CONFIGURATIONS

TECHNICAL REPORT 2708-7

20 January 1970

Contract No. DAAD 05-69-C-0031

Department of the Army
Ballistic Research Laboratory
Aberdeen Proving Ground Maryland 21005

Preceding page blank

TABLE OF CONTENTS

ANALYSIS AND DESIGN OF SPECIAL ANTENNA CONFIGURATIONS

I. OBJECTIVES

The objective of this program was to develop digital computer techniques for analyzing the impedance, efficiency and pattern characteristics of wire antennas. In particular, studies were to be made of halo and multi-turn loop antennas.

II. INTRODUCTION

In the past, antenna development has progressed via experimental methods guided by intuition and experience. An antenna is built and its characteristics are measured in the laboratory. The antenna dimensions and/or shape are then modified and the measurements are repeated until satisfactory performance is obtained. This approach is slow and tedious. Accurate measurements require skill, care and sophisticated instrumentation. The final antenna design is seldom optimized, since it represents simply the best of all the models tested.

Now the experimental approach cannot and should not be eliminated, but it should be augmented and coordinated with modern computational techniques. Indeed, the state of the art now permits computer simulation of many laboratory experiments, and results can be predicted with greater speed and accuracy and lower costs. With a suitable program, a modern computer can deliver a design in one day that might require several months with the experimental cut-and-try approach.

The ElectroScience Laboratory has developed significant capability and experience in the analysis of thin-wire antenna problems. Thiele[1]* has developed and published a solution for the current distributions and radiation patterns of a Yagi array, and is now able to calculate the impedance as well.[2] Richmond[3] carried out a computer analysis of an array of V-antennas for a NASA satellite system. Agrawal[4] measured and calculated the impedance of a planar array of three TEM-line antennas interconnected with transmission lines, and obtained excellent results. Jennetti and Agrawal[5] measured and calculated patterns and impedance of a broadside array of TEM-line loops. To optimize the array, they programmed a computer to analyze 10,000 different designs per minute and display the best results. A purely experimental approach would have required several months to achieve the excellent bandwidth, VSWR and directivity of their final design.

Thiele, Travieso-Diaz and Jones[6] measured and calculated the radiation patterns of a dipole antenna mounted on the base of a conducting cone. In their solution, a computer is programmed to enforce boundary conditions at many points on the cone. Tsai and Otto[7,8] employed the Fourier transform, discrete boundary matching and computer

*References are listed on page 15.

optimization to calculate the impedance of dipoles mounted on spheres and cylinders. Their results agree closely with measurements.

The ElectroScience Laboratory has made significant progress in the past year in the investigation of wire antennas for the Ballistic Research Laboratory. This progress is surveyed in the next sections, and the details may be found in the Technical Reports included as Appendices.

III. TASKS 1 AND 3: MULTI-TURN LOOPS

A new reaction solution was formulated for three-dimensional wire antennas located in free space or over a ground plane. In this approach, a piecewise-sinusoidal expansion is employed for the unknown current distribution on the antenna. To determine the expansion coefficients, we force the antenna current function to have the correct reactions with a set of interior test sources. This yields a set of simultaneous linear equations. These equations are solved on a digital computer to determine the current distribution, and it is found that the solution is stationary. Then it is not difficult to calculate the impedance, radiation efficiency, field patterns, gain and directivity.

Computer programs based on this new formulation were found to be exceptionally fast, accurate and versatile. These programs were used to determine the impedance versus frequency for various loop antennas. Technical Reports 2708-1 and 2708-5 (Appendices A and B) show the results for several one-turn polygon loops. The accuracy of the calculations was verified by comparison with experimental measurements for the square loop and with Storer's solution for the circular loop. It was found that our new technique is highly accurate not only for the impedance but also for the current distribution.

Report 2708-6 (Appendix C) presents experimental and theoretical results for two-turn and three-turn loops over a ground plane.

IV. TASKS 2 AND 4: HALO ANTENNAS

In developing the techniques and computer programs for halo antennas, preliminary studies were necessary with simplified configurations. Technical Reports 2708-2 and 2708-3 (Appendices D and E) show the results for coplanar-skew and nonplanar-skew cylindrical wire arrays.

Report 2708-4 (Appendix F) shows calculated and measured results for several three-dimensional dipoles and a square halo antenna. The calculations show excellent agreement with the measurements. This report also develops in detail our theoretical formulation for three-dimensional

wire antennas with finite conductivity, multiple excitation and lumped loading. The report includes the computer program and the theory for the current distribution, impedance, radiation efficiency and patterns.

V. RECOMMENDATIONS

As indicated above, we have developed excellent computer techniques for wire antennas located in free space or over a ground plane. These techniques are also applicable to slot and dipole antennas mounted on a rocket or projectile with axial symmetry. For example, Figure 1 compares our measurements and calculations for a dipole mounted on a cylindrical vehicle. The same computer program, based on the reaction formulation, handles a variety of configurations including biconical antennas, slotted cones and slotted cylinders.

We recommend an extension of this program to apply these techniques to a configuration of direct interest to the Ballistic Research Laboratory: a loop or halo antenna exciting a slot in a conical rocket or projectile. Our experience in this area is illustrated in References 6 through 8 and in Figure 1. The theory and computational techniques would be applied to optimize the impedance, patterns, bandwidth, efficiency and voltage-breakdown characteristics of the projectile-mounted antenna.

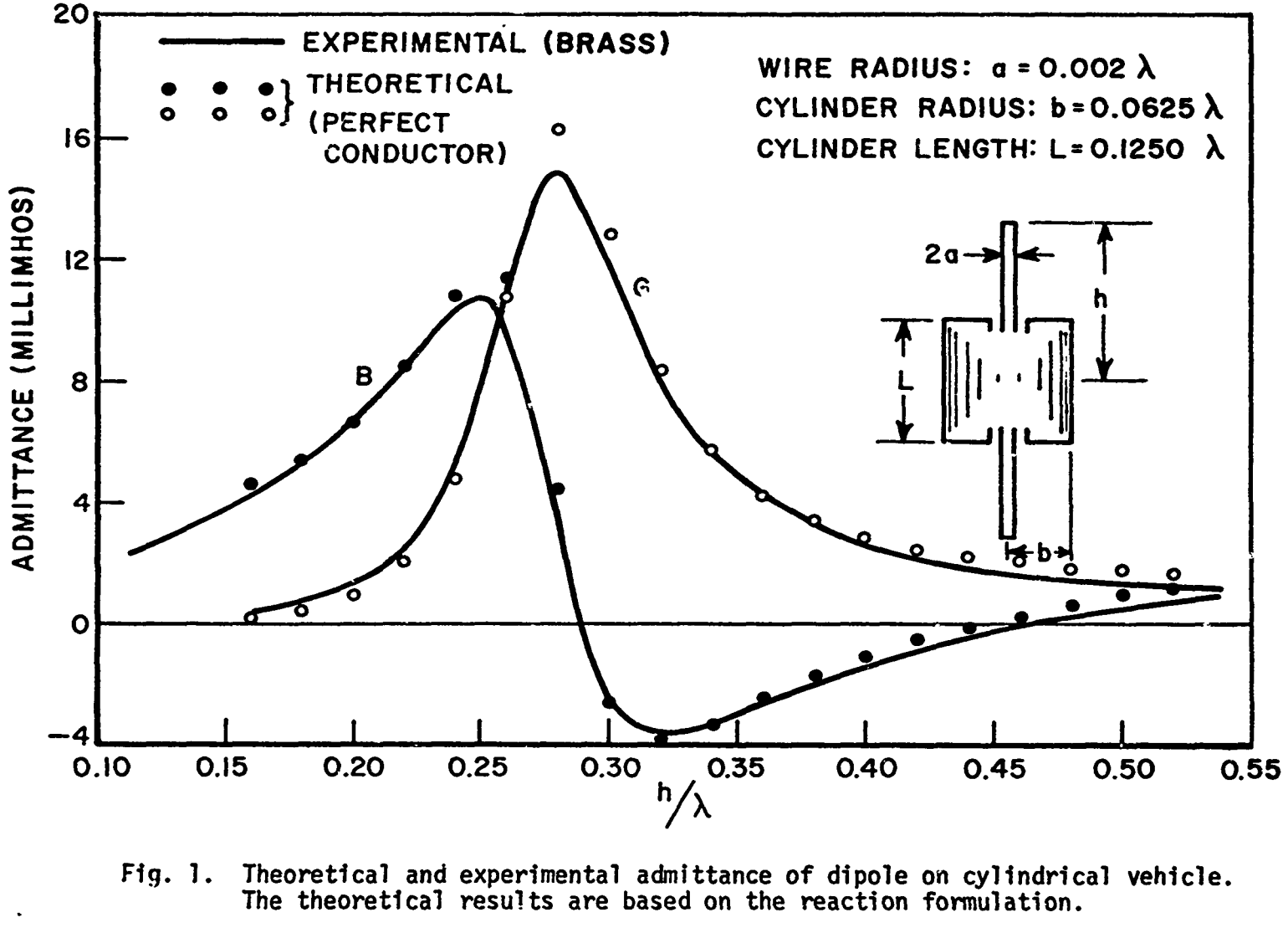

Fig. 1. Theoretical and experimental admittance of dipole on cylindrical vehicle. The theoretical results are based on the reaction formulation.

VI. REFERENCES

1. Thiele, G.A., "Analysis of Yagi-Uda Type Antennas," IEEE Trans., Vol. AP-17, January 1969.

2. Thiele, G.A., "Impedance Analysis of Yagi-Uda Type Antennas," URSI-PGAP Fall Meeting, Austin, Texas, 8-10 December 1969.

3. Richmond, J.H., "Theoretical Study of V Antenna Characteristics for the ATS-E Radio Astronomy Experiment," Report 2619-1, 13 February 1969, Contract NAS5-11543.

4. Agrawal, P.K., "Analysis of Coplanar TEM-Line Antenna Using Reaction Technique," M.Sc. Thesis, The Ohio State University, Department of Electrical Engineering, 1969.

5. Jennetti, A.G. and Agrawal, P.K., "A New Design Technique for TEM-Line Antennas," Nineteenth Annual Symposium, USAF Antenna Research and Development Program, October 1969.

6. Thiele, G.A., Travieso-Diaz, M., and Jones, H.S., "Radiation of a Monopole Antenna on the Base of a Conical Structure," Conference on Environmental Effects on Antenna Performance, Boulder, Colorado, 15 July 1969.

7. Tsai, L.L. and Otto, D.V., "Theory of the Cylindrical Dipole on a Sphere," Report 2648-2, 17 May 1969.

8. Tsai, L.L., "Analysis and Measurement of a Dipole Antenna Mounted Symmetrically on a Conducting Sphere or Cylinder," Report 2648-3 (In Preparation).

VII. BIBLIOGRAPHY OF TECHNICAL REPORTS ISSUED UNDER THIS CONTRACT

1. Richards, G.A., "Input Admittance of Planar Polygon Antennas," Report 2708-1, April 1969.

2. Richmond, J.H., and Geary, N.H., "Mutual Impedance Between Coplanar-Skew Dipoles," Report 2708-2, 6 August 1969.

3. Richmond, J.H., "Coupled Linear Antennas with Skew Orientation," Report 2708-3, 16 August 1969

4. Richmond, J.H., "Computer Analysis of Three-Dimensional Wire Antennas," Report 2708-4, 22 December 1969.

5. Richards, G.A., "Computer Analysis of Polygon Loop Antennas," Report 2708-5, 17 December 1969.

6. Richards, G.A., "Computer Analysis of Multi-Turn Loop Antennas," Report 2708-6, (In Preparation).

7. "Analysis and Design of Special Antenna Configurations, Final Report 2708-7.

VIII. LIST OF PUBLISHED PAPERS RESULTING FROM THIS PROJECT

1. Richmond, J.H., and Geary, N.H., "Mutual Impedance Between Coplanar-Skew Dipoles," IEEE Transactions on Antennas and Propagation, May 1970.

2. Richmond, J.H., "Coupled Linear Antennas with Skew Orientation," IEEE Transactions on Antennas and Propagation, May 1970.

APPENDIX A

INPUT ADMITTANCE OF PLANAR POLYGON ANTENNAS

G. A. Richards

ElectroScience Laboratory
The Ohio State University
Columbus, Ohio 43212

TECHNICAL REPORT 2708-1

Department of the Army
Ballistic Research Laboratory
Aberdeen Proving Ground Maryland 21005

ABSTRACT

A brief summary of the application of the reaction concept to calculate mutual coupling between thin linear dipoles is given. Using reaction, a basis is developed for a multisegment piecewise-sinusoidal approach to the calculation of mutual coupling. This technique is applied to compute the input admittance of a planar polygon loop antenna, and results are presented which show good agreement between these calculations and similar theoretical values for a circular loop of equal area.

INPUT ADMITTANCE OF PLANAR POLYGON ANTENNAS

INTRODUCTION

In recent years greater attention has been directed to the accurate calculation of antenna impedance. In the area of coupled linear antennas, much of this work has been based upon the induced-emf technique first used by Carter.[1]* Others, including Storer[2] and Tai,[3] have attacked the problem using variational techniques with significant success. A third approach, which can be obtained through variational considerations and which is reducible to the induced-emf technique as one case, is the reaction concept introduced by Rumsey.[4]

The first two techniques mentioned above assume that an antenna is represented by two collinear thin cylindrical segments. Differences between these first two techniques center around the choice of the current distribution function to be used. The induced-emf approach, which assumes a piecewise-sinusoidal current on each of the two antenna arms fails for the full-wavelength dipole case, while the variational approach of Tai yields finite terminal impedance for all lengths.

The reaction concept, like the other techniques, has in the past been concerned mainly with the two-segment representation of a linear antenna.

Harrington,[5] Chang and King[6], and more recently Richmond,[7] have successfully reformulated the coupling problem. Their approach is to represent a dipole by several collinear segments on each of which the current distribution is described by some fairly simple function. Application of the reaction principle results in a system of linear equations relating the unknown current coefficients to the voltage at each junction between segments. The set of equations is then solved with the aid of the digital computer.

The form of the technique developed by Richmond is general enough to be applied in a straightforward way to a much larger class of antennas than the coupled thin linear dipoles with which the approach was initially concerned. The purpose of this communication is to describe the technique briefly and to show its application to the case of a planar polygon antenna.

THEORETICAL DISCUSSION

In any reference to the use of reciprocity or reaction to compute coupling between antennas, an important consideration is the form

**References are listed on page 25.*

of the current distribution that is assumed to exist on the antennas. One is at liberty to approximate the true current distribution in any way he desires, but the amount of work one must then do to obtain accurate results depends greatly on his particular choice of an approximation. This discussion will consider a piecewise-sinusoidal approximation for reasons other than just its obviously close relation to the true current distribution on an electric line source.

The use of reaction to calculate coupling between two cylindrical dipoles, where each is composed of two segments with an assumed piecewise-sinusoidal current, is identical to the induced-emf technique. This method relates the unknown short-circuit terminal current I_2 induced on antenna 2 by voltage V_1 impressed at the terminals of antenna 1 (with unit terminal current) by

$$(1) \qquad Z_{12} I_2 = V_1$$

where

$$(2) \qquad Z_{12} = -\frac{1}{I_2} \oint\!\!\oint_S \underline{J}_2 \cdot \underline{E}_1 \, ds \ .$$

and the integration is over the surface of antenna 2. Here $(\underline{E}_1, \underline{H}_1)$ denote the free-space fields generated by a linear test source located along the axis of antenna 1. Eq. (2) is obtained by enforcing reciprocity between the test source and antenna 2. In most practical situations the surface current density $\underline{J}_2$ on antenna 2 can be adequately represented by a line current $\underline{I}_2$ along the surface. This reduces Eq. (2) to a line integral,

$$(3) \qquad Z_{12} = -\frac{1}{I_2} \int \underline{I}_2(\ell) \cdot \underline{E}_1 \, d\ell \quad .$$

Schelkunoff and Friis[8] give the cylindrical polar components of the free-space field of an electric line source on the z-axis with sinusoidal current distribution as

$$(4) \qquad E_z(\rho,z) = \frac{\sqrt{\mu/\varepsilon}}{4\pi jk} \left[I'(z_1) \frac{e^{-jkr_1}}{r_1} - I'(z_2) \frac{e^{-jkr_2}}{r_2} - \frac{\partial V}{\partial z} \right]$$

$$(5) \qquad E_\rho(\rho,z) = \frac{\sqrt{\mu/\epsilon}}{4\pi jk\rho} \left\{ \left[I'(z_2)\cos\theta_2 - jk\, I(z_2) \right] e^{-jkr_2} - \left[I'(z_1)\cos\theta_1 - jk\, I(z_1) \right] e^{-jkr_1} - \rho \frac{\partial V}{\partial \rho} \right\}$$

where

$$(6) \qquad k = \omega\sqrt{\mu\epsilon} \quad ,$$

V is the potential due to end charges, and the primes denote derivatives with respect to z. Fig. 1 illustrates the geometry related to Eqs. (4)

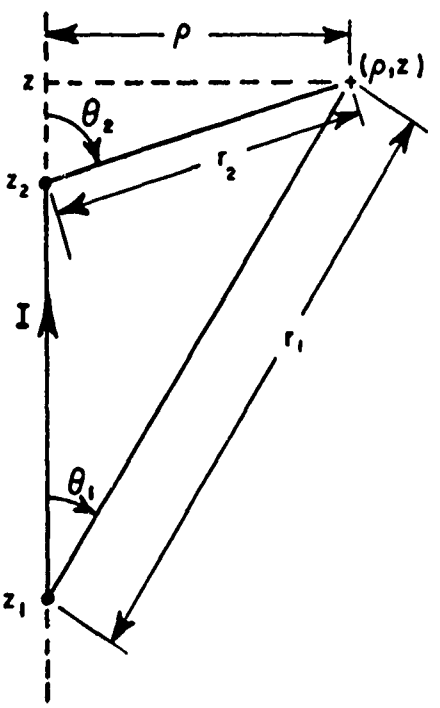

Fig. 1. Geometric relations for an electric line source on the z-axis with an observation point at (ρ,z).

and (5). If an antenna is represented by a collection of these line sources joined end to end in some fashion, and if the current is forced to vanish at any free ends, then the partial derivatives of V in Eqs. (4) and (5) contribute nothing to the field expressions for the whole structure and may be neglected providing the end charges are negligible.

The collection of line segments representing one or more antennas forms an N-port network, where N represents the number of junctions which have a segment on each side (i.e., no open end can be a junction). An equivalent viewpoint is that the collection consists of N overlapping dipole and/or Vee antennas on each of which the current vanishes at either end.

Let an ordinary dipole be a special case of a Vee antenna. Also, let a test Vee antenna be located on axis with terminals at junction i and with arms the same lengths as those of the i^{th} true surface-current Vee antenna. Then the coupling between the i^{th} junction any any other junction, say the j^{th} junction, can be calculated by enforcing reciprocity between the test Vee antenna on axis at junction i and the true surface-current Vee antenna whose terminals are located at the j^{th} junction. This is done through Eq. (3) which for every possible pair of junctions i and j generates a matrix of coefficients $[Z_{ij}]$. These are the coefficients of a system of linear equations each having the form

$$(6) \qquad \sum_j Z_{ij} I_j = V_i \ , \ i = 1, 2, \cdots, N \ .$$

By assuming a known voltage source, usually a unit voltage source, at a junction of interest and by requiring short circuits at all other junctions, the unknown current coefficients at all the junctions can be determined. The current coefficient at the junction with the voltage source is the input admittance of the system if the voltage source is a unit source. The input impedance is easily obtained as the reciprocal of the input admittance.

Richmond realized several advantages by using the piecewise-sinusoidal current description on the test Vee antenna and on the overlapping true surface-current antennas. First, the reaction between any two (nonintersecting) coplanar dipole or Vee antennas may be calculated in closed form in terms of sine and cosine integrals. The arms of either antenna can be of unequal length, and their Vee angles need not be equal. Also, a good value for the mutual coupling may be obtained for individual antenna arms up to a quarter-wavelength in extent. Of course, greater accuracy may be had by using more segments, especially when the test source and the true surface-current antenna are relatively close together. However, this technique has been used, for example, to calculate the input impedance of a linear dipole to the same degree of accuracy but with far fewer segments than were needed for a similar technique employing a different current distribution.[7]

These, then, are the advantages of the piecewise-sinusoidal multi-segment approach to coupling between coplanar linear antennas: relative simplicity of concepts; speed and accuracy of numerical calculations; and, as the next section attempts to demonstrate, applicability to a

more general class of wire antennas.

PRESENTATION OF RESULTS

The technique discussed in the previous section has been employed successfully to calculate the self-impedance of linear dipoles, to obtain the mutual impedance between two linear dipoles in various orientations, and to calculate driving-point impedance and current distributions for coupled coplanar Vee antennas.[7]

The results to be reported here deal with the calculation of driving-point admittances and current distributions for square loops and polygons. Part of the motivation for this investigation was the desire to find some representation for a circular loop antenna that could be analyzed by the reaction technique using straight wire segments. The regular polygon antenna was proposed to fill this need. The criterion chosen to relate the approximating polygon to a circular loop was that of equal enclosed areas. There are at least two reasons for enforcing this relationship. First, a circle is more closely approximated geometrically by a concentric N-sided polygon with equal enclosed area than by either an inscribed or circumscribed N-sided polygon. Second, the dependence of both the field expressions and the input impedance of the circular loop antenna on its enclosed area suggested that this feature be incorporated in any approximating structure.

Figure 2 is a plot of the input conductance and susceptance of a square loop antenna as a function of frequency. These calculations bear a strong resemblance to the comparison shown in Fig. 3. These plots compare the input conductance and susceptance of an octagonal loop antenna to those of a circular loop antenna with equal enclosed area. The circular loop data were taken from a paper by Storer[9] in which the input admittance was obtained through consideration of a Fourier series solution obtained by Hallén. Notice that the comparison extends beyond a full wavelength in circumference.

The input admittance data for the octagon were calculated by using two segments to represent each side of the figure. There was negligible difference between admittances calculated by placing the input terminals at a vertex of the octagon and those calculated with the input at the middle of one of the sides. In addition, the agreement shown in Fig. 3 over the entire range of frequencies is only slightly different from that obtained by using an approximating octagon having only one segment per side with input terminals at a vertex. The data for the square loop were calculated using two segments per side at the higher frequencies and only one segment per side at the lower frequencies.

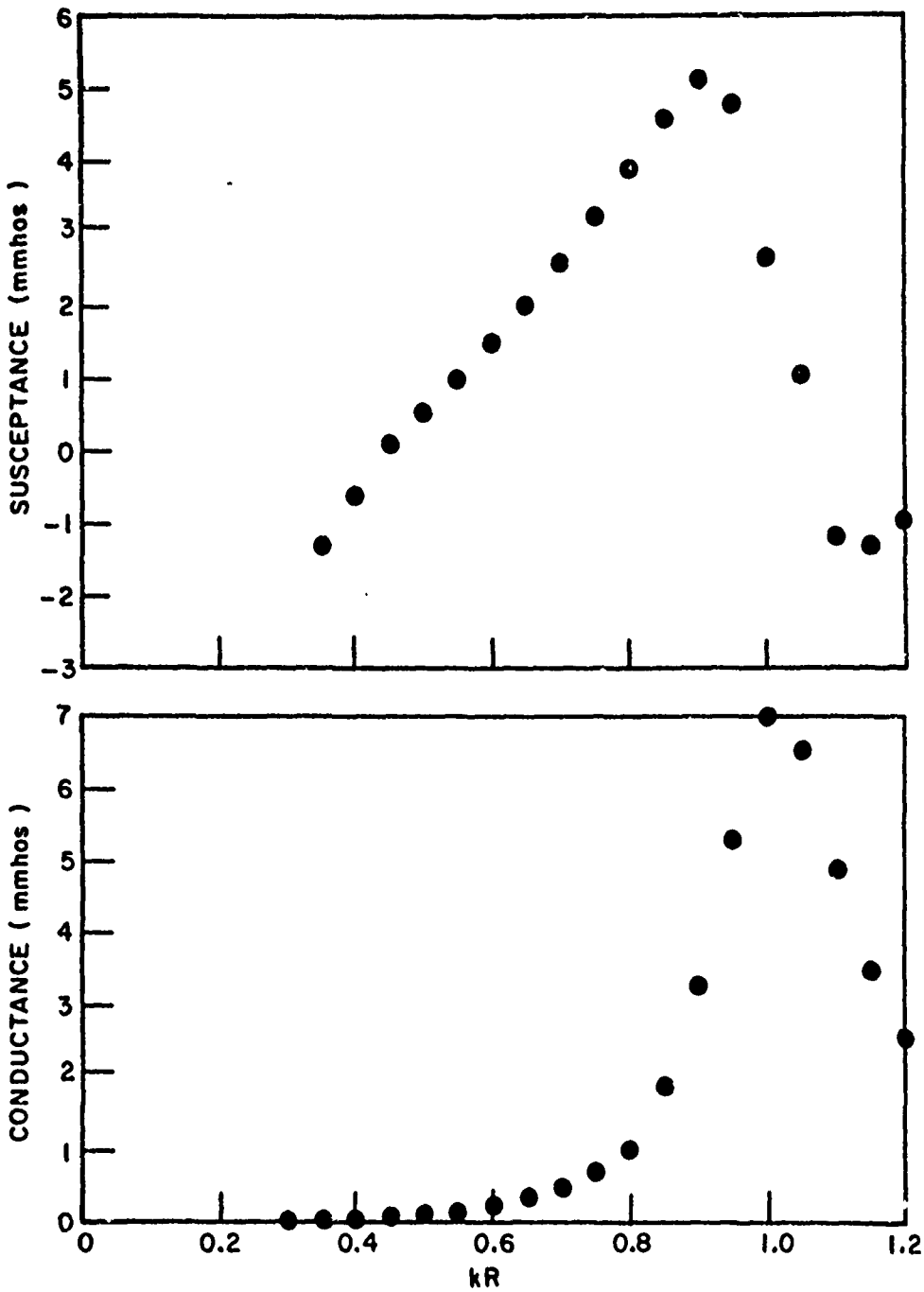

Fig. 2. Input conductance and susceptance of a square loop vs. circumference of a circle (in wavelengths)having the same enclosed area. R is the radius of the circle, and $k = 2\pi/\lambda$.

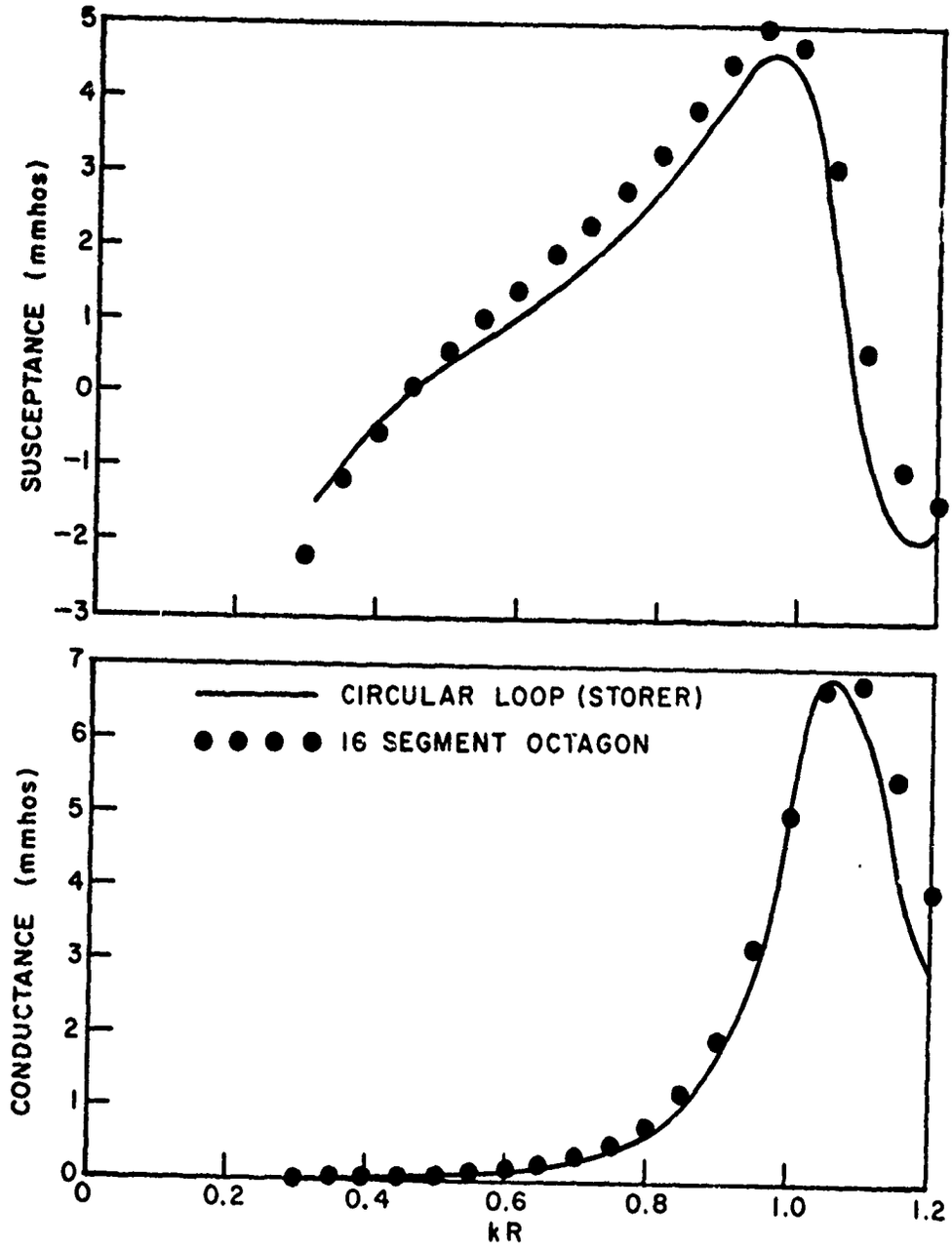

Fig. 3. A comparison of input conductances and susceptances for a planar octagonal loop and a circular loop of equal area. The horizontal scale is the circumference of the circle in wavelengths.

The current distribution on the octagon as determined from the values of the current coefficients at the junctions between segments shows good agreement with circular loop data in both form and phase, but the magnitude does not show good agreement for circumferences under half a wavelength. At approximately one wavelength in circumference, however, the current coefficients at the junctions of the sixteen-segment octagon show excellent agreement in both magnitude and phase with corresponding values of the current distribution on a circular loop antenna as published by Storer.[9]

CONCLUSIONS

The multisegment reaction technique developed by Richmond for coupled straight-wire antennas and coupled Vee dipoles has been utilized to calculate the input admittance and current distribution of the polygon loop antenna. Moreover, the polygon loop has been shown to approximate a circular loop for the purpose of calculating input admittance and current distribution.

This method forms the basis for computing the impedance, current distribution, and far-field patterns of an antenna or a system of antennas composed of loops or of combinations of loops, such as multiturn loops, and, in general, any antenna made up of or approximated by piecewise straight-wire segments.

ACKNOWLEDGMENT

The author wishes to thank Prof. J. H. Richmond for his guidance during many informative discussions.

REFERENCES

1. Carter, P.S., "Circuit Relations in Radiating Systems and Applications to Antenna Problems," Proc. IRE, Vol. 20, June 1932, pp. 1004-1041.

2. Storer, J.E., "Variational Solution to the Problem of the Symmetrical Cylindrical Antenna," Cruft Laboratory, Harvard University, Technical Report No. 101, 1950.

3. Tai, C.T., "A Variational Solution to the Problem of Cylindrical Antennas," Aircraft Radiation Systems Lab., Stanford Research Institute, Stanford, California, Tech. Rep. No. 12, 1950.

4. Rumsey, V.H., "The Reaction Concept in Electromagnetic Theory," Physical Review, Ser. 2, Vol. 94, June 1954, pp 1483-1491.

5. Harrington, R.F., Field Computation by Moment Methods, The Macmillan Company, New York, 1968.

6. Chang, V.W.H. and King, R.W.P., "On Two Arbitrarily Located Identical Parallel Antennas," IEEE Trans, Vol. AP-16, May 1968, pp. 309-317.

7. Richmond, J.H., "Theoretical Study of V Antenna Characteristics for the ATS-E Radio Astronomy Experiment," ElectroScience Laboratory, Ohio State University, Report 2619-1, February 1969, Contract No. NAS5-11543, National Aeronautical and Space Administration.

8. Schelkunoff, S.A., and Friis, H.T., Antennas: Theory and Practice, John Wiley and Sons, Inc., New York, 1952.

9. Storer, J.E., "Impedance of Thin-Wire Loop Antennas," AIEE Trans., Vol. 75, Part 1, November 1956, pp. 606-619.

APPENDIX B

COMPUTER ANALYSIS OF POLYGON LOOP ANTENNAS

G.A. Richards

ElectroScience Laboratory
The Ohio State University
Columbus, Ohio 43212

TECHNICAL REPORT 2708-5

17 December 1969

Department of the Army
Ballistic Research Laboratory
Aberdeen Proving Ground Maryland 21005

ABSTRACT

The reaction concept is applied to wire antennas in the shape of regular polygons to calculate the input impedance (or admittance) and current distribution. The calculated results are found to give excellent agreement with experimental measurements and independent theoretical data.

COMPUTER ANALYSIS OF POLYGON LOOP ANTENNAS

I. INTRODUCTION

This report deals with a class of wire antennas that has heretofore been largely ignored. Except for some preliminary results[1]* this report constitutes the first presentation of a rapid, efficient technique for calculating current distribution and impedance for piecewise - straight wire loop antennas. Results are shown for planar examples in this report; a future report will deal with the analysis of three-dimensional multiturn loop antennas based on the same method reported here.

A brief review of the theory precedes the numerical results.

II. THEORY

Consider the polygon antenna as a piecewise - straight wire loop with $\underline{E}$ and $\underline{H}$ its radiated electric and magnetic field intensities everywhere in space. The surface-equivalence principle of Schelkunoff[2] is used to replace the antenna by equivalent electric and magnetic surface current densities, $\underline{J}$ and $\underline{M}$, radiating in free space. These quantities are obtained from the relations $\underline{J} = \hat{n} \times \underline{H}$ and $\underline{M} = \underline{E} \times \hat{n}$ evaluated at the antenna surface with $\hat{n}$ the unit normal outward from the surface. The current densities $\underline{J}$ and $\underline{M}$ radiate the actual field intensities ($\underline{E}$, $\underline{H}$) in the region exterior to the antenna and generate a null field in the interior of the antenna itself. Thus there would exist no coupling, or reaction, between the source distribution ($\underline{J}$, $\underline{M}$) and any source located entirely within the interior region.

This zero-reaction condition has been utilized previously[3-5] to solve problems involving dipole antennas and is here extended to include polygon loops. The loop is represented by a set of N tubular segments, each having a piecewise - sinusoidal current distribution. If the radius of the wire is small compared with the circumference of the loop, then for the purpose of calculating reaction the surface current density $\underline{J}$ may be replaced by a filamentary current $\underline{I}$ on the surface of the antenna. In this way the set of N tubular segments is replaced by a set of filamentary segments which can be considered as a collection of N overlapping dipoles.

The zero-reaction condition is implemented by enforcing reciprocity between the collection of filamentary surface-current dipoles and a

**References are listed on p. 43.*

collection of N filamentary test dipoles located along the axis of the loop. Figure 1 illustrates the situation for a typical pair of elements. The coordinate s_j along the j-th surface dipole has unit vector $\hat{s}_j$. The reciprocity relation between the j-th true surface-current dipole and the i-th axial test dipole has the following form:

$$(1) \qquad \iint \underline{H}_i \cdot \underline{M}_j \, dS_j = \int \underline{E}_i \cdot \underline{I}_j \, ds_j \quad .$$

In Eq. (1) the currents $(\underline{I}_j, \underline{M}_j)$ are that portion of the surface-current distribution associated with the j-th surface dipole, and $(\underline{E}_i, \underline{H}_i)$ are the free-space fields of the i-th test dipole. The surface integral on the left side of Eq. (1) exists in the vicinity of the j-th junction where $\underline{M}_j$ is nonzero, and the line integral on the right side is evaluated along the j-th dipole filament.

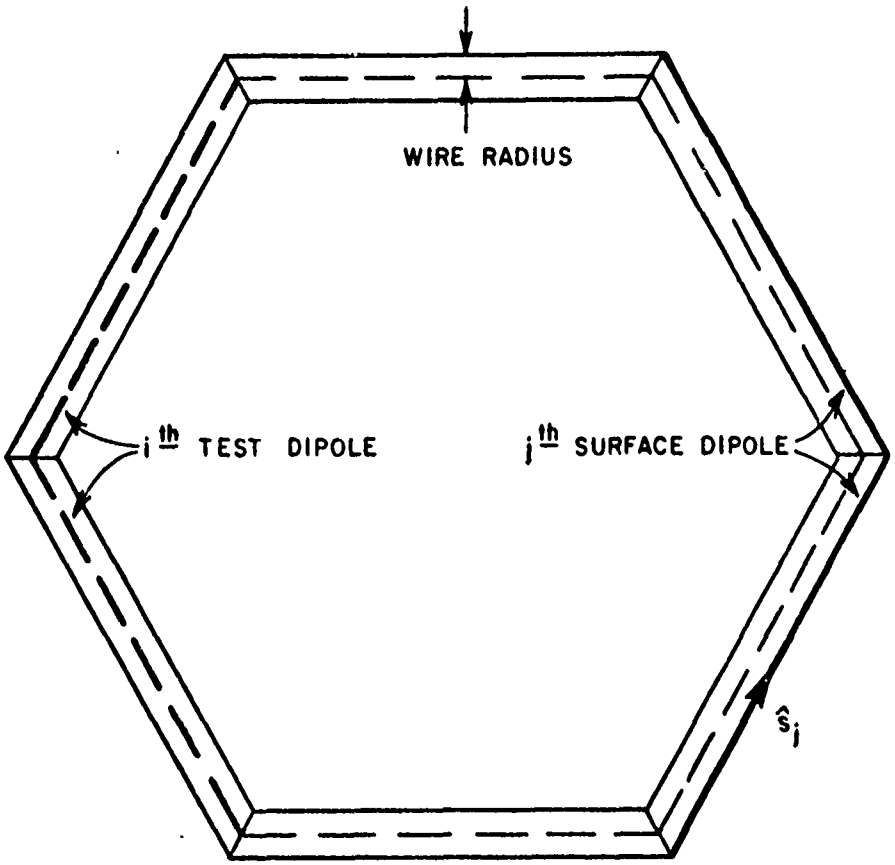

Fig. 1. Typical locations for i-th test dipole on axis and j-th true surface-current dipole.

After the scalar product has been taken, the right side of Eq. (1) normalized by the j-th terminal current I_j has the form of mutual impedance:

$$(2) \qquad Z_{ij} = -\frac{1}{I_j} \int E_{i_t}(s_j)\, I_j(s_j)\, ds_j \quad .$$

The quantity $E_{i_t}(s_j)$ represents the component of the free-space electric field radiated by the i-th test dipole that is tangential to the j-th surface dipole. If a delta-gap voltage generator ($\underline{M}_j$ in this case is a ring of magnetic current) is assumed at the terminals of the j-th surface dipole, then the left-hand side of Eq. (1) reduces to zero except when i and j coincide. For this case, the integral is equal to V_i, the applied voltage at that junction.

By enforcing reciprocity via Eqs. (1) and (2) between the i-th test dipole and all N true surface-current dipoles, a set of N mutual impedance coefficients is obtained. The coefficients relate the terminal voltages and currents as follows:

$$(3) \qquad \sum_{j=1}^{N} Z_{ij}\, I_j = V_i \quad .$$

Equation (3) represents one linear equation out of a whole system of N equations that are obtained by successively enforcing reciprocity between the N surface dipoles and each of the N axial test dipoles in turn. This system of equations is solved by fixing a unit voltage source at the feed terminals and short-circuiting the other terminals. Solution of the equations yields values for the current samples at the N junctions, thus determining the current distribution over the entire perimeter of the antenna.

Impedance information is obtained from the current sample at the feed terminals. Since a unit voltage source was assumed, this quantity is itself the input admittance and its reciprocal is the input impedance of the antenna.

In the next section numerical data are compared with experimental data and independent theoretical calculations.

III. NUMERICAL RESULTS

Comparison with experiment and comparison with results from independent theory are two important ways to demonstrate the accuracy of the multisegment reaction technique. Both comparisons will be shown in this section, along with results for which there are no direct comparisons, but which are nevertheless interesting, useful, and, it is believed, accurate.

Figure 2 compares measured and calculated admittances for half a square loop mounted vertically over a ground plane. One end of the antenna is coaxially fed out of the ground plane. The agreement between

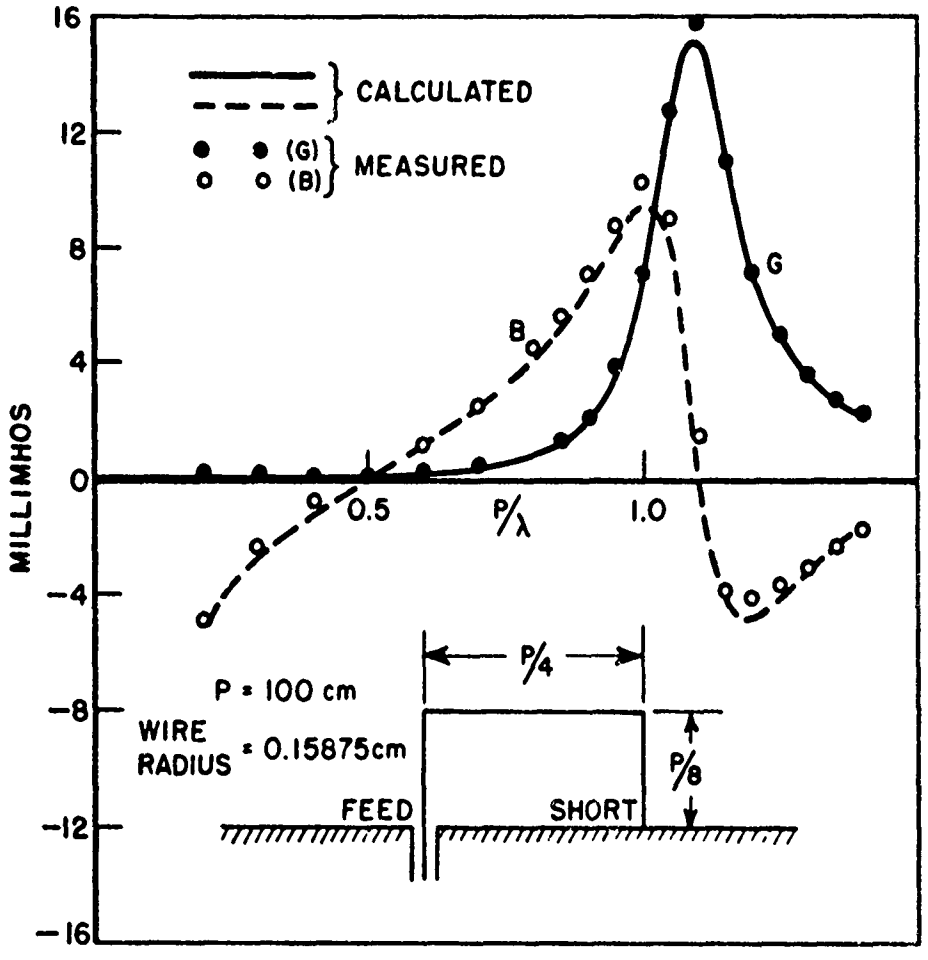

Fig. 2. Calculated and measured data for the conductance (G) and susceptance (B) of a vertical half-loop over a ground plane.

experiment and theory that is shown in Fig. 2 demonstrates that the multisegment reaction technique can be applied successfully to closed, piecewise-straight wire antenna shapes.

Figures 3-6 are a series of comparisons between the admittance of a regular polygon and that of a circular loop of the same perimeter. The data for the circular loop are those of Storer,[6] who obtained his results by numerically solving the integral equation for a circular loop antenna. The polygon data were calculated for symmetrical side-driven loops using the multisegment reaction technique.

It seems reasonable that, of all the possible polygonal shapes (for logical development, we have chosen regular polygons), the one whose shape most nearly resembled a circular loop of the same perimeter would have impedance (or admittance) properties closely resembling those of the circular loop. Figures 3-6 bear out this reasoning. Notice that, as the number of sides is increased, the admittance curves more nearly resemble the circular loop data; for a 12-sided polygon, the data are virtually indistinguishable over the entire range of values. (Data calculated for a 16-sided polygon essentially lie on that for the circular loop.) Notice also that the electrically small polygon ($P/\lambda < 0.5$) behaves quite like a circular loop for any number of sides. This bears out the expected result - electrically small single-turn loops behave much the same whether they are circular or polygonal in shape.

Figures 7 and 8 show that the admittance of a planar polygon with few sides is altered when the feed point is changed from a side to a corner. The curves in Figs. 7 and 8 are for corner-driven polygons of three and four sides, respectively. These data differ from the data of Figs. 3 and 4 most noticeably for higher values of P/λ. As the number of sides is increased, though, the admittances for the corner-driven and the side-driven cases become nearly identical. Thus the curves in Fig. 5 and Fig. 6 apply to either driving-point situation.

Figures 9 and 10 demonstrate that the multisegment reaction technique gives an accurate description of the current distribution over the entire length of an antenna. The current samples at junctions between segments for a 12-sided, 24-segment polygon are compared with data by Storer[6] for the circular loop antenna. The current sample values compare well with the circular loop data for perimeters of both one and two wavelengths. The currents are plotted for half of the perimeter, since the current on the other half is symmetric with respect to the feed point. The sample data in Figs. 9 and 10 represent either the side-driven or the corner-driven case, since the difference in currents between the two cases at any junction is less than one-tenth of one milliampere.

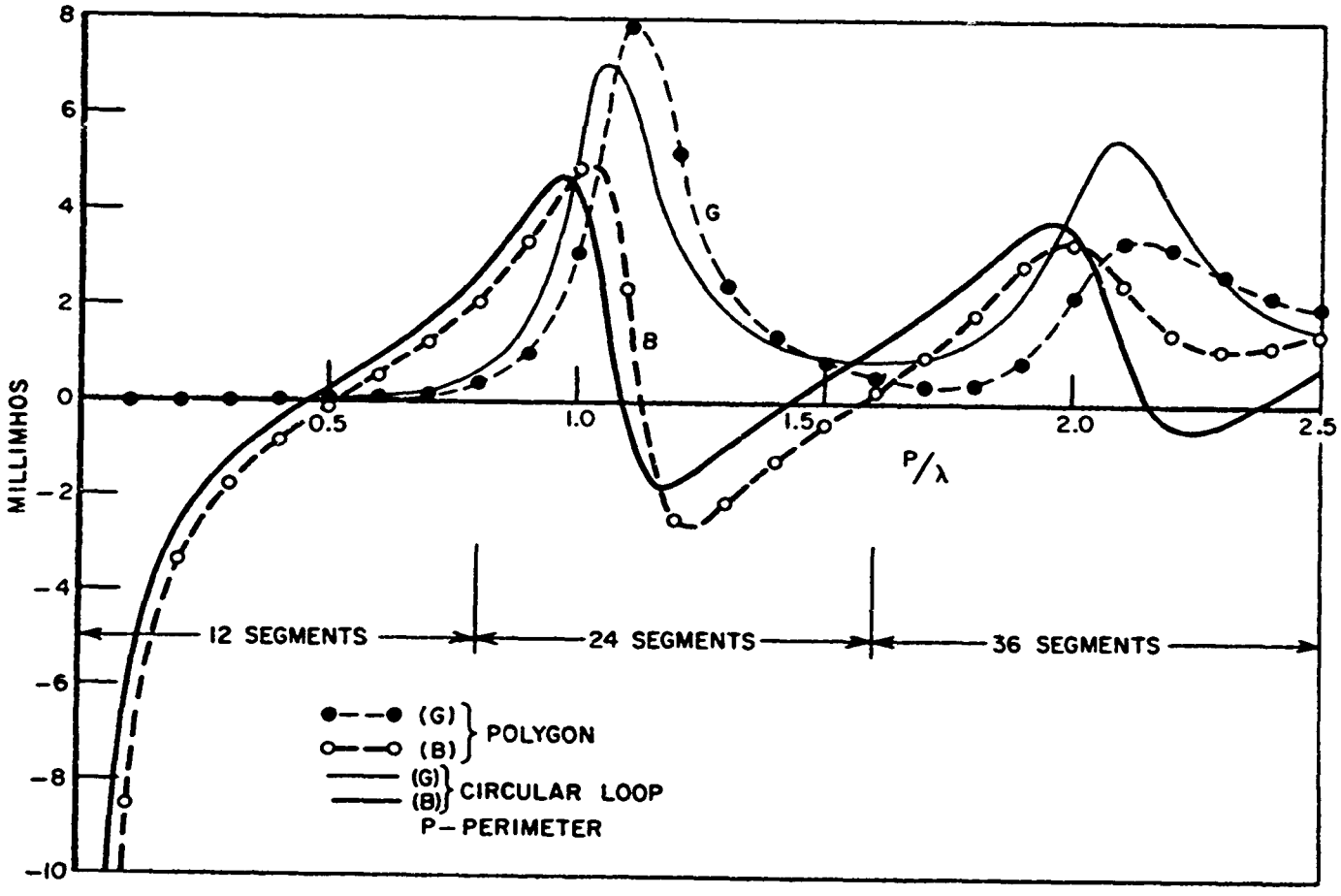

Fig. 3. Conductance (G) and susceptance (B) vs. P/λ: side-driven three-sided polygon (Richards) and circular loop (Storer). ($P/\alpha = 403.43$, where α is wire radius.)

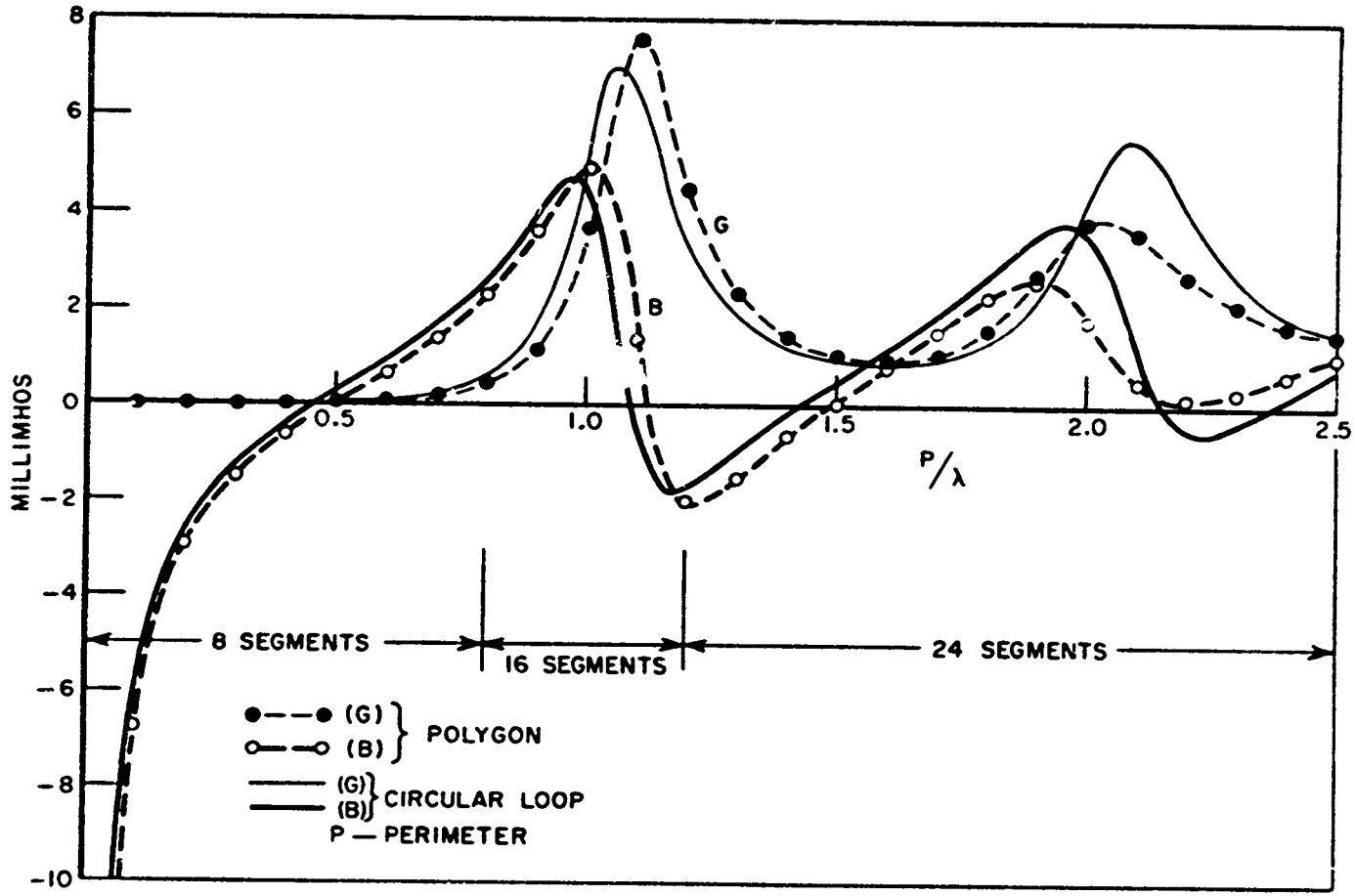

Fig. 4. Conductance (G) and susceptance (B) vs. P/λ: side-driven four-sided polygon (Richards) and circular loop (Storer). ($P/\alpha = 403.43$, where α is wire radius.)

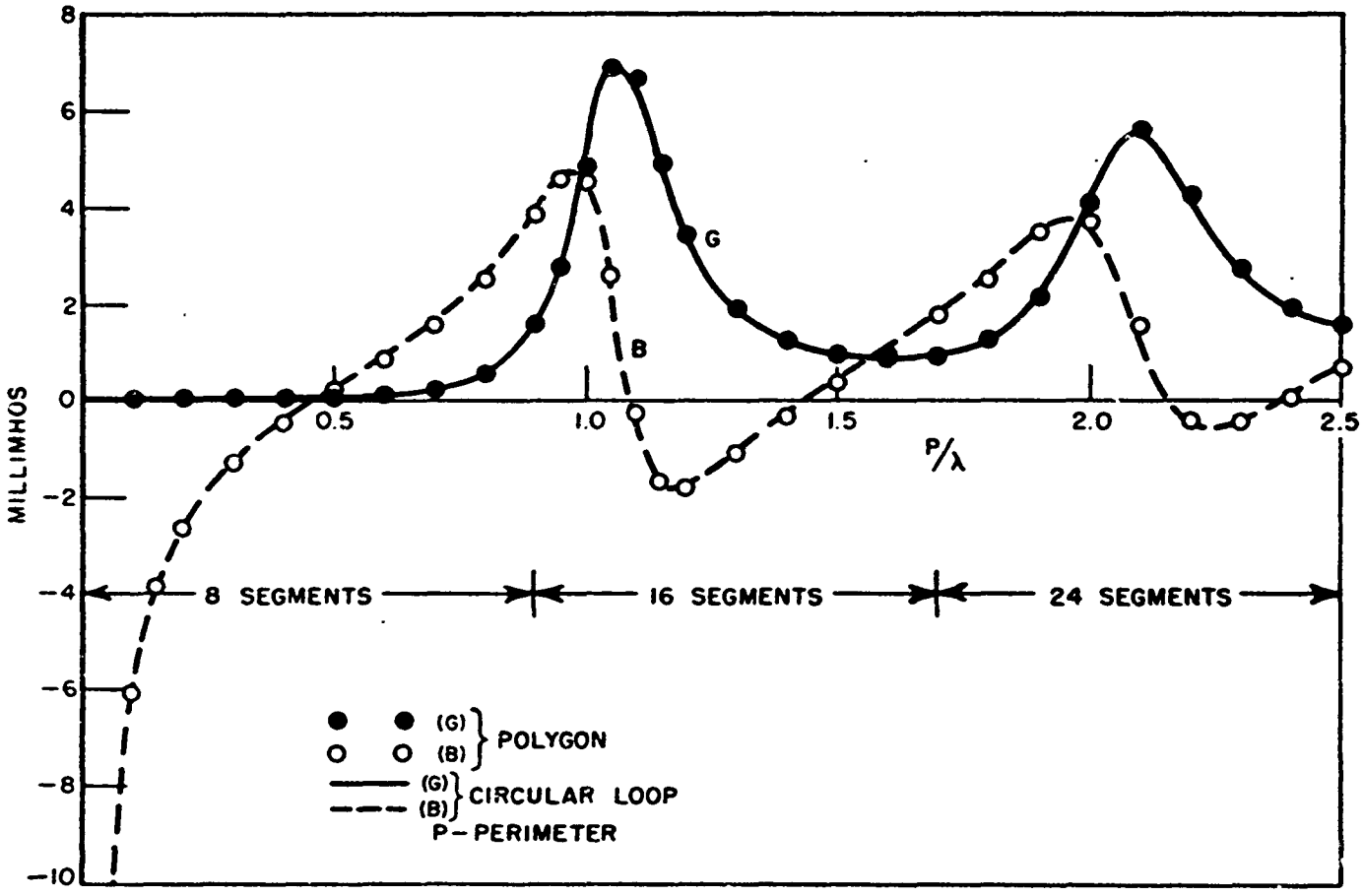

Fig. 5. Conductance (G) and susceptance (B) vs. P/λ: side-driven eight-sided polygon (Richards) and circular loop (Storer). ($P/\alpha = 403.43$, where α is wire radius.)

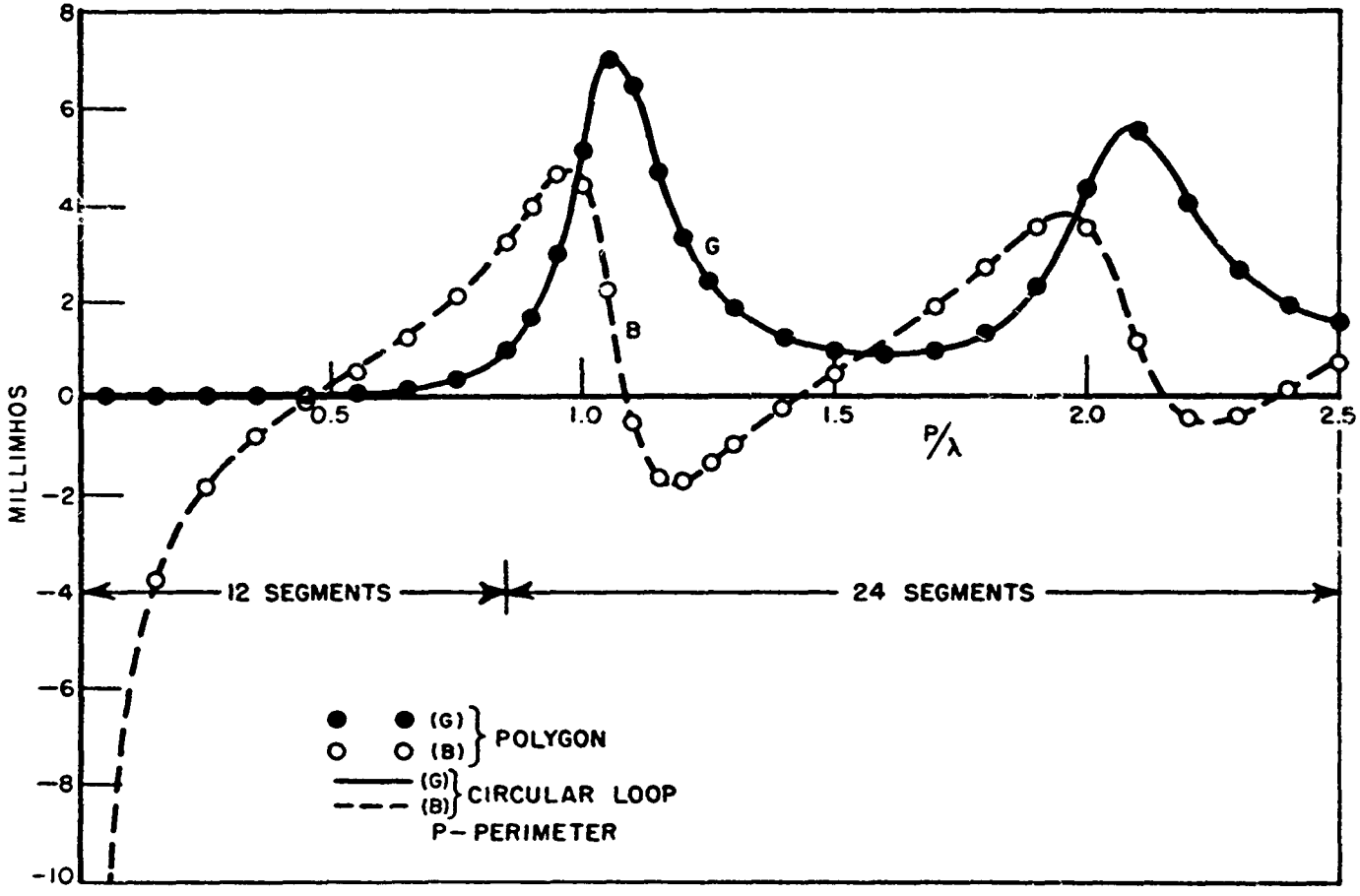

Fig. 6. Conductance (G) and susceptance (B) vs. P/λ: side-driven twelve-sided polygon (Richards) and circular loop (Storer). ($P/\alpha = 403.43$, where α is wire radius.)

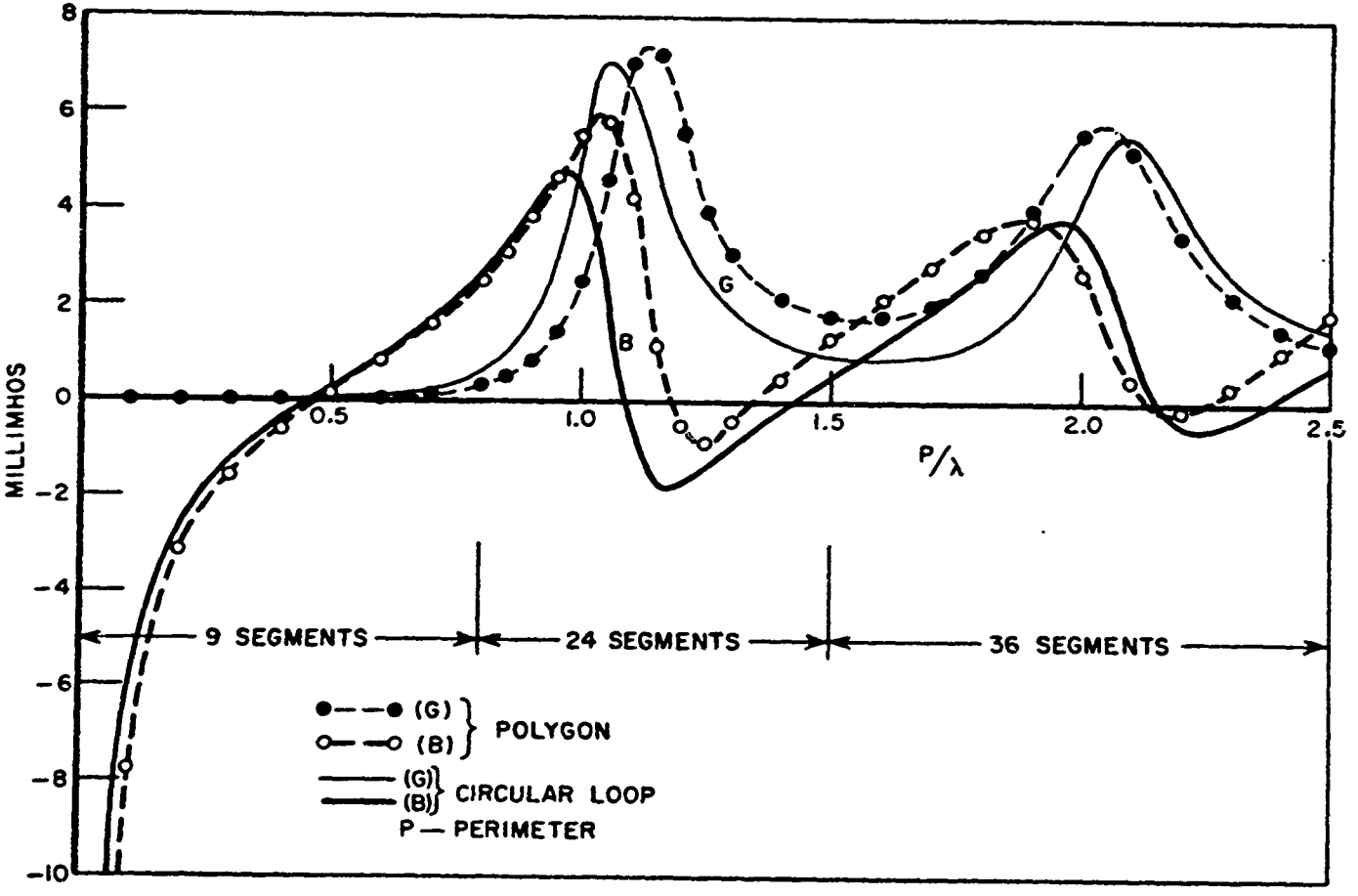

Fig. 7. Conductance (G) and susceptance (B) vs. P/λ: corner-driven three-sided polygon (Richards) and circular loop (Storer). (P/α = 403.43, where α is wire radius.)

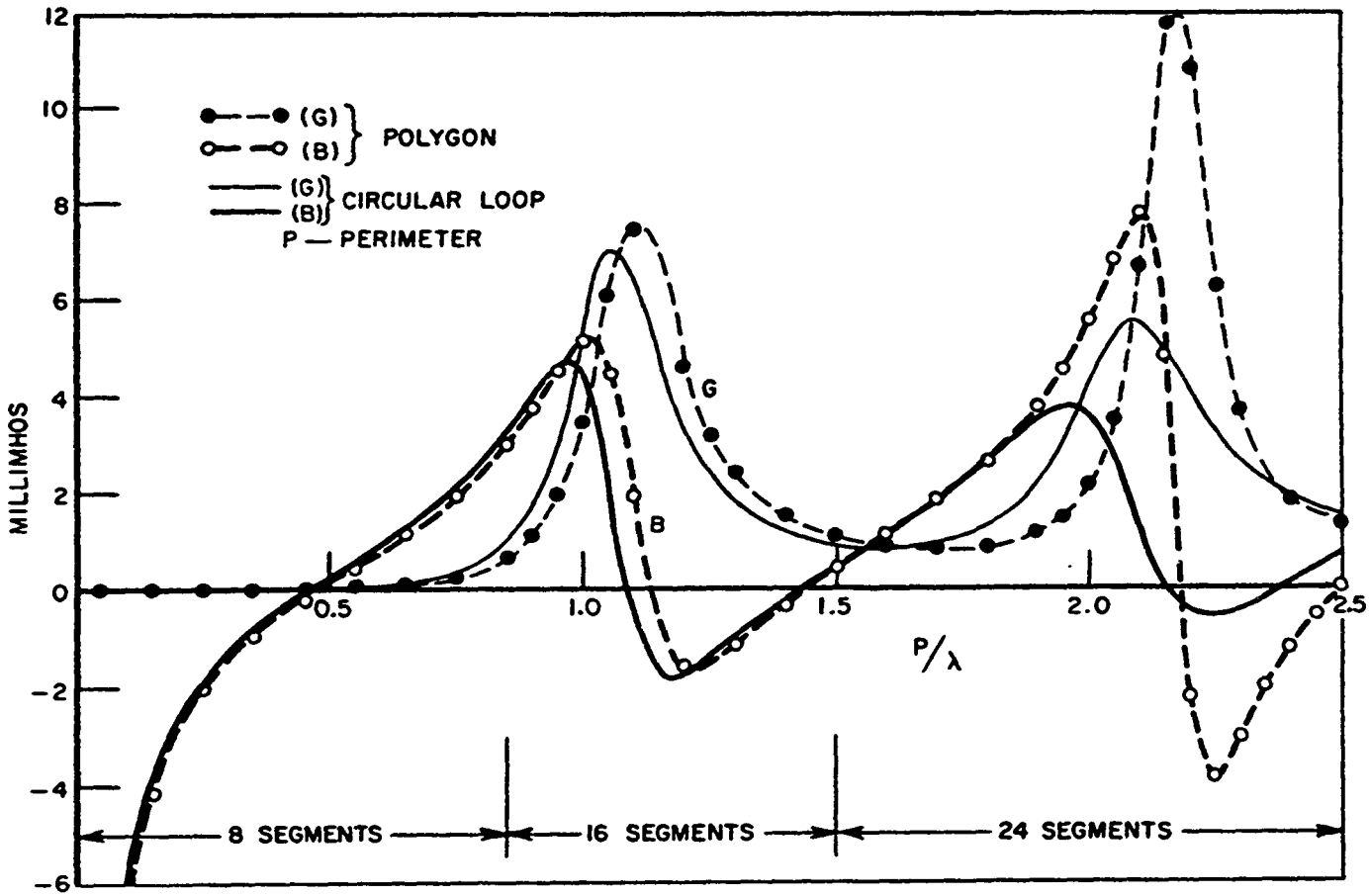

Fig. 8. Conductance (G) and susceptance (B) vs P/λ: corner-driven four-sided polygon (Richards) and circular loop (Storer). ($P/\alpha = 403.43$, where α is wire radius.)

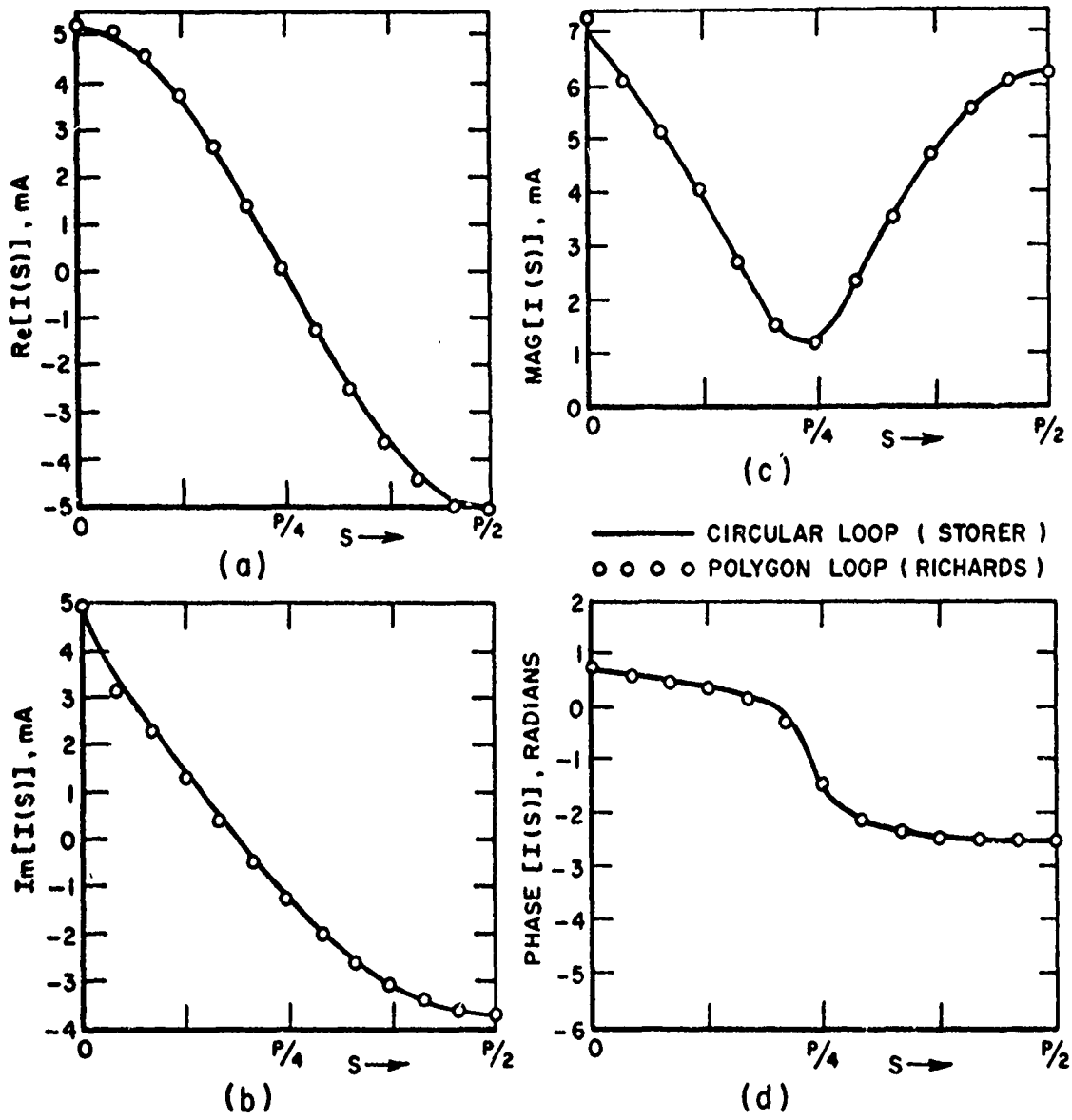

Fig. 9. Current distribution on twelve-sided polygon and circular loop: $P/\lambda = 1.0$ and $P/\alpha = 148.41$, where α is wire radius. a - real part of current distribution; b - imaginary part of current distribution; c - magnitude of current distribution; d - phase of current distribution.

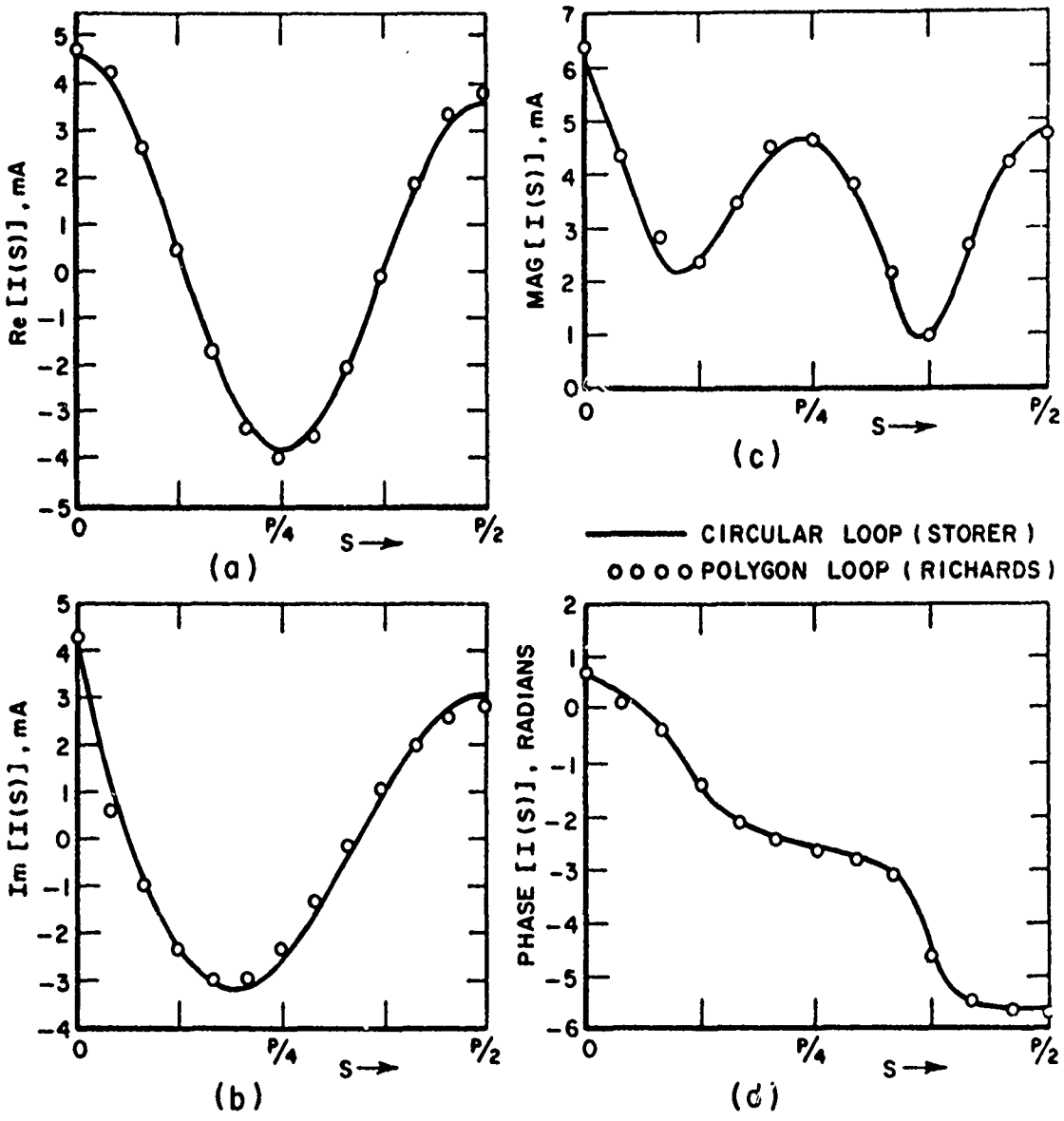

Fig. 10. Current distribution on twelve-sided polygon and circular loop: $P/\lambda = 2.0$ and $P/\alpha = 148.41$, where α is wire radius. a - real part of current distribution, b - imaginary part of current distribution; c - magnitude of current distribution; d - phase of current distribution.

The above data were calculated with a program written in Fortran IV and executed on an IBM 7094 digital computer. Most of the computation is performed by a part of the program that has been written for much more general antenna shapes. As an example of the time required, the calculation of the input admittance and current distribution for a 24-segment polygon loop antenna takes only 10 seconds.

IV. CONCLUSIONS AND RECOMMENDATIONS

The multisegment reaction technique has been applied to calculate the admittance of regular polygon antennas. It has been shown to give good agreement both with measurements and with independent theoretical calculations. Moreover, the calculated current distribution has been shown to be in good agreement with that obtained from an independent theory; hence, accurate far-field patterns of polygon antennas can easily be calculated.

Work will continue on the application of this technique to three-dimensional polygon loops and multiturn loops. It is recommended that this effort include a study of how finite conductivity affects the operating bandwidth and radiation efficiency of such antennas. The use of lumped loading to alter the current distribution along an antenna should be investigated for bandwidth effects and impedance-matching possibilities. Finally, the effect of a finite gap at the feed point should be included to represent physical situations more accurately.

REFERENCES

1. Richards, G.A., "Input Admittance of Planar Polygon Antennas," Report 2708-1, 10 April 1969, ElectroScience Laboratory, The Ohio State University Research Foundation. For Internal Distribution.

2. Schelkunoff, S.A., "On Diffraction and Radiation of Electromagnetic Waves," Physical Review, Vol. 56, (August 1939), pp. 308-316.

3. Richmond, J.H., and Geary, N.H., "Mutual Impedance Between Coplanar-Skew Dipoles," Report 2708-2, 6 August 1969, ElectroScience Laboratory, The Ohio State University Research Foundation. For Internal Distribution.

4. Richmond, J.H., "Coupled Linear Antennas with Skew Orientation," Report 2708-3, 15 August 1969, ElectroScience Laboratory, The Ohio State University Research Foundation. For Internal Distribution.

5. Richmond, J.H., "Computer Analysis of Three-Dimensional Wire Antennas," Report 2708-4, (in process), ElectroScience Laboratory, The Ohio State University Research Foundation. For Internal Distribution.

6. Storer, J.E., "Impedance of Thin-Wire Loop Antennas," AIEE Trans., Vol. 75, Part 1 (November 1956), pp. 606-619.

APPENDIX C

COMPUTER ANALYSIS OF THREE-DIMENSIONAL LOOP ANTENNAS

G. Richards

ElectroScience Laboratory
The Ohio State University
Columbus, Ohio 43212

TECHNICAL REPORT 2708-6
Contract No. DAAD 05-69-C-0031

Department of the Army
Ballistic Research Laboratory
Aberdeen Proving Ground Maryland 21005

ABSTRACT

The multisegment reaction technique is an accurate, efficient analytic tool for the analysis and synthesis of novel wire antenna configurations. The highlights in the development of this technique are first presented.

The above technique is employed to analyze the impedance properties of multiturn loops in free space and fed over a ground plane. A shift in the antiresonant frequency is observed and discussed. The ability to control the antiresonance with tunable lumped elements is developed. Finally, calculated and measured data for square halo antennas of one and two turns are shown. Comparison between the two sets of data is seen to be good.

COMPUTER ANALYSIS OF THREE-DIMENSIONAL LOOP ANTENNAS

I. INTRODUCTION

It is the intent of this report to relate results of a computer analysis of three-dimensional wire antennas. The particular shapes which were analyzed were chosen because of their similarity to certain antennas of interest to the Ballistic Research Laboratory. Two of these antennas are the halo-type antenna and the multiturn loop antenna. Previous efforts to improve the operation of these antennas have been carried out on a cut-and-try experimental basis. While noteworthy improvements have been made, it is possible that still better performance could be achieved by implementing a computerized technique to sort through many more alternate designs than it would be possible to test experimentally.

A first step toward a computerized approach of the sort mentioned above is the subject of this report. The multisegment reaction technique is a theoretically sound analytic tool which has been proven on many previous antenna configurations, including straight and Vee dipoles, polygon loops, and three-dimensional antennas of various shapes. The shapes to be analyzed in this report will further demonstrate the versatility of this technique. The ability of the multisegment reaction technique to handle novel antenna configurations and to handle them accurately and efficiently is perhaps its greatest asset as a tool for antenna design.

A very brief review of the theory and development of the multisegment technique is presented in the following section. A later section presents the results of computer analysis along with comments and observations.

A. The Multisegment Reaction Technique

The theoretical development of this technique has been presented several times previous to this report. For completeness, the important points in the development will be repeated here.

A wire antenna radiates the time-harmonic fields ($\underline{E},\underline{H}$) in free space. The surface equivalence theorem of Schelkunoff [1]* is invoked to replace the antenna by equivalent surface current densities ($\underline{J},\underline{M}$) which radiate the fields ($\underline{E},\underline{H}$) exterior to the surface and generate a null field in the interior region. Reciprocity is enforced between the surface currents and a test source located in the interior region, and a zero-reaction [2] (coupling) situation is seen to exist. The surface is subdivided into a collection of straight segments each having an assumed current distribution that is sinusoidal. By considering the segments

**References are listed on p. 76.*

as a set of overlapping dipoles and by calculating the reaction between each surface-current dipole and each member of an equinumerous set of test dipoles all located along the axis of the wire antenna, a system of linear equations is obtained which relates the currents at the junctions between each pair of connected segments to the terminal voltages at those junctions. Assumption of an appropriate set of voltage source conditions (unit source at driving terminals, zero volts at wire junctions, etc.) results in a solution of the system of equations for the unknown current samples. The input impedance is obtained as the reciprocal of the current sample at the driving terminal, and the current over the whole antenna is obtained in terms of the sample point currents.

B. Multiturn Loop in Free Space

The multiturn loop antenna resembles a coil with several turns. An individual turn may be circular, rectangular, or some other shape and the spacing between successive turns is generally small compared to the length of a single turn. In free space the multiturn loop is fed as a balanced configuration and this presents a problem if a coax feed line is used. For operation at a single frequency a balanced feed may be achieved with a tuned balancing network or a fixed-length balun. However, for operation over a band of frequencies a wide-band balun of the transformer type would be preferable.

Figure 1 indicates the shape of the loops with which this section is concerned. A two-turn loop is shown, but this analysis will cover loops up to four turns and spacings between turns of both 2 cm and 4 cm. For 1/8-inch diameter wire, this represents a turn spacing-to-wire radius ratio of about 12.5 and 25, respectively.

Figure 2 is a plot of input impedance versus frequency (L/λ) for a 4-turn multiturn loop with 4 cm turn spacing. The shape of this impedance curve is generally the same for all antennas of this configuration. Antiresonant peaks are found roughly at the odd-numbered half wavelength points (L/λ = 1/2, 3/2, etc.) and, between peaks, the real part of the impedance is small. The number, relative width, and location of these peaks depend on both the number of turns and the spacing between turns. The figures that follow demonstrate how these parameters affect the input impedance of a multiturn loop antenna.

One of the most interesting phenomena associated with the performance of the multiturn loop antenna is the influence of the coupling between turns on the frequencies at which antiresonances occur. The mechanism which induces this variation in the location of the peaks of the impedance curve has been the subject of discussion for some time. It is believed that a firmer understanding of this phenomenon is now available through analysis of these loops via the multisegment reaction

technique. Figure 3 shows the input impedance around the first antiresonant point for three square multiturn loops of two, three, and four turns. The turn spacing for each loop is 4 cm. Note that the value of L/λ at which antiresonance occurs is almost identical for all three antennas. Note also that the total wire length is almost identical for the three antennas. For a given length L of wire, the size of each individual turn decreases as antennas with more turns are formed from the wire. From this figure it is apparent that within the range of sizes investigated, the cross-sectional size of the individual loop (turn) has little if anything to do with the antiresonant frequency.

Another interesting observation on the data of Fig. 3 is that increasing the number of turns while holding length constant does not change the antiresonant frequency, given the same turn spacing. This tends to indicate that a balance is maintained between the change in inductance due to a change in the deformation of the wire into more turns and the change in the distributed capacitance between neighboring turns due to the same deformation. This involvement of electromagnetic coupling in the shifting of an antiresonant frequency (the thin-wire single-turn loop of just about any shape has a natural antiresonance very near $L/\lambda = 0.5$) is admittedly of a complex nature, but these data definitely indicate the presence of the effect on the impedance of the antenna.

Figure 4 reinforces the arguments made above. The impedance data shown here are concerned with two, three, and four turn loops each having a turn spacing of 2 cm. Again, essentially the same length of wire was used for all three antennas. This length was the same as that used for the antennas in Fig. 3. Again, all three antennas exhibit an antiresonance at nearly exactly the same value of L/λ (same frequency). All the statements made before about the antennas of Fig. 3 could be made about these antennas. The only essential change is that the turn spacing has been halved for the antennas of Fig. 4 from 4 cm to 2 cm. The inductance would not be appreciably affected, but the distributed capacitance between turns would definitely be increased. Notice that, for the antennas in Fig. 4, the antiresonant frequency occurs at a value of L/λ near 0.33. For the 4 cm-spaced antennas of Fig. 3 the antiresonant frequency occurs at about $L/\lambda = 0.38$. Thus a reduction in the turn spacing has a definite tendency to lower the antiresonant frequency of a multiturn loop antenna.

Figures 5 and 6 present additional evidence that the turn spacing really controls the antiresonance shift. Figure 5 is quite similar to Fig. 3 except that the antennas in Fig. 5 all have the same turn size as the 3-turn antenna of Fig. 3. Figure 6 is like Fig. 5 except for the turn spacing of 2 cm instead of 4 cm. The results are essentially identical to those in the corresponding previous figures. The antiresonant frequency for all three antennas in Fig. 5 is very near $L/\lambda = 0.38$,

while that for the antennas in Fig. 6 occurs near $L/\lambda = 0.33$. These data emphasize the dependence of the antiresonant point on the turn spacing, since the turn size for these latter cases is the same for all three antennas.

Figure 7 compares the impedances of two-turn loops of 4 cm spacing and 2 cm spacing. The frequency-shifting effect of the turn spacing on the antiresonant point is less pronounced at the second antiresonance. The situation is somewhat different in Fig. 8, which compares impedance data for four-turn loops of 2 cm and 4 cm turn spacings. Here the loop with the closer turn spacing shows a lowered second antiresonance as well as the first. This indicates that there is still significant interaction between turns at the higher frequency. This study, though, has not dwelt on the impedance properties at higher frequencies for reasons which will be given in the following paragraph.

The primary motivation for a study of these antennas near the first antiresonant peak is that this is the region where the antenna is ordinarily designed to operate [3]. It has been seen that the real part of the input impedance is low for values of L/λ not near the antiresonant point. Hence, if one is to obtain a meaningful amount of radiated energy from the antenna, he must operate the antenna near an antiresonance. Another consideration is that of matching the antenna impedance to the characteristic impedance of the feed system. Only near antiresonance is there at least some chance of matching an antenna of this configuration to a reasonable impedance level, such as 50 ohms or 100 ohms. There is always the possibility of tuning out the reactive component of the impedance; however, more will be said of this point in a later section. One problem associated with this attempt to match impedance levels by operating near antiresonance is the very steep slope of the impedance curve in this region. As one adds turns (see Fig. 5) in order to operate at a lower actual frequency, the antiresonant peak becomes more narrow and the slope is even steeper. Thus, the range of frequencies within which a given antenna performs satisfactorily is quite narrow, and this range becomes even more narrow as more turns are added. This performance characteristic severely limits the applications for which an antenna of this sort is useful. Any implementation more ambitious than very narrowband operation would necessitate a rather elaborate compensating system due to the rapid rate of change of the antenna impedance in the operating frequency range. This problem is not insurmountable, however, and material presented in the next section may be of use in alleviating the problem.

C. Three-Dimensional Loop over a Ground Plane

The basic advantage to be gained by placing the three-dimensional or multiturn loop over a ground plane is that it can be fed from a coaxial

line in an unbalanced configuration. The presence of the ground plane alters the behavior of the antenna, but if the way in which these alterations occur is known, then steps can be taken to obtain satisfactory performance from the antenna. Because the problem of the balanced feed is overcome, more attention can be directed toward tuning the antenna itself to obtain improved radiation properties.

Figure 9 is an example of the sort of antenna configuration with which this section is concerned. The antenna in the figure is shown with 2-1/2 turns. This discussion will include antennas from 1-1/2 to 4-1/2 turns, with turn spacings of both 5 cm and 2 cm.

Figures 10 and 11 contain the information pertinent to this discussion. Figure 10 is input impedance vs L/λ for 2-1/2 turn loops of both 5 cm and 2 cm turn spacings. Figure 11 shows the same data for 4-1/2 turn loops of the same two spacings. (Note: L stands for the length of the antenna plus its image.) Notice that, in the case of the 5 cm turn spacings, the first antiresonance actually occurs at a value of L/λ greater than 0.5. This would seem to indicate that, due to the ground plane symmetry, there is a tendency to detune the antenna so antiresonance occurs at L/λ above 0.5, rather than below 0.5 as was the case for the free-space configuration. Still, when the turn spacing is reduced to 2 cm, it can be seen that the antiresonant point drops below $L/\lambda = 0.5$. Evidently, the proximity effect of nearest-neighbor turns is at least partially offset by the presence of the ground plane.

The use of lumped elements to adjust the impedance properties of this antenna has been probed only slightly. Experimental work on a multiturn loop over a ground plane by Shreve [4] indicates that the impedance of a loop terminated in an adjustable capacitance can be shifted significantly. Figure 12 shows the net effect on the impedance curve is to shift the whole curve to higher values of L/λ. The amount of shift is, of course, dependent on the value of the adjustable capacitor. This illustration of tunability with regard to the impedance of an antenna is valuable if one is to consider operating the antenna over any reasonable range of frequencies.

Results of an alternate tuning technique are given in Fig. 13. Here the input impedance of a 1-1/2 turn loop is plotted against L/λ for several cases of distributed lumped capacitances. In the computer program implementing the multisegment reaction technique a small capacitor is inserted at every wire junction (the corners, in this case) except the driving terminal. The impedance data in Fig. 13 show a marked similarity to those of Fig. 12. As the value of capacitance is increased (capacitive reactance is decreased), notice that the impedance plots come closer to that of the unloaded wire antenna. Thus a collection of adjustable capacitors distributed along the antenna can have much the same effect on the input impedance as a single adjustable

capacitor at the far end of the loop. The advantage of the single-element tuning is its simplicity. The advantage possessed by the antenna with several capacitors is the possibility of reducing voltage breakdown [5]. The capacitors, in addition to providing a distributed tuning network, may redistribute among themselves the voltage drop around the loop, possibly reducing a build-up of a large potential gradient at a single region on the loop. This would be most useful if the antenna were being operated at a high level of input power, or if the surrounding medium contained ionized gases.

Finally, the ability to match the input impedance to a desired value as the frequency is changed is important. Figures 12 and 13 indicate that, for operation on the low-frequency side of the antiresonant peak, the reactive component of the input impedance is inductive when the real part is around 50 ohms. Shreve [6] has shown that this inductive reactance may be tuned out at the input terminals with a series capacitor. Thus, the antenna may be continuously matched to the feed system over a significant frequency range through the use of adjustable lumped elements with the antenna.

Another sort of loop antenna over a ground plane which has received some attention is the so-called halo antenna. The models with which this study has been concerned are only a first step toward a true halo antenna, but the results which have been obtained serve to demonstrate the accuracy and power of the multisegment reaction technique as a tool both for analysis and for synthesis of novel antenna shapes.

Figure 14 shows a Smith chart impedance plot of calculated and measured data for the one-turn square halo depicted in the upper corner of that figure. The total length of the antenna plus its image is 300 cm, so the range of values of L/λ represented is from $L/\lambda = 2$ to $L/\lambda = 3$. Notice that the antiresonance is delayed, occurring at a value of L/λ near 2.7, instead of very close to $L/\lambda = 2.5$. This is the same effect noted previously when the turns of the multiturn loop were too far apart for the proximity effect to lower the antiresonant point noticeably. Note also the good comparison between calculated and measured data.

Figure 15 illustrates a two-turn halo antenna similar to the one just discussed. Figure 16 is a Smith chart impedance plot for the antenna of Fig. 15, again comparing calculated and measured data. The error between calculations and measurements at the highest frequency shown is less than 2 percent. The good comparison which Fig. 16 shows between theory and experiment lends weight to the validity of the multisegment reaction technique. Notice once again that, although the total wire length plus its image equals the odd-numbered half-wavelengths at frequencies of 100 MHz and 300 MHz, the antiresonant points are delayed in both instances. Again, this is attributed to the effect of the ground plane on the impedance properties of the antennas involved in this study.

II. CONCLUSIONS AND RECOMMENDATIONS

The multisegment reaction technique has proven effective for analyzing novel antenna configurations. Through the use of this technique the input impedance of the multiturn loop has been shown to possess a predictable antiresonance feature. The turn spacing is a controlling factor in determining the frequency at which this antiresonance occurs. The same effect has been seen for multiturn loops fed over a ground plane, but the effect of the ground plane itself seems to diminish the proximity effect between successive turns. The antenna has been seen to be tunable by several techniques, two of which are the termination in an adjustable capacitor and the distributed loading with several capacitors. By either means it is possible to adjust the frequency at which antiresonance occurs, or to realize a given input impedance.

The results which this report presents are only the completion of some basic steps toward the realization of a completely analytic, computerized technique for wire antenna design. Yet, the accuracy with which these calculations have been made, as demonstrated by their comparison with experimental measurements, shows that these have indeed been large steps. A greater understanding of the operation of these new antenna configurations is unfolding via the computerized analysis. Further investigation of the properties and possibilities of these antennas is necessary. More improvements ought to be made in the analytic technique to allow more general configurations to be handled. The alternatives of tunability through lumped loading should be further explored.

ACKNOWLEDGMENTS

The author wishes to thank Professor J. H. Richmond for his continual support and advice concerning the implementation of the multisegment reaction technique. Mr. D. H. Shreve is gratefully acknowledged for allowing the use of his experimental data on the multiturn loop terminated in an adjustable capacitor.

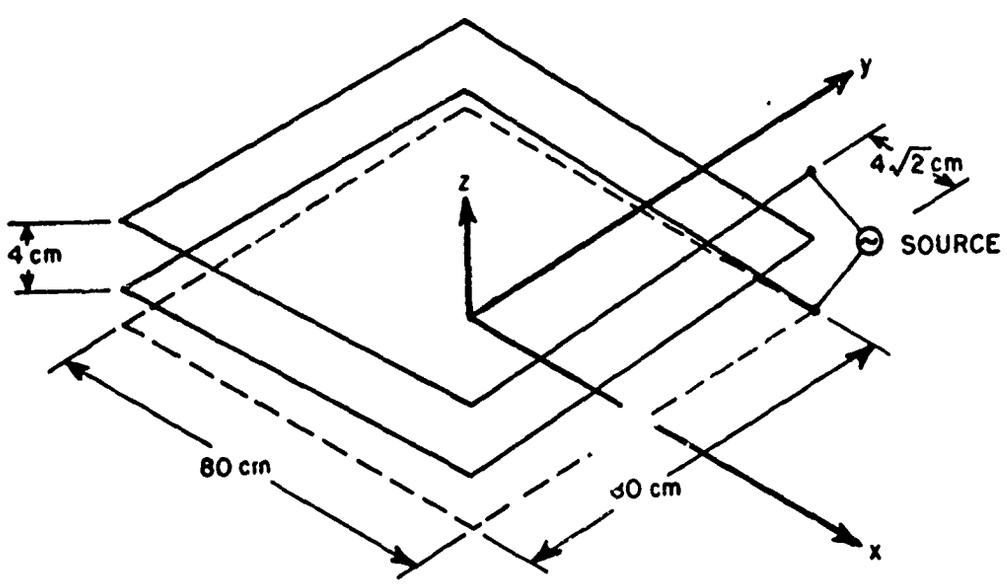

WIRE RADIUS: 0.1588 cm

Fig. 1. Two-turn square loop in free space; turn spacing = 4 cm.

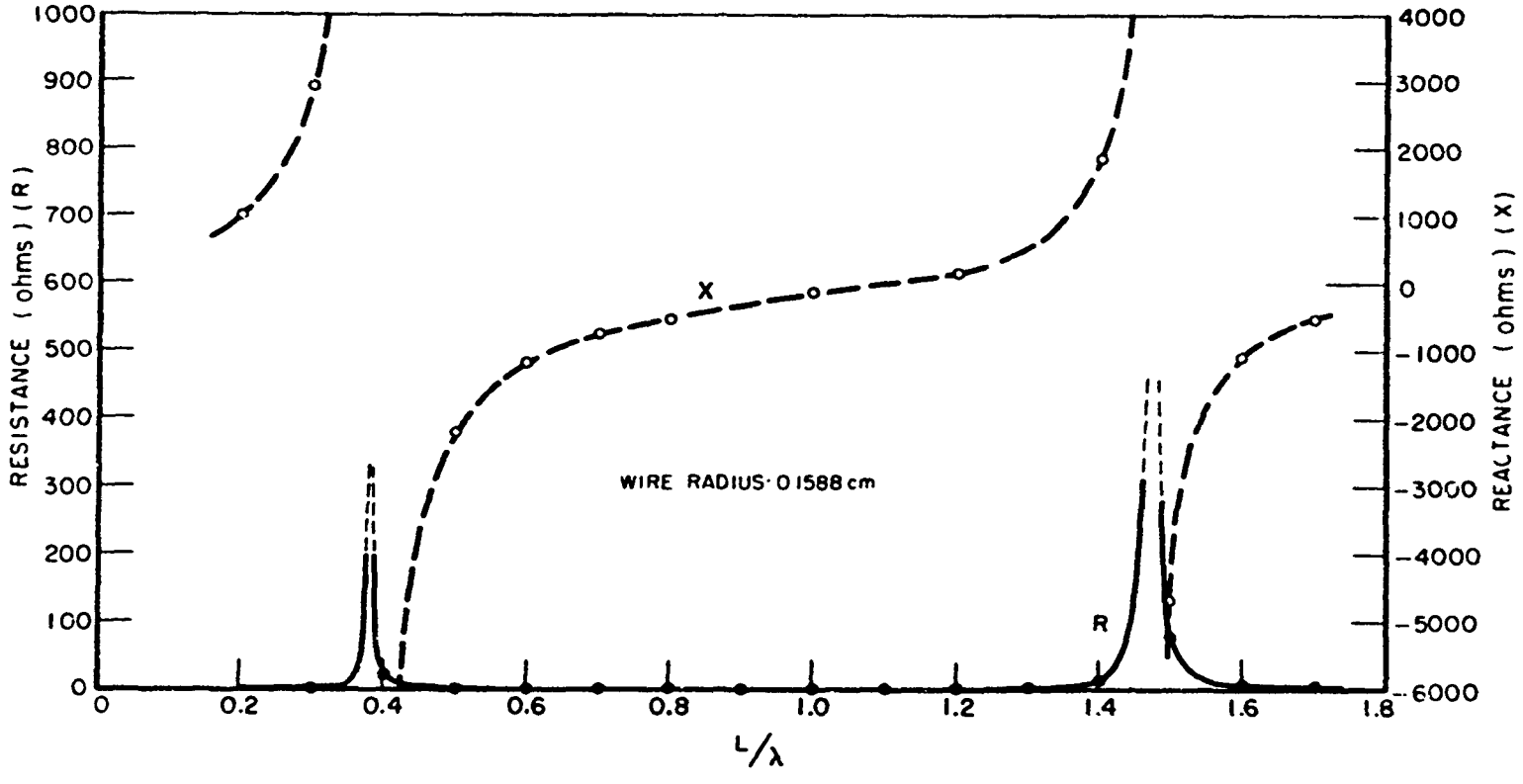

Fig. 2. Input impedance (R and X) vs. L/λ for four-turn square loop in free space (turn spacing = 4 cm).

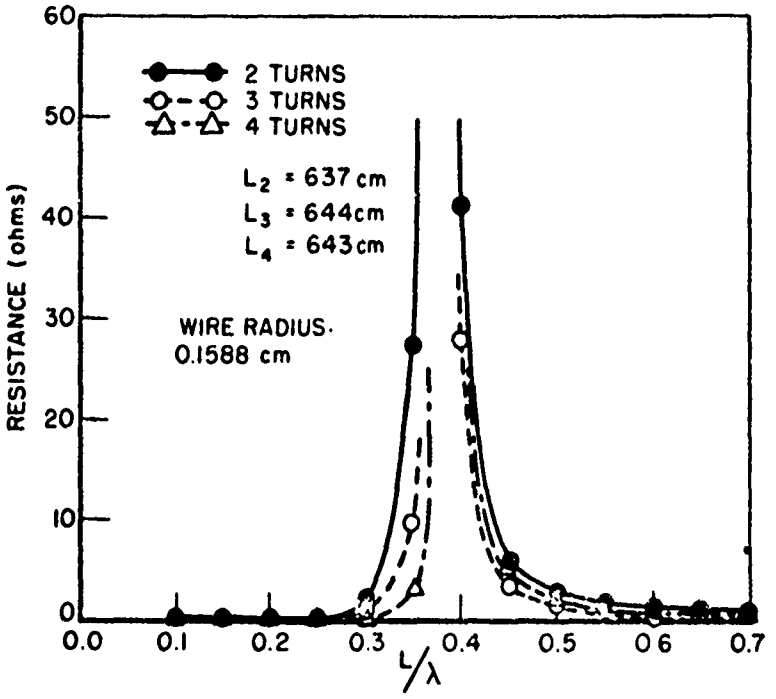

Fig. 3(a). Input resistance near first antiresonance: square loops of two, three, and four turns (turn spacing = 4 cm, same total wire length).

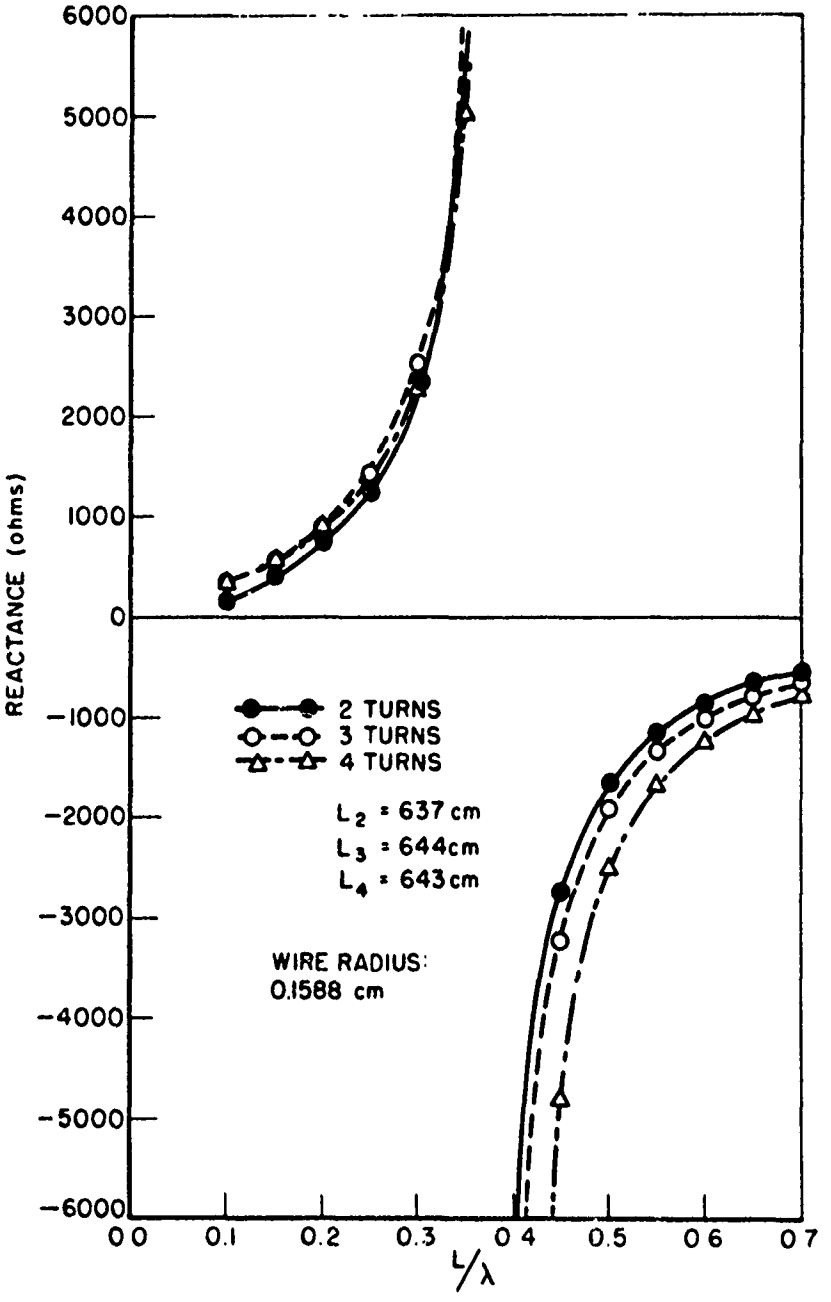

Fig. 3(b). Input reactance near first antiresonance: square loops of two, three, and four truns (turn spacing = 4 cm, same total wire length).

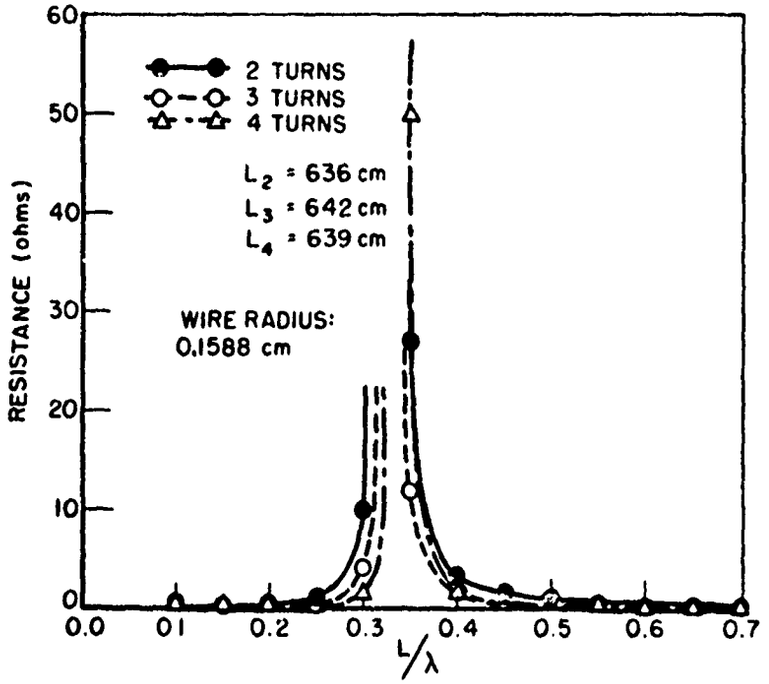

Fig. 4(a). Input resistance near first antiresonance: square loops of two, three, and four turns (turn spacing = 2 cm, same total wire length).

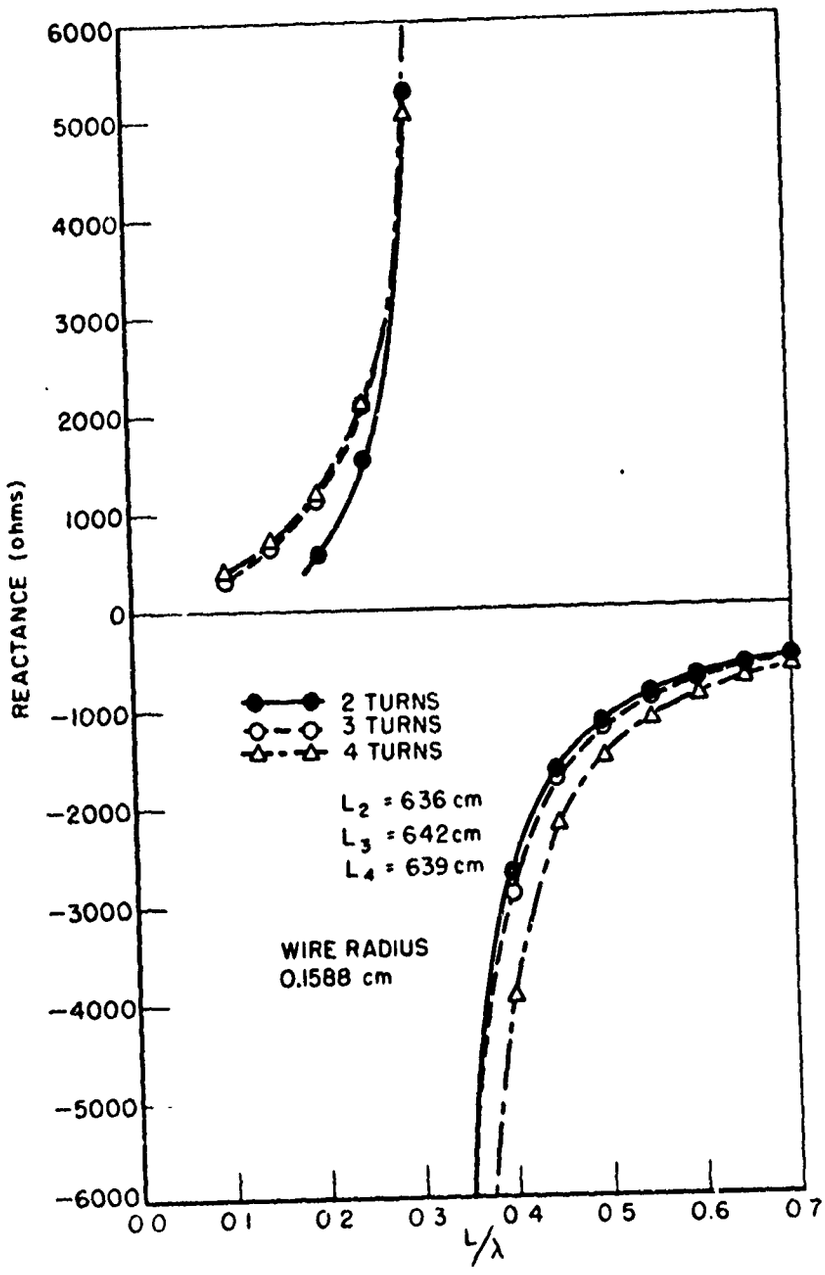

Fig. 4(b). Input reactance near first antiresonance: square loops of two, three, and four turns (turn spacing = 2 cm, same total wire length).

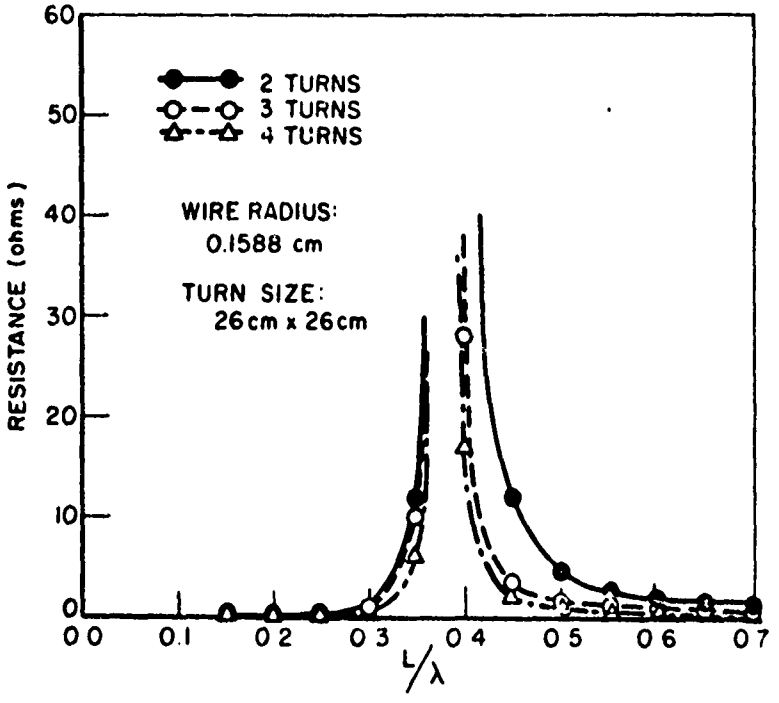

Fig. 5(a). Input resistance near first antiresonance: square loops of twc three, and four turns (turn spacing = 4 cm, same turn size).

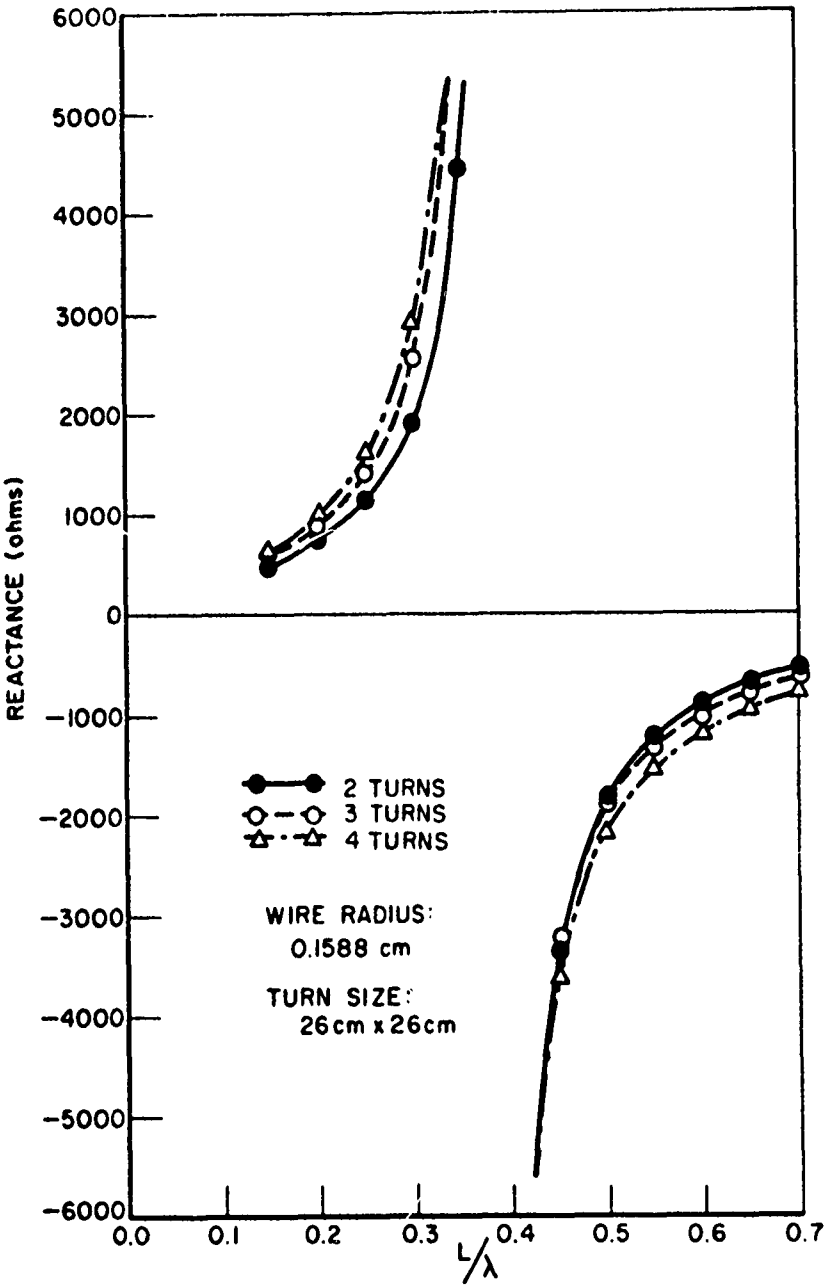

Fig. 5(b). Input reactance near first antiresonance: Square loops of two, three, and four turns (turn spacing = 4 cm, same turn size).

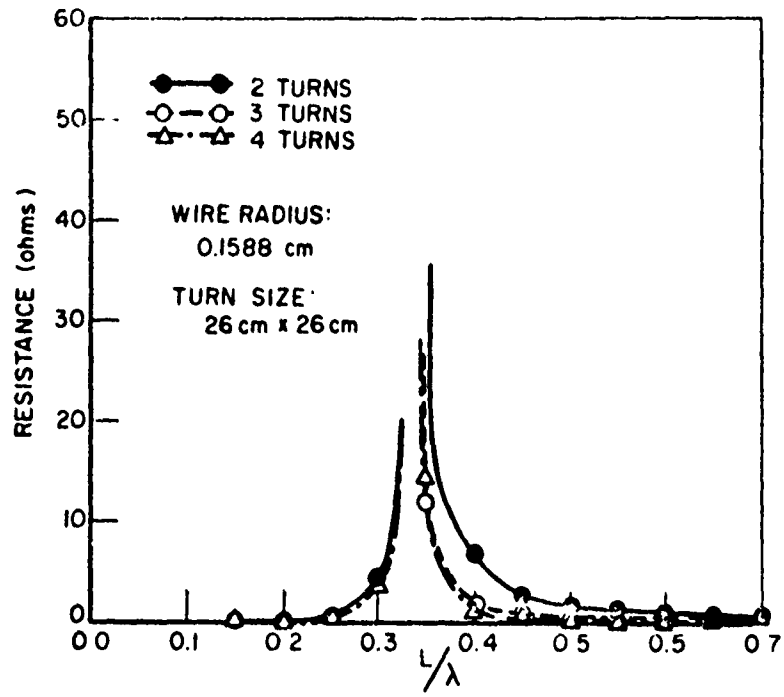

Fig. 6(a). Input resistance near first antiresonance: square loops of two, three, and four turns (turn spacing = 2 cm, same turn size).

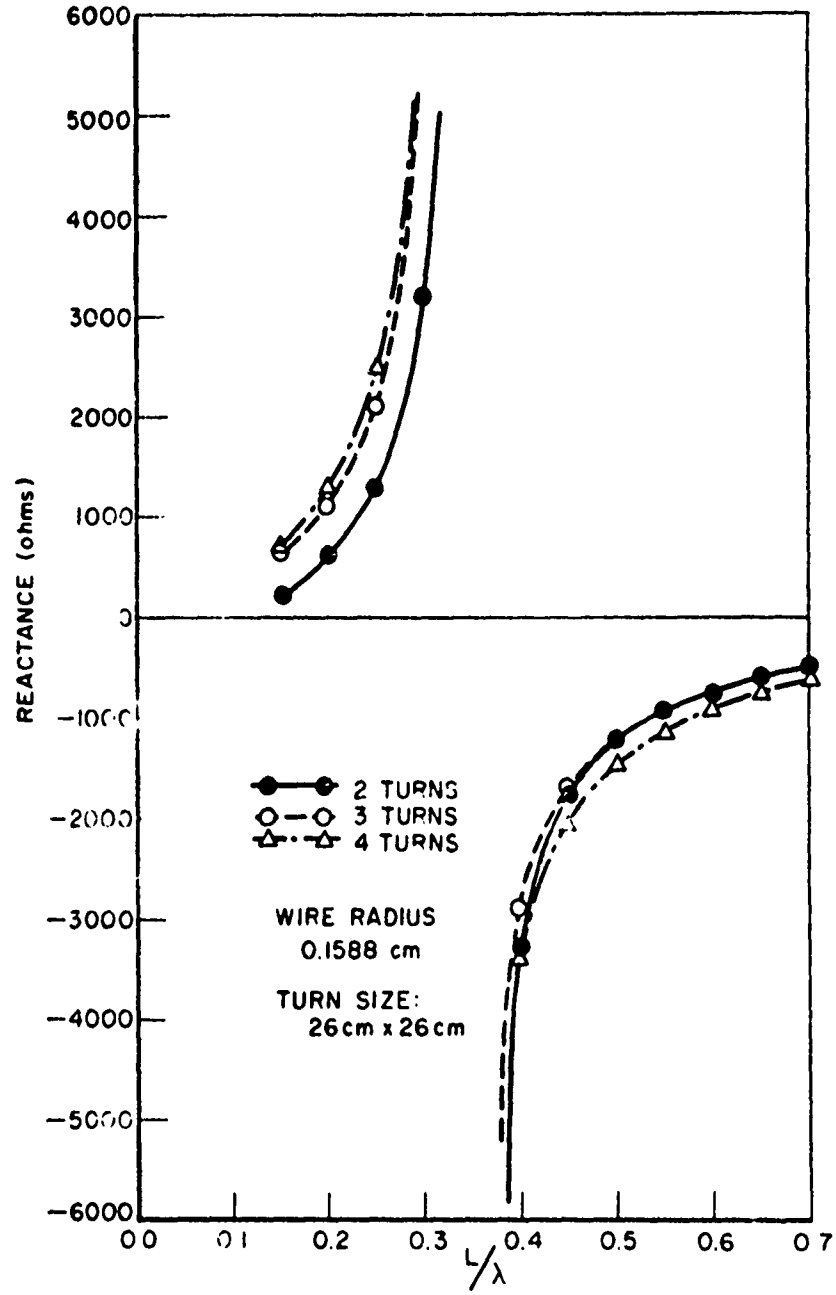

Fig. 6(b). Input reactance near first antiresonance: square loops of two, three, and four turns (turn spacing = 2 cm, same turn size).

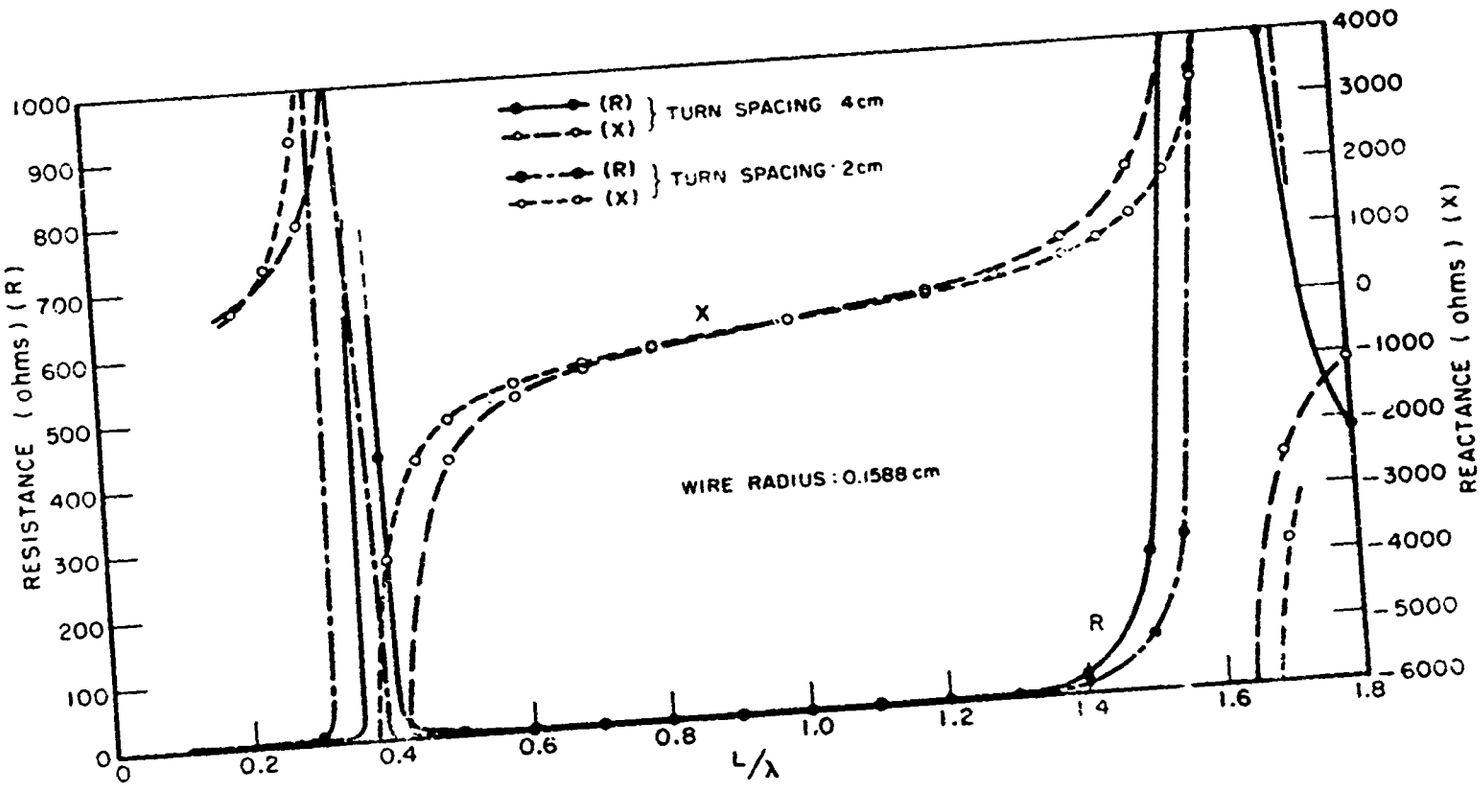

Fig. 7. Comparison of input impedances vs. L/λ for two-turn square loops with spacings of 4 cm and 2 cm.

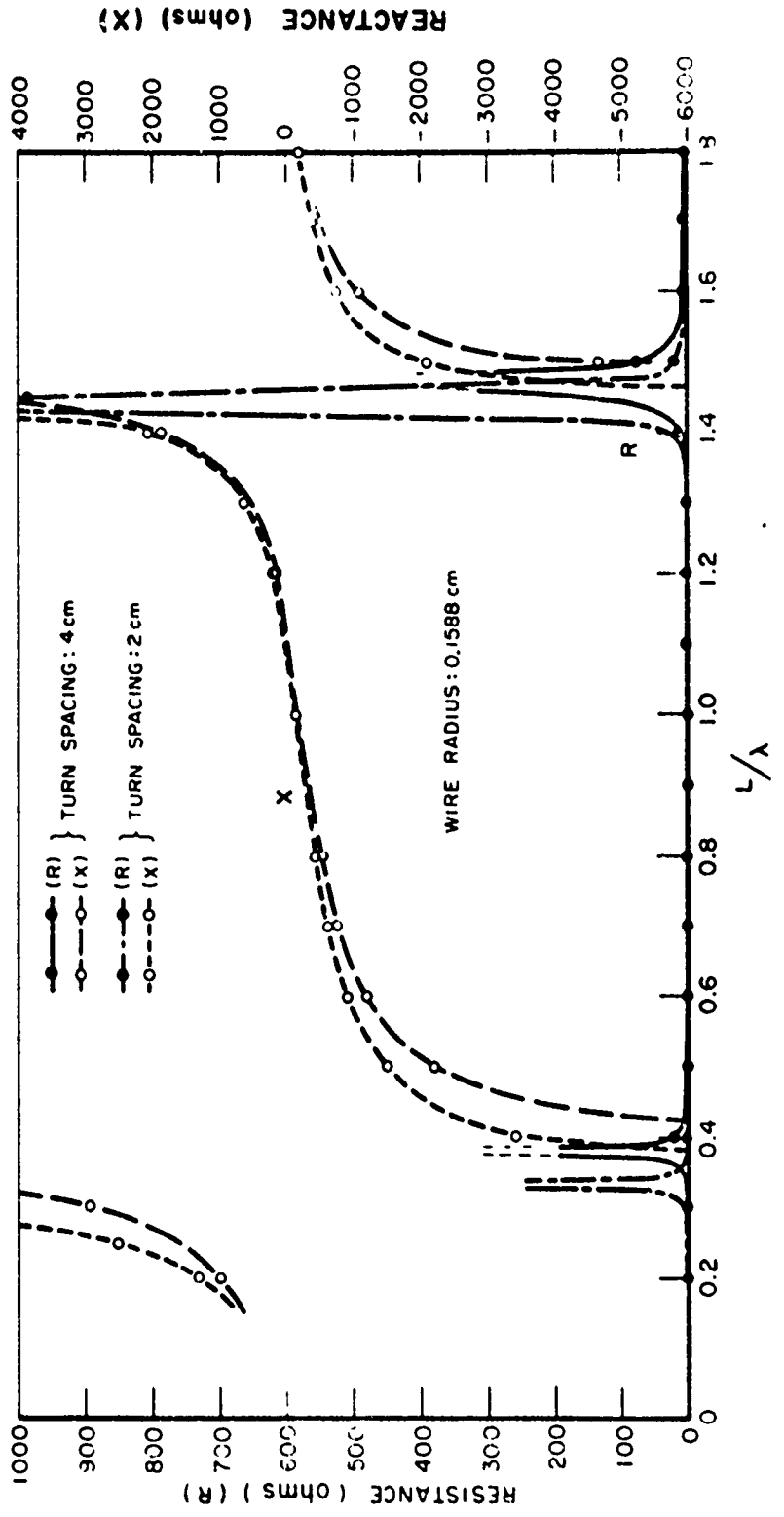

Fig. 8. Comparison of input impedances vs. L/λ for four-turn square loops with spacings of 4 cm and 2 cm.

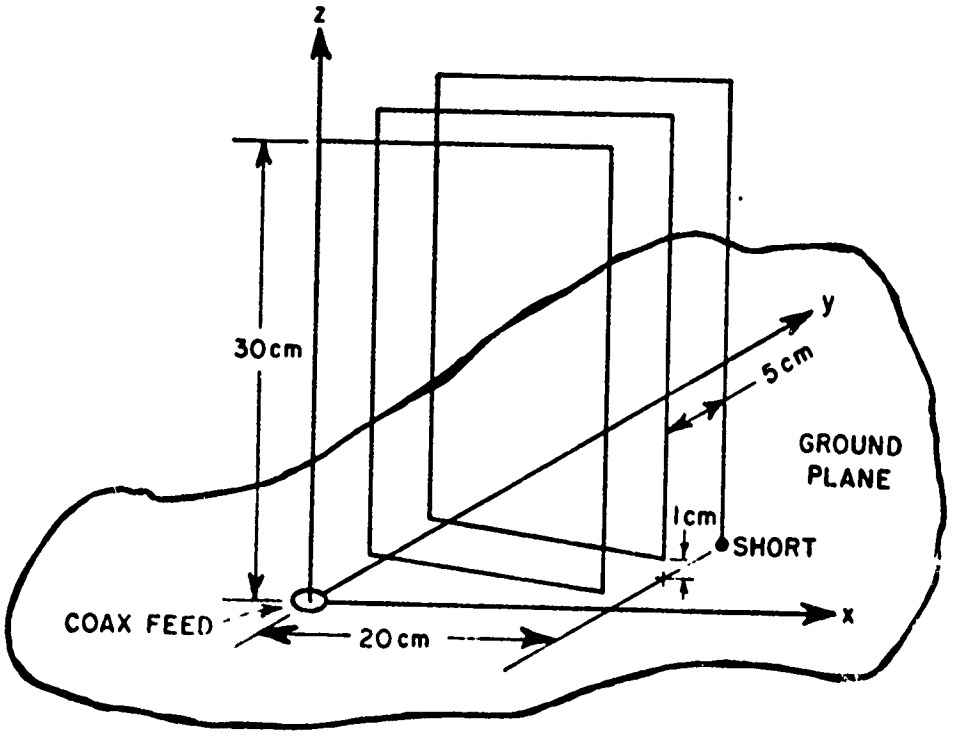

Fig. 9. Two and one-half turn vertical half-loop over ground plane.

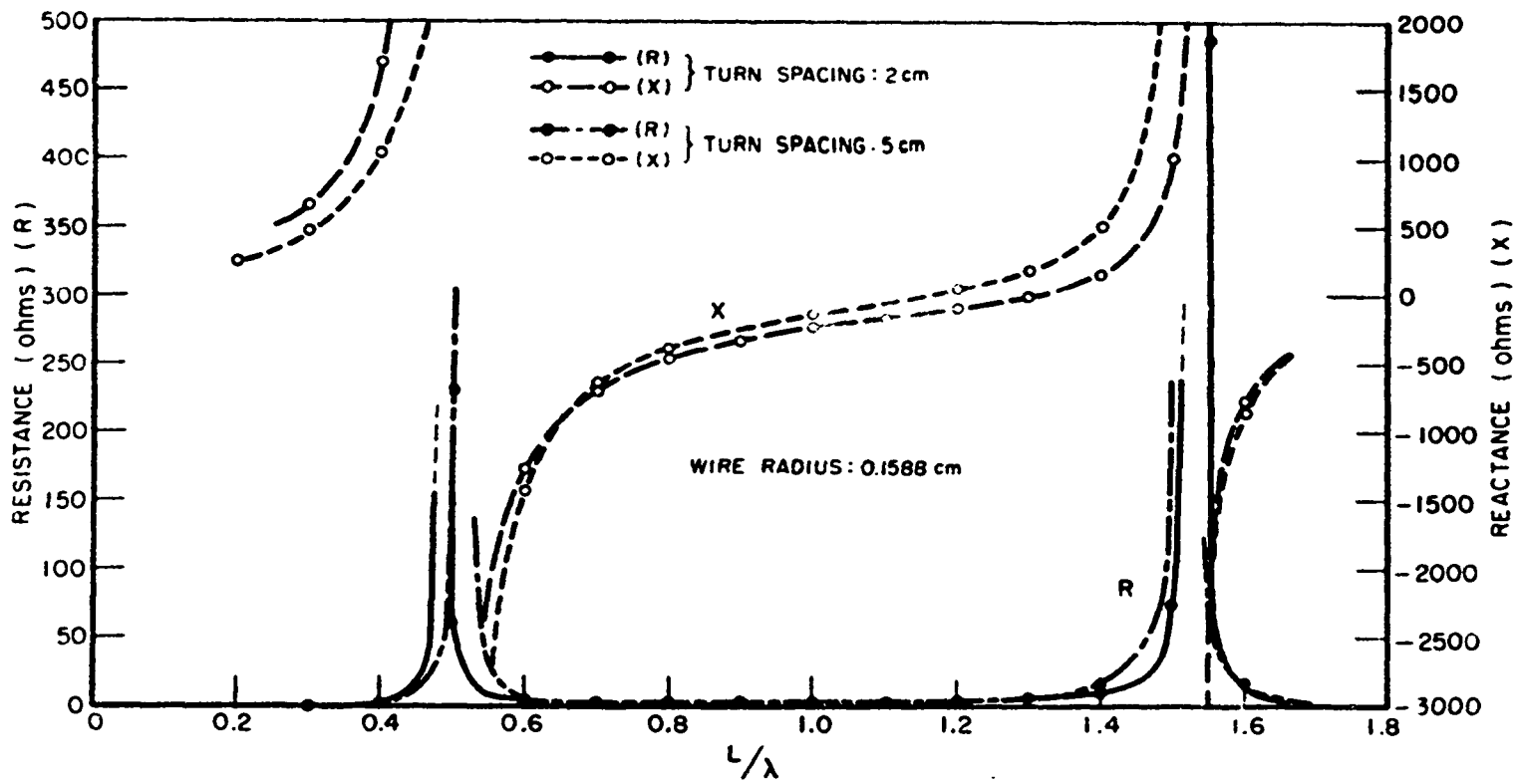

Fig. 10. Comparison of input impedances: two and one-half turn vertical half-loop over ground plane with turn spacings of 5 cm and 2 cm.

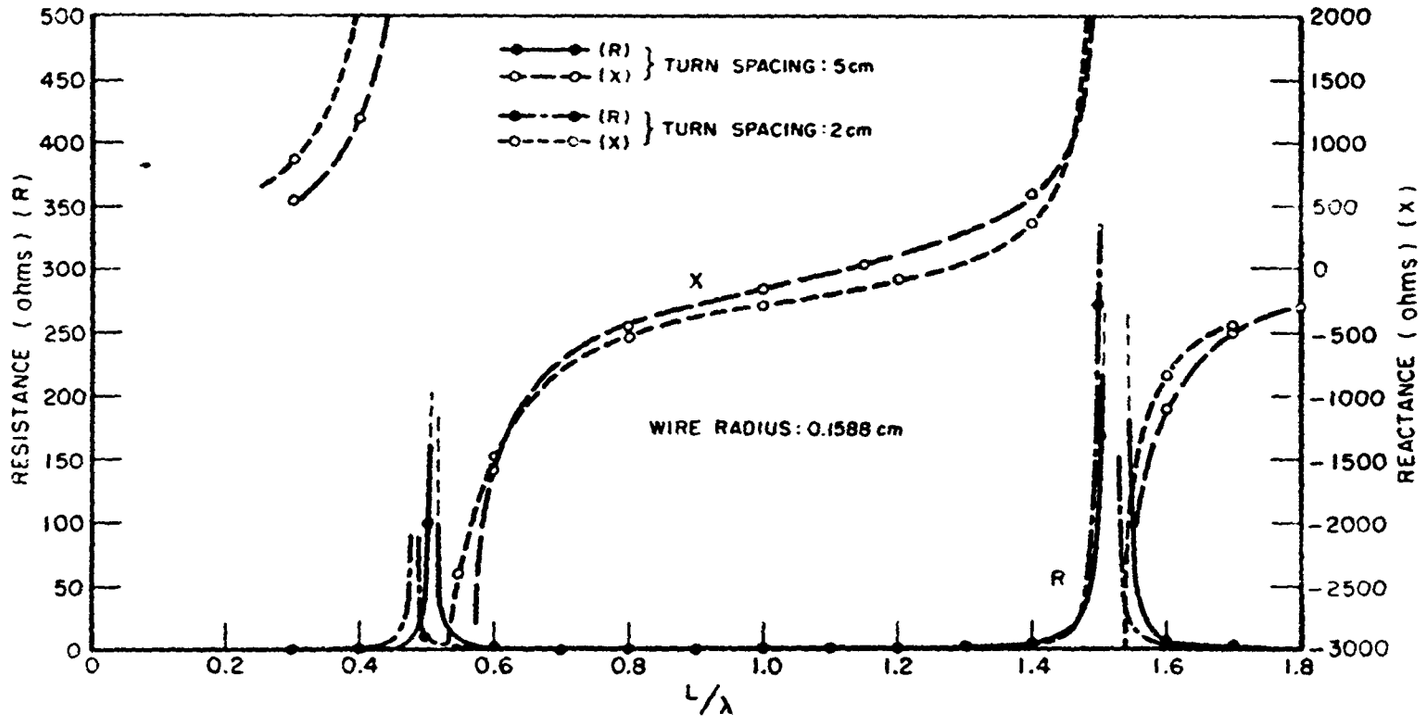

Fig. 11. Comparison of input impedances: four and one-half turn vertical half-loop over ground plane with turn spacings of 5 cm and 2 cm.

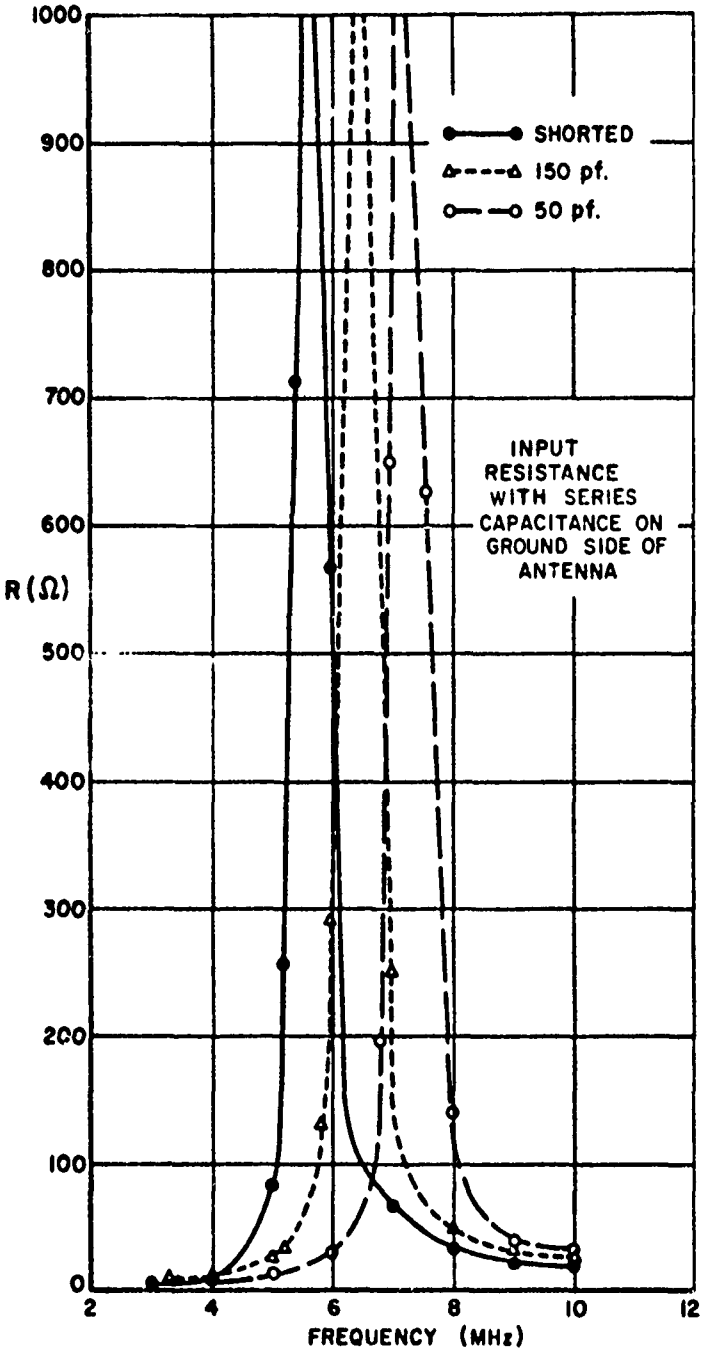

Fig. 12(a). Input resistance showing effect of capacitor between multiturn loop and ground (Shreve).

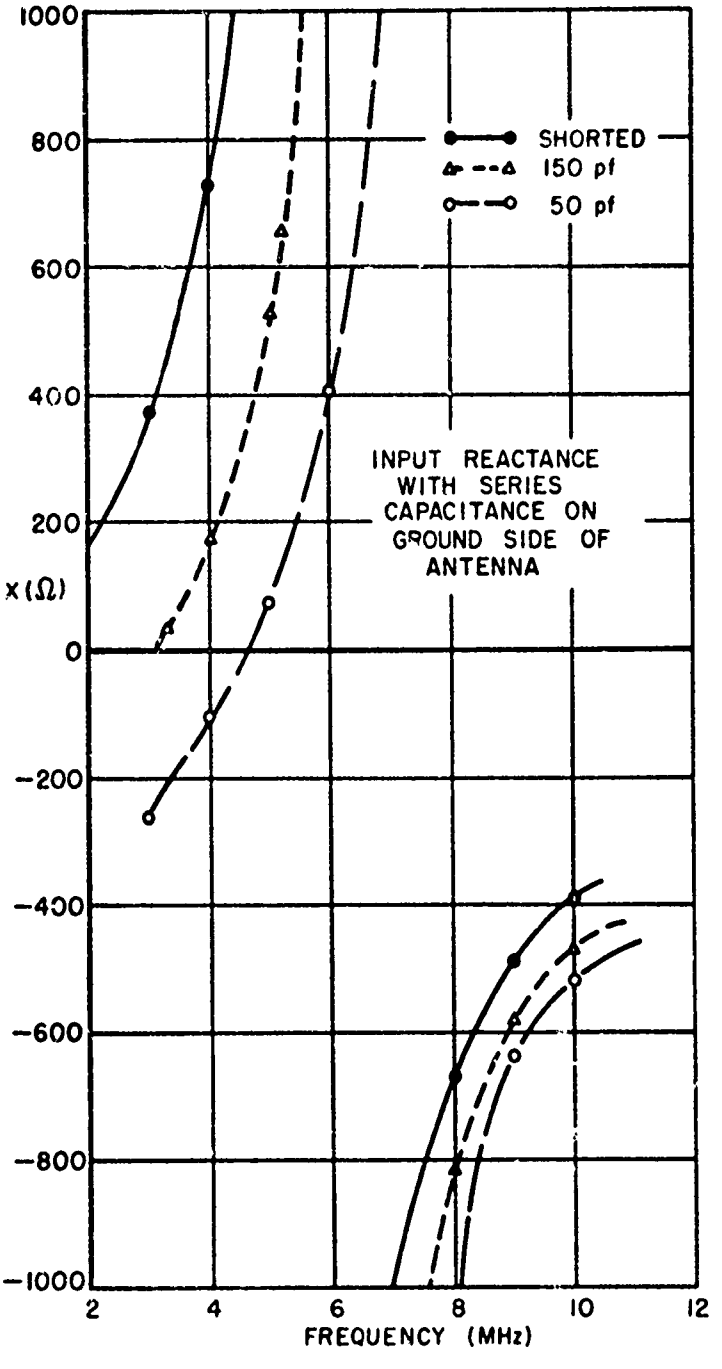

Fig. 12(b). Input reactance showing effect of capacitor between multiturn loop and ground (Shreve).

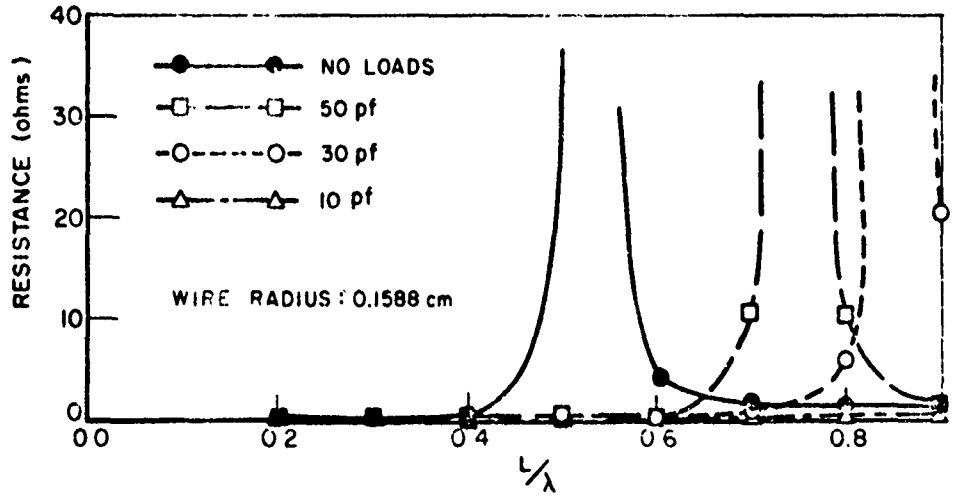

Fig. 13(a). Variation of input resistance near first antiresonance for several cases of multiple reactive lumped loads: one and one-half turn vertical half-loop over ground plane.

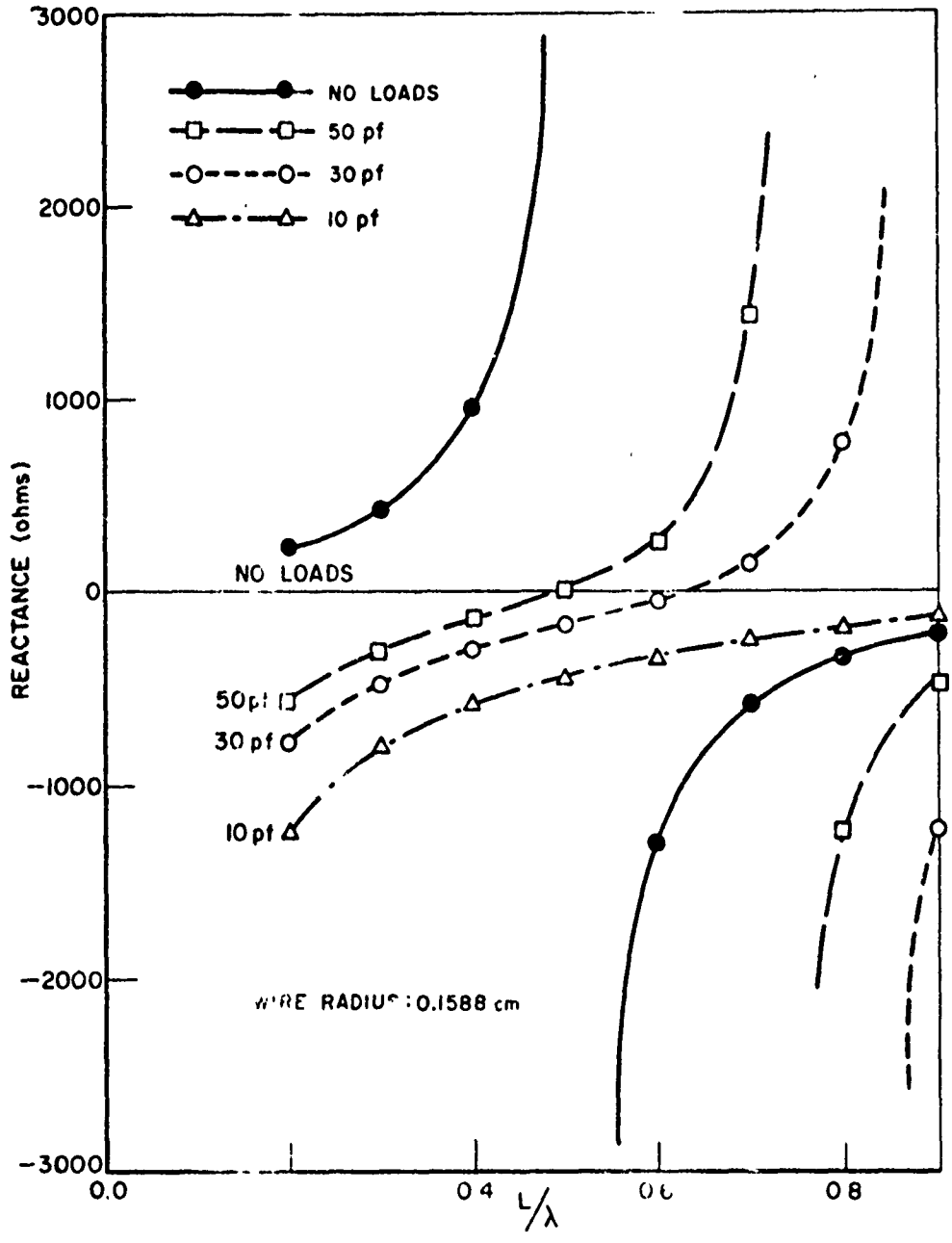

Fig. 13(b). Variation of input reactance near first antiresonance for several cases of multiple reactive lumped loads: one and one-half turn vertical half-loop over ground plane.

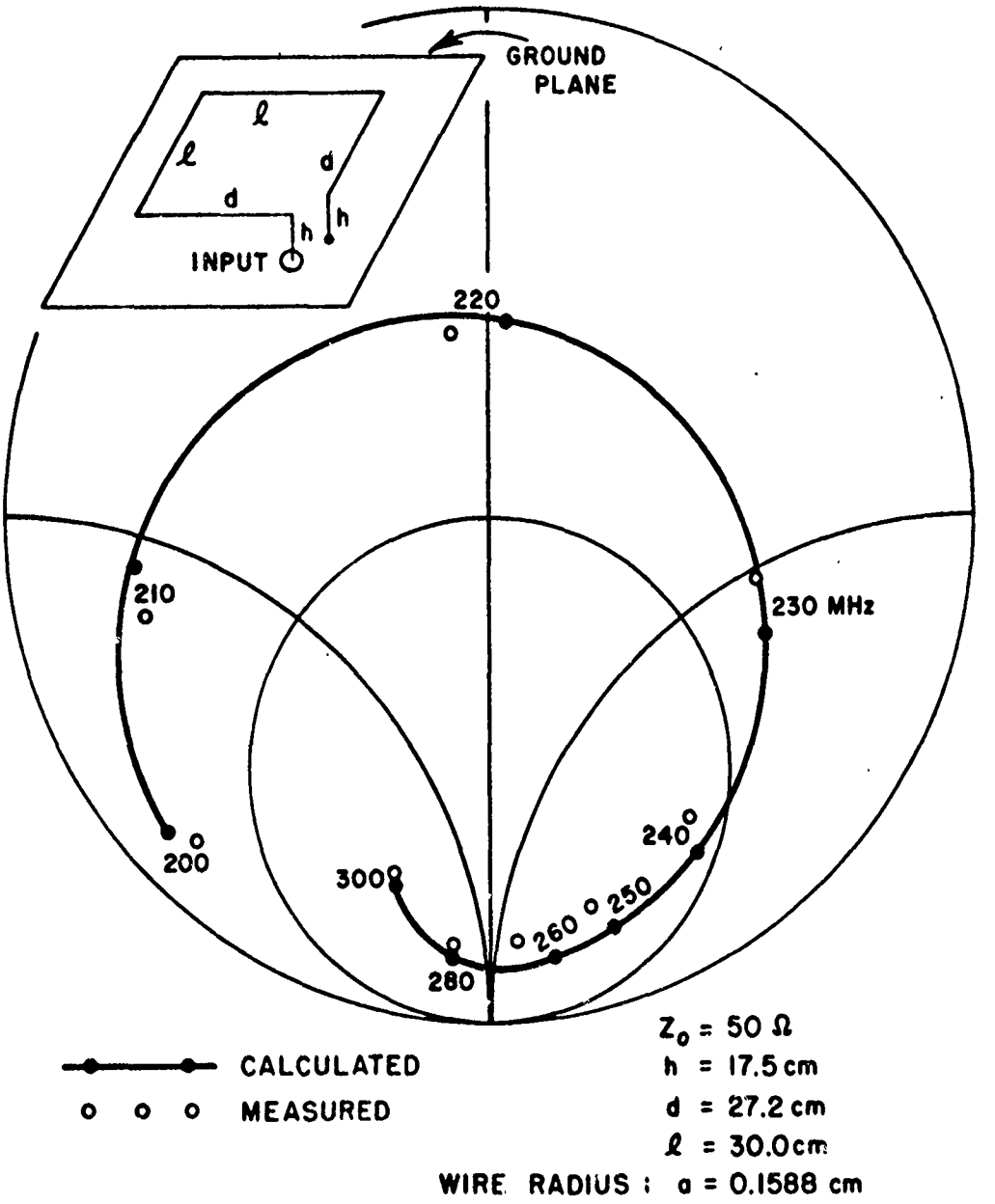

Fig. 14. Calculated and measured input impedance of one-turn halo antenna.

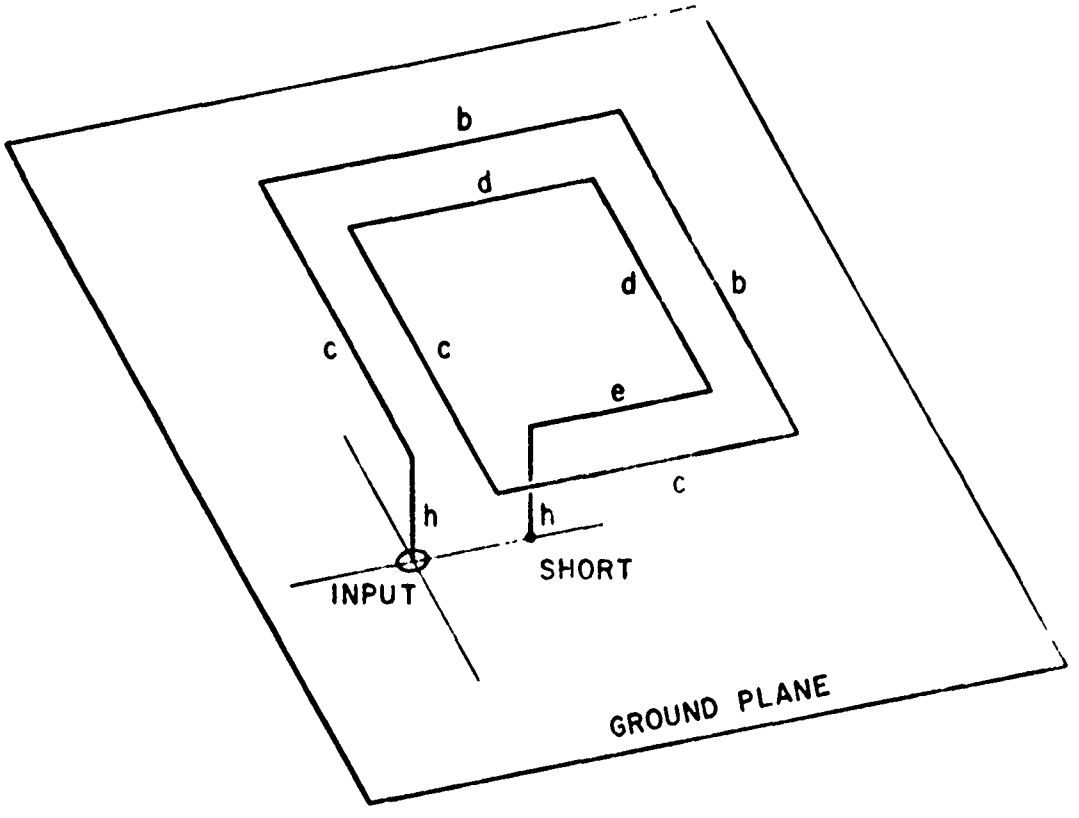

WIRE MATERIAL : BRASS
WIRE RADIUS : a = 0.1588 cm
WIRE LENGTH : L = 75 cm

b = 10 cm	d = 6 cm
c = 8 cm	e = 4 cm
	h = 7.5 cm

Fig. 15. Two-turn halo-type loop antenna over ground plane.

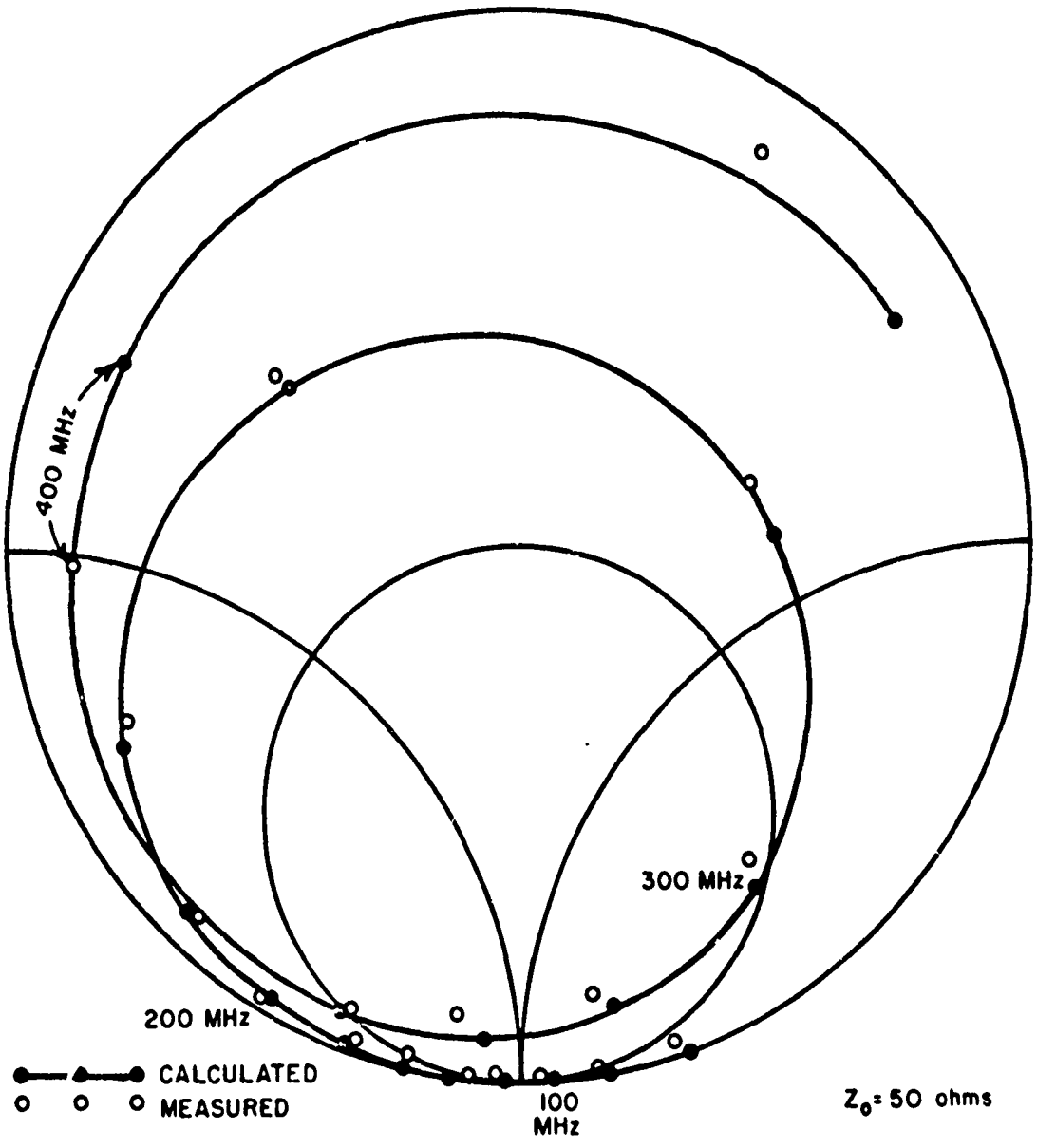

Fig. 16. Calculated and measured input impedance of two-turn halo-type antenna over ground plane.

REFERENCES

1. Schelkunoff, S.A., "On Diffraction and Radiation of Electromagnetic Waves," Physical Review, Vol. 56, (August 15, 1939), pp. 308-316.

2. Rumsey, V.H., "The Reaction Concept in Electromagnetic Theory," Physical Review, Ser. 2, Vol. 94, (June, 1954), pp. 1983-1991.

3. Flaig, T.L., "The Impedance and Efficiency of Multiturn Loop Antennas," M.Sc. Thesis, The Ohio State University, 1968.

4. Shreve, D.H., "Numerical and Experimental Investigation of Impedance and Matching Techniques Associated with Multiturn Loop Antennas," M.Sc. Thesis, The Ohio State University, 1970.

5. Ermatinger, C.E., "A Technique for Improving Voltage Breakdown Threshold," IEEE Trans. on Antennas and Propagation, Vol. AP-16, (July, 1968), p. 488.

6. Shreve, D.H., op. cit.

APPENDIX D

MUTUAL IMPEDANCE BETWEEN COPLANAR-SKEW DIPOLES

J.H. Richmond and N.H. Geary

ElectroScience Laboratory
The Ohio State University
Columbus, Ohio 43212

TECHNICAL REPORT 2708-2

Contract No. DAAD05-69-C-0031

6 August 1969

Department of the Army
Ballistic Research Laboratory
Aberdeen Proving Ground Maryland 21005

ABSTRACT

The induced emf formulation is employed to develop a closed form expression for the mutual impedance between coplanar-skew dipoles. Numerical results are presented in graphical form.

MUTUAL IMPEDANCE BETWEEN COPLANAR-SKEW DIPOLES

I. INTRODUCTION

H.E. King[1*] has determined the mutual impedance between parallel dipoles, and Lewin[2] has analyzed the coplanar-skew dipoles. Lewin's analysis, however, is restricted to half-wave center-fed dipoles. In this paper we derive an expression for the mutual impedance between coplanar-skew dipoles with arbitrary lengths and terminal positions. This expression is relatively simple and convenient for computer programming. Future reports will use this result to develop a multi-segment reaction formulation for multi-turn loops and halo antennas.

In the following section we present a new expression for the near-zone field of a linear dipole, in a form most convenient for the mutual-impedance analysis.

II. THE NEAR-ZONE FIELD OF THE LINEAR DIPOLE

As shown in Fig. 1, we consider a dipole located on the z axis and let z_1 and z_3 denote the endpoints and z_2 the terminals. In the induced emf method, the dipole current is given by

$$(1)\quad \underline{I}(z) = \hat{z}\, I_1 \frac{\sin k(z-z_1)}{\sin kc_1} \qquad \text{for } z_1 < z < z_2$$

$$(2)\quad \underline{I}(z) = \hat{z}\, I_1 \frac{\sin k(z_3-z)}{\sin kc_2} \qquad \text{for } z_2 < z < z_3$$

The time dependence $e^{j\omega t}$ is suppressed, c_1 and c_2 denote the dipole arm lengths, $\hat{z}$ is a unit vector, I_1 is the terminal current, and $k = 2\pi/\lambda$. The field generated in free space by this dipole (or sinusoidal line source) is determined most readily from the expressions of Schelkunoff.[3] The cylindrical components of the electric field intensity are

$$(3)\quad E_\rho = \frac{j30I_1}{\rho}\left[\frac{(z-z_1)e^{-jkR_1}}{R_1 \sin kc_1} - \frac{(z-z_2)e^{-jkR_2}\sin kc}{R_2 \sin kc_1 \sin kc_2} + \frac{(z-z_3)e^{-jkR_3}}{R_3 \sin kc_2}\right]$$

$$(4)\quad E_z = j30I_1\left[-\frac{e^{-jkR_1}}{R_1 \sin kc_1} + \frac{e^{-jkR_2}\sin kc}{R_2 \sin kc_1 \sin kc_2} - \frac{e^{-jkR_3}}{R_3 \sin kc_2}\right]$$

---

* *References are listed on p. 85.*

where c is the dipole length and R_1, R_2 and R_3 are the distances defined in Fig. 1.

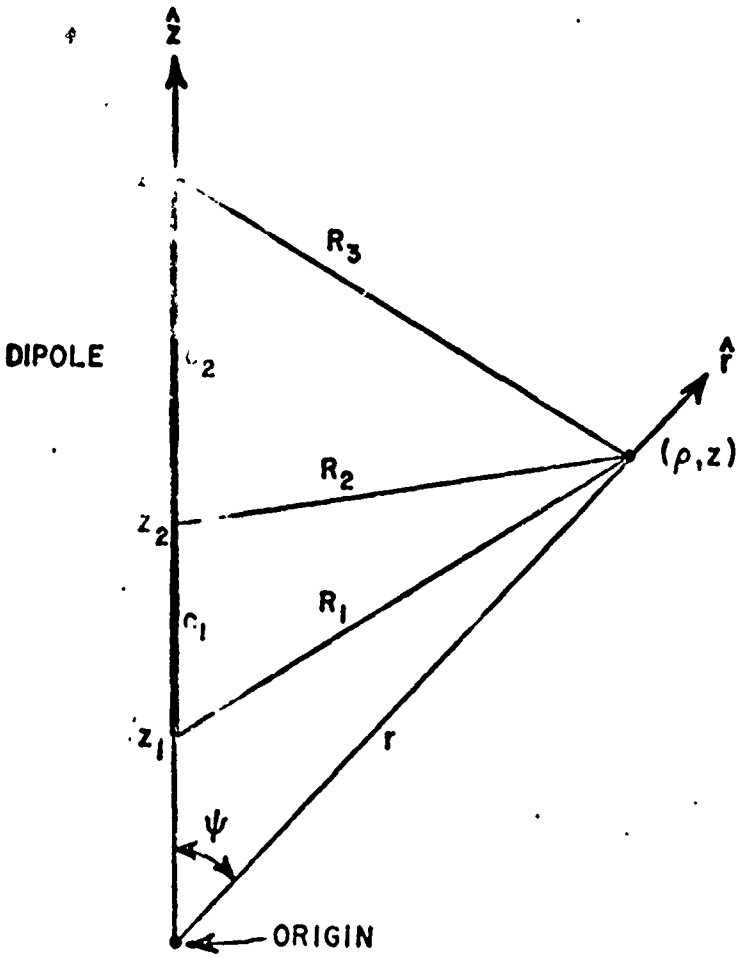

Fig. 1. A linear dipole and the coordinate system.

The radial component of the field is obtained from a linear combination of E_ρ and E_z:

$$(5) \qquad E_r = \frac{-j30I_1}{r} \sum_{m=1}^{3} C_m z_m \frac{e^{-jkR_m}}{R_m}$$

where

$$(6) \qquad C_1 = \frac{1}{\sin kc_1}$$

$$(7) \qquad C_2 = - \frac{\sin kc}{\sin kc_1 \sin kc_2}$$

$$(8) \qquad C_3 = \frac{1}{\sin kc_2}$$

Equation (5) is believed to be a new and useful form for the rigorous near-zone field of the linear dipole.

III. THE MUTUAL IMPEDANCE

For the coplanar-skew dipoles shown in Fig. 2, the mutual impedance is

$$(9) \qquad Z_{12} = - \frac{1}{I_1 I_2} \int_{r_1}^{r_3} \underline{I}_2(r) \cdot \underline{E}_1(r) dr$$

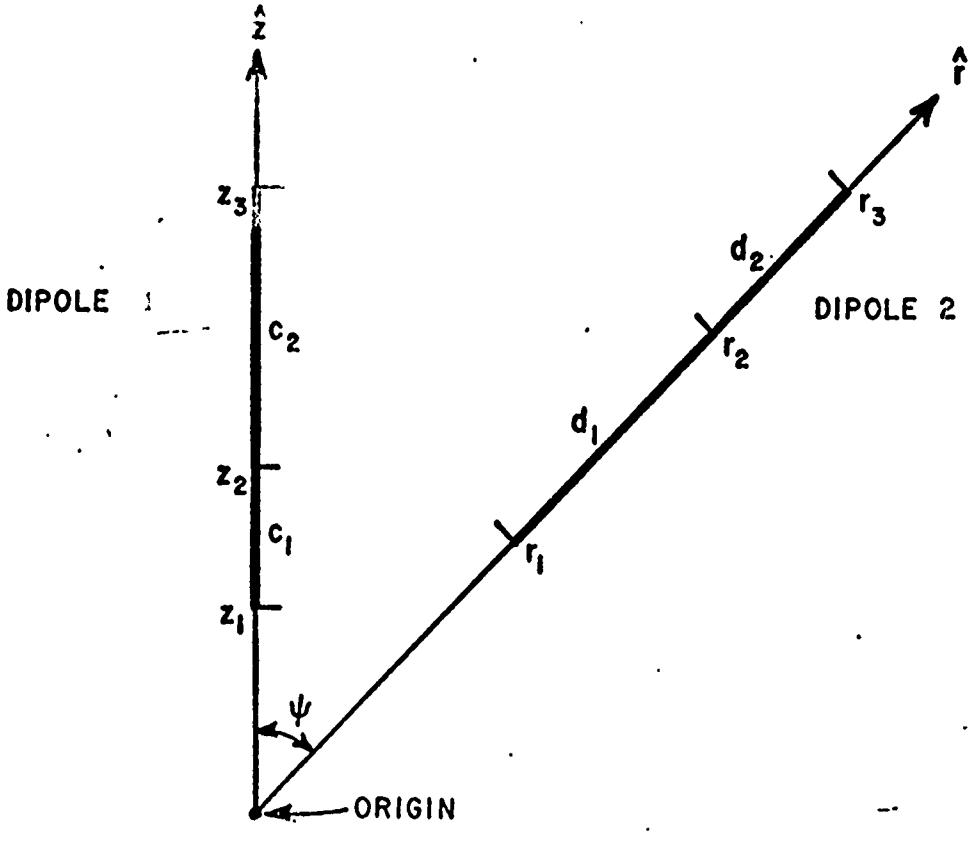

Fig. 2. Coplanar-skew dipoles.

The current on dipole 2 is

$$(10)\quad \underline{I}_2(r) = \hat{r}\,\frac{I_2 \sin k(r-r_1)}{\sin kd_1} \qquad \text{for } r_1 < r < r_2$$

$$(11)\quad \underline{I}_2(r) = \hat{r}\,\frac{I_2 \sin k(r_3-r)}{\sin kd_2} \qquad \text{for } r_2 < r < r_3$$

From Eqs. (5) and (9),

$$(12)\quad Z_{12} = \frac{j30}{I_2} \sum_{m=1}^{3} z_m C_m \int_{r_1}^{r_3} \frac{I_2(r) e^{-jkR_m}\, dr}{r\, R_m}$$

These integrals are given in terms of the sine- and cosine-integrals as follows

$$(13)\quad z_m \int_{r_1}^{r_2} \frac{e^{\pm jr}\, e^{-jR_m}\, dr}{r\, R_m} = \left[e^{-jz_m} E(R_m - z_m \mp r) - e^{jz_m} E(R_m + z_m \mp r)\right]_{r=r_1}^{r=r_2}$$

where

$$(14)\quad E(x) = Ci(|x|) - j\, Si(x).$$

From Eqs. (12) and (13), the mutual impedance is

$$(15)\quad Z_{12} = -15 \sum_{m=1}^{3} \sum_{n=1}^{3} C_m D_n \sum_{p=-1}^{1} \sum_{q=-1}^{1} pq e^{jk(pz_m + qr_n)} E(kR_{mn} + kpz_m + kqr_n)$$

where p and q assume only the values ±1 and R_{mn} is the distance from point z_m on dipole 1 to point r_n on dipole 2:

$$(16)\quad R_{mn} = \sqrt{z_m^2 + r_n^2 - 2z_m r_n \cos \psi}\ .$$

The coefficients D_n have the same form as the C_m:

$$(17)\quad D_1 = \frac{1}{\sin kd_1}$$

$$(18) \qquad D_2 = - \frac{\sin kd}{\sin kd_1 \sin kd_2}$$

$$(19) \qquad D_3 = \frac{1}{\sin kd_2}$$

The coordinates z_m and r_n are measured from the coordinate origin at the intersection of the axes of the coplanar skew dipoles. For center-fed half-wave dipoles, Eq. (15) reduces to Eq. (15) of Lewin's paper.[2]

For parallel dipoles, z_m and r_n go to infinity and it is not difficult to show that Eq. (15) reduces to the expression published by H.E. King.[1]

IV. NUMERICAL RESULTS

Figure 3 illustrates the mutual impedance between half-wave center-fed dipoles as a function of the angle ψ between their axes. Using Eq. (15), the calculations require 0.15 seconds on an IBM 7094 computer for each value of ψ.

Although the numerical approach of Baker and LaGrone[4] is efficient when the dipoles are adequately separated, Eq. (15) is preferable for closely spaced dipoles.

V. CONCLUSIONS

A convenient new form is presented for the rigorous near-zone field of the linear dipole with sinusoidal current distribution. This is employed to derive a closed-form expression for the mutual impedance between coplanar-skew dipoles. Future reports will use these results to develop a multi-segment reaction formulation for halo antennas and multi-turn loops.

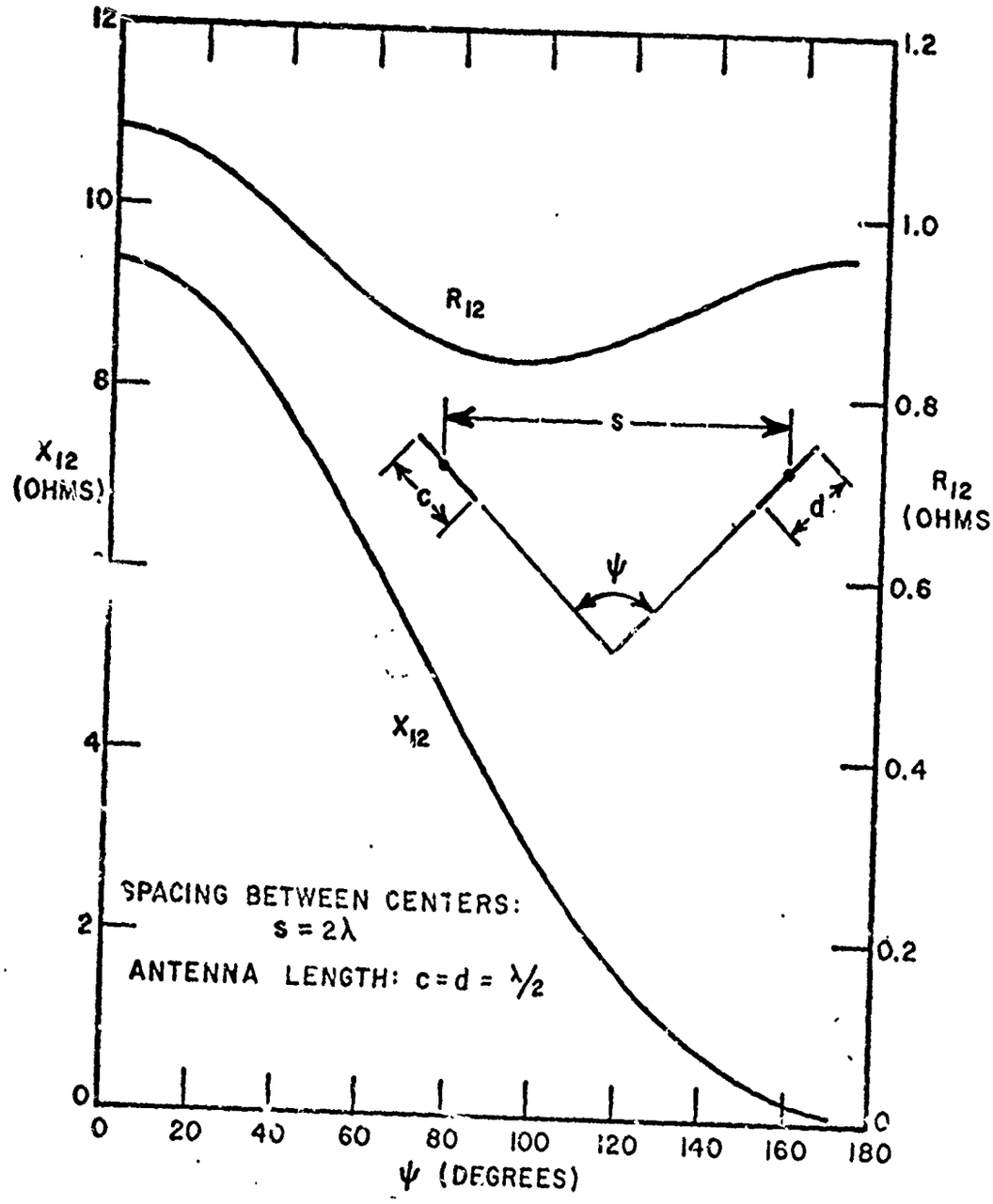

Fig. 3. Mut i impedance between coplanar-
sk dipoles.

REFERENCES

1. H.E. King, "Mutual Impedance of Unequal Length Antennas in Echelon," IRE Trans., vol. AP-5, pp. 306-313; July 1957.

2. L. Lewin, "Mutual Impedance of Wire Aerials," Wireless Engr., vol. 28, pp. 352-355; December 1951.

3. S.A. Schelkunoff and H.T. Friis, Antennas, Theory and Practice, New York: Wiley, 1952, pp. 370, 401.

4. H.C. Baker and A.H. LaGrone, "Digital Computation of the Mutual Impedance Between Thin Dipoles," IEEE Trans., vol. AP-10, pp. 172-178, March 1962.

APPENDIX E

COUPLED LINEAR ANTENNAS WITH SKEW ORIENTATION

J.H. Richmond

ElectroScience Laboratory
The Ohio State University
Columbus, Ohio 43212

TECHNICAL REPORT 2708-3
15 August 1969

Contract No. DAAD05-69-C-0031

Department of the Army
Ballistic Research Laboratory
Aberdeen Proving Ground Maryland 21005

ABSTRACT

The reaction concept is applied to determine the self- and mutual-admittances of coupled linear antennas with arbitrary positions and angular orientations. Numerical results are presented in graphical form for parallel, coplanar-skew, and nonplanar-skew cylindrical-wire antennas.

COUPLED LINEAR ANTENNAS WITH SKEW ORIENTATION

I. INTRODUCTION

Chang and King[1*] have solved the coupled-dipole problem for the special case where the antennas are parallel. In this report we consider the skew array of linear antennas. Future reports will extend the techniques to various three-dimensional antennas such as the multi-turn loop and the halo.

The theory is developed in the next section, followed by numerical results for some parallel and skew configurations.

II. THEORY

Consider the coupled linear antennas shown in Fig. 1. These antennas are assumed to be perfectly conducting, but they may be parallel, coplanar skew, or non-planar skew. The wire is divided into segments, and the complex constants I_1, I_2, . . I_N denote the current function sampled at the junctions of these segments. If the radius of these cylindrical-wire antennas is small, we assume the current vanishes at the ends. Furthermore, the current density is assumed uniform around the circumference of each wire; this is reasonable if the spacing between them is not too small.

If antenna 1 is divided into four equal segments as illustrated in Fig. 1, a convenient expansion for the current is

$$(1) \qquad \underline{I}(s) = \hat{s} \sum_{n=1}^{3} I_n P_n(s) \frac{\sin k(\ell - |s - s_n|)}{\sin k\ell}$$

where ℓ is the segment length, $k = 2\pi/\lambda$, and s is the coordinate distance measured along the axis of antenna 1. The pulse function $P_n(s)$ has unit value for $s_{n-1} < s < s_{n+1}$ and vanishes elsewhere. The unit vector $\hat{s}$ defines the reference direction for positive current flow. The time dependence $e^{j\omega t}$ is assumed and suppressed.

The current on antenna 2 is given in a similar manner by

$$(2) \qquad \underline{I}(t) = \hat{t} \sum_{n=4}^{N} I_n P_n(t) \frac{\sin k(\ell' - |t - t_n|)}{\sin k\ell'}$$

---

*References are listed on p. 106.

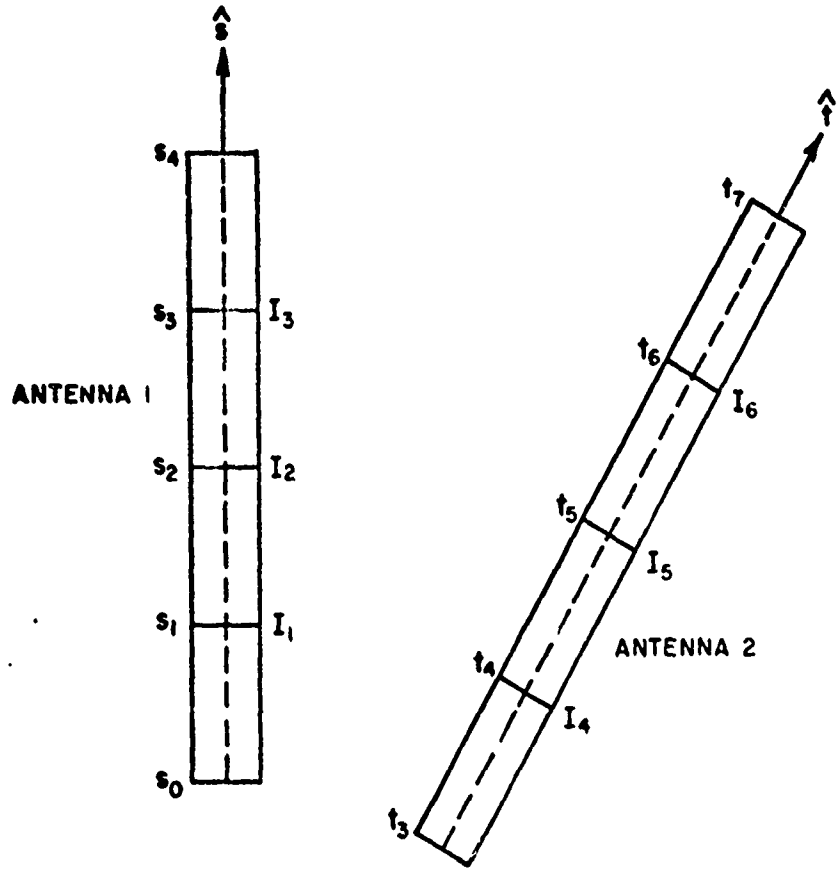

Fig. 1. The coupled antennas are divided into segments for the piecewise-sinusoidal current expansion.

The segment length ℓ' on antenna 2 may differ from that on antenna 1.

Of course, Eqs. (1) and (2) are not rigorous expressions for the current functions. However, they represent current distributions which are continuous and vanish at the ends of each antenna. Furthermore, they allow for slope discontinuities across any generators or lumped loads located at the current sampling points. A tradeoff between accuracy and computational expense can be achieved simply by dividing each wire into a suitable number of segments. Our objective is to determine the expansion coefficients or the current samples I_n and thereby the self- and mutual-admittances of the coupled antennas.

It is helpful to apply the surface-equivalence principle of Schelkunoff[2] to the coupled antenna problem. Let S denote the circular-cylindrical surfaces of the antennas. To make S a closed surface, we include the flat ends of each antenna. Let $\underline{E}$ and $\underline{H}$ represent the electric

and magnetic field intensities generated by the antenna array. Then the equivalent electric current density is $\underline{J} = \hat{n} \times \underline{H}$ and the equivalent magnetic current density is $\underline{M} = \underline{E} \times \hat{n}$. These currents, located on S and radiating in free space, generate the true field $(\underline{E}, \underline{H})$ in the exterior region and a null field in the interior. The outward unit normal vector on S is denoted by $\hat{n}$.

Since $\underline{J}$ and $\underline{M}$ generate a null field in the interior region of the antennas, they have no coupling or reaction with any source located in the interior. The reaction with an electric line source I'(s) or I'(t) on the axis of antenna 1 or antenna 2 is given by

$$(3) \qquad \oint\!\!\oint_S (\underline{J} \cdot \underline{E}' - \underline{M} \cdot \underline{H}')\, dS = 0$$

where $(\underline{E}', \underline{H}')$ denotes the free-space field generated by the interior line source. Equation (3) follows from the reciprocity theorem and the fact that $\underline{J}$ and $\underline{M}$ generate a null field in the interior. The current density $\underline{J}$ is related to the current I as follows

$$(4) \qquad \underline{J} = \frac{\underline{I}}{2\pi a}$$

where a denotes the wire radius.

Let us enforce Eq. (3) with a sinusoidal electric dipole located on the axis of antenna 1 or antenna 2. We assume there are no lumped loads and there is only one generator: a one-volt generator at the center of antenna 1. In the first reaction test, the electric dipole extends from s_0 to s_2 on the axis of antenna 1. In the second reaction test, the dipole extends from s_1 to s_3. In reaction tests 4, 5, and 6, the test dipole is located at various positions on the axis of antenna 2, and in reaction test m the field on the test dipole is denoted $(\underline{E}_m', \underline{H}_m')$. If the test dipole has unit terminal current, Eq. (3) reduces to

$$5. \qquad -\int_{s_0}^{s_4} \underline{I}(s) \cdot \underline{E}_m'\, ds - \int_{t_3}^{t_7} \underline{I}(t) \cdot \underline{E}_m'\, dt = V_m \quad .$$

In Eq. (5), the field $\underline{E}_m'$ is evaluated on the surface of antenna 1 or 2. V_m has unit value if $m = 2$ and is zero otherwise. As stated earlier, it is assumed that the wire radius "a" is small. Furthermore, we are using a "delta-gap" model for the voltage generator although it is

not difficult to develop the theory for a more realistic generator with finite extent.

From Eqs. (1), (2) and (5) we find that

$$(6) \qquad \sum_{n=1}^{N} I_n Z_{mn} = V_m$$

where Z_{mn} is the mutual impedance between the axial test dipole m and the surface dipole mode n. Specifically,

$$(7) \qquad Z_{mn} = -\int_{s_{n-1}}^{s_{n+1}} \hat{s} \cdot \underline{E}_m'(s) \frac{\sin k(\ell - |s - s_n|)}{\sin k\ell} \, ds \quad \text{if } 1 \le n \le 3$$

and

$$(8) \qquad Z_{mn} = -\int_{t_{n-1}}^{t_{n+1}} \hat{t} \cdot \underline{E}_m'(t) \frac{\sin k(\ell' - |t - t_n|)}{\sin k\ell'} \, dt \quad \text{if } 4 \le n \le N \ .$$

Dipoles m and n are filamentary dipoles with sinusoidal current distributions. Thus, the elements in our mutual-impedance matrix are given by classical induced emf theory. If dipoles m and n are located on the same antenna, they form essentially a collinear array, but with a slight displacement equal to the wire radius a. Then Z_{mn} can be expressed in terms of sine integrals and cosine integrals.[3] If dipoles m and n are located on opposite antennas, the numerical technique of Baker and LaGrone[4] is applicable. Alternatively, if antennas 1 and 2 are coplanar-skew, the closed-form expression of Richmond and Geary[5] may be employed.

Letting N represent the total number of unknown current samples on our two-antenna array, we enforce N reaction tests by letting m = 1, 2, .. N in Eq. (6). This yields a system of simultaneous linear equations. This system is solved numerically to determine the current samples I_n. The impedance matrix Z_{mn} is, of course, symmetric. The self admittance is $Y_{11} = I_2$ and the mutual admittance is $Y_{12} = I_5$.

If each antenna is divided into just two segments, our solution reduces to the classical induced emf theory and the accuracy is limited. As each antenna is subdivided into more segments, our solution converges rapidly and shows excellent agreement with experimental measurements. (An exception is the self-susceptance B_{11} which has

poor convergence with the delta-gap model. This problem disappears, however, when the finite extent of the generator gap is taken into account.)

III. NUMERICAL RESULTS

Figures 2, 3 and 4 illustrate our numerical results for the self- and mutual-admittance versus the displacement d for an array of parallel nonstaggered antennas. Each antenna is divided into ten segments for the reaction solution. It may be noted that the results show excellent agreement with the data published by Chang and King.[1]

Figures 5 and 6 show numerical results for the mutual admittance between coplanar-skew antennas versus the angle ψ between their axes. When $\psi = 0$ the antennas are parallel and nonstaggered, and when $\psi = 180°$ they are collinear. In these limiting cases our results agree closely with those of Chang and King.[1]

Figure 7 shows the mutual admittance between nonplanar-skew antennas versus the angle ϕ. When $\phi = 0$ the antennas are parallel and nonstaggered. When $\phi = 90°$ they are orthogonal and the mutual admittance vanishes.

The computer program developed for this study handles linear antennas with arbitrary lengths L_1 and L_2, displacement d, stagger s and angles ψ and ϕ. The output data include the current distributions, radiation patterns and radiation efficiency. Using an IBM 7094 computer, the computation time is four seconds for each coupled antenna problem.

IV. CONCLUSIONS

A multi-segment reaction technique is developed and applied to coupled linear antennas. Numerical results are presented in graphical form for parallel, coplanar-skew and nonplanar-skew cylindrical-wire antennas. When the antennas are parallel or collinear, the calculated results show excellent agreement with previously published data.

Future reports will extend these techniques to various three-dimensional antennas such as the multi-turn loop and the halo.

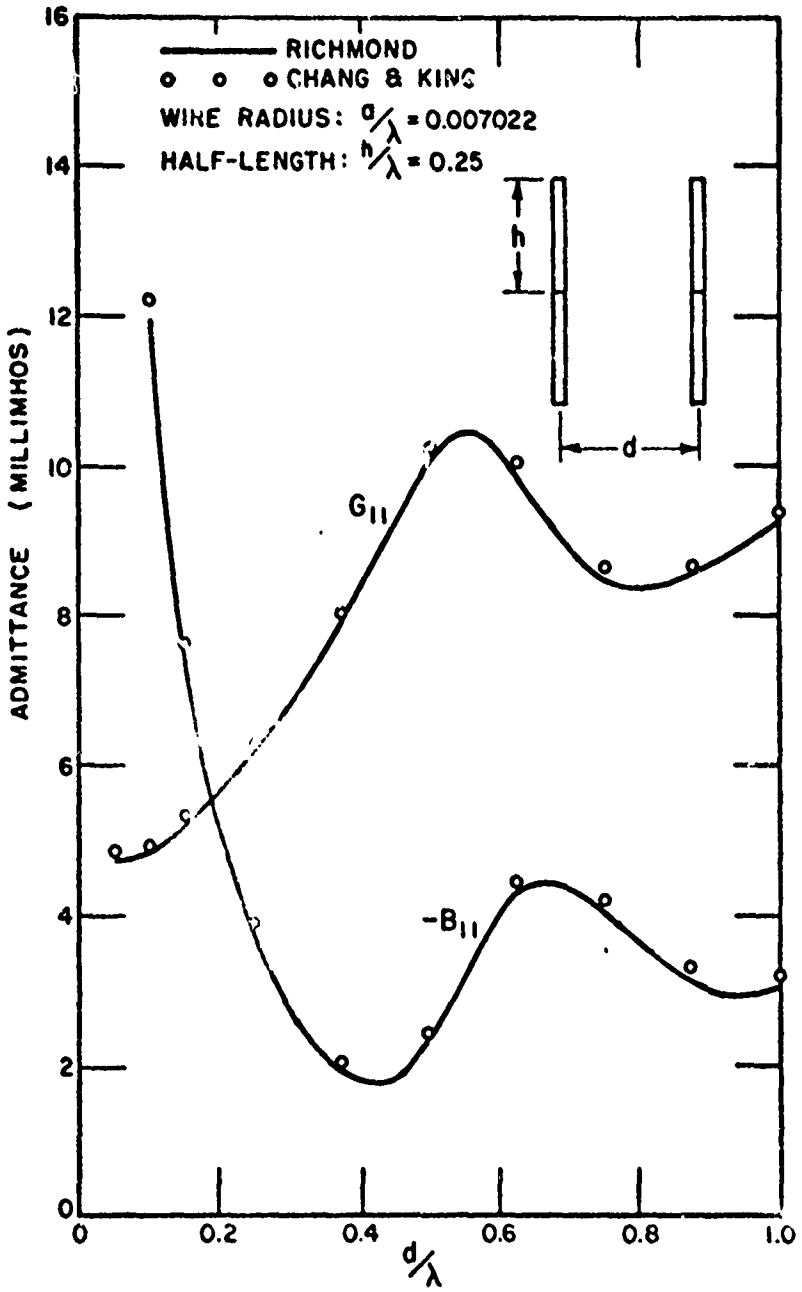

Fig. 2. Self admittance vs. spacing for parallel half-wave antennas.

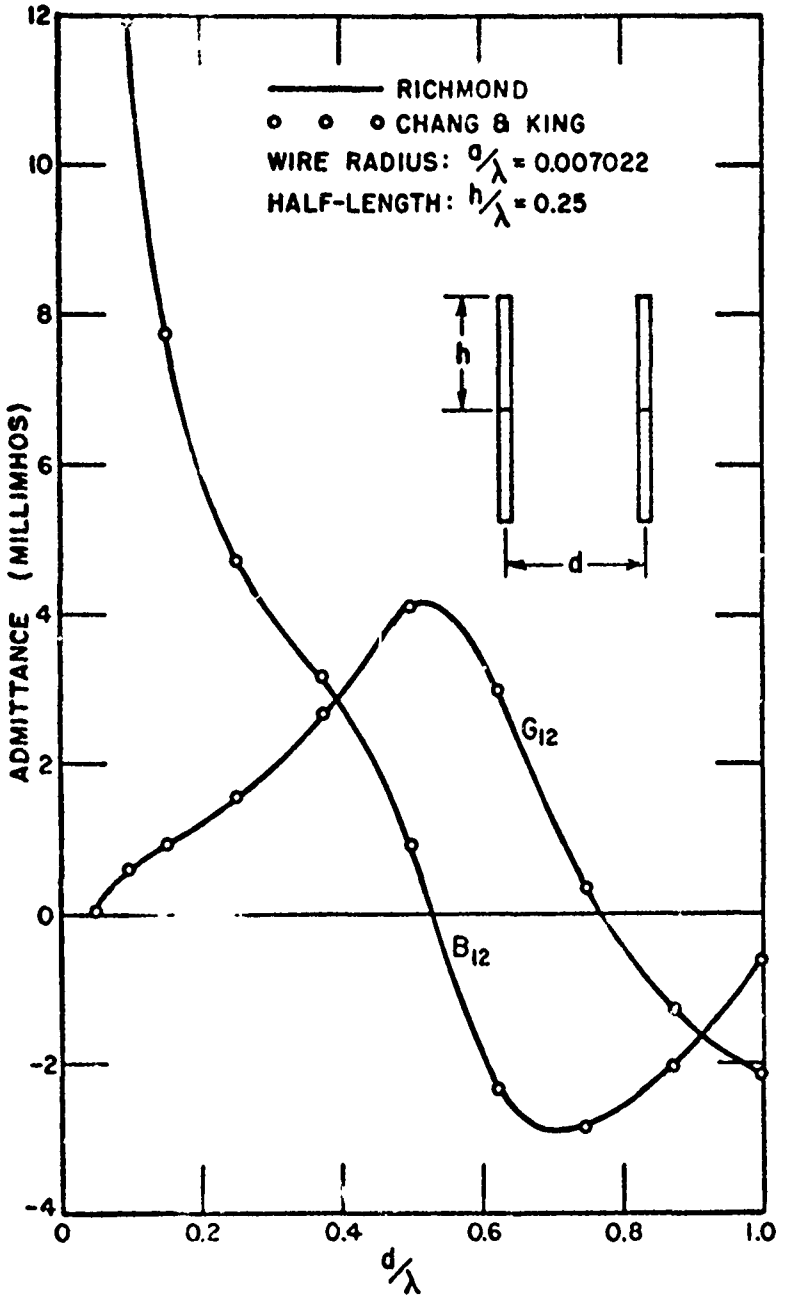

Fig. 3. Mutual admittance vs. spacing for parallel half-wave antennas.

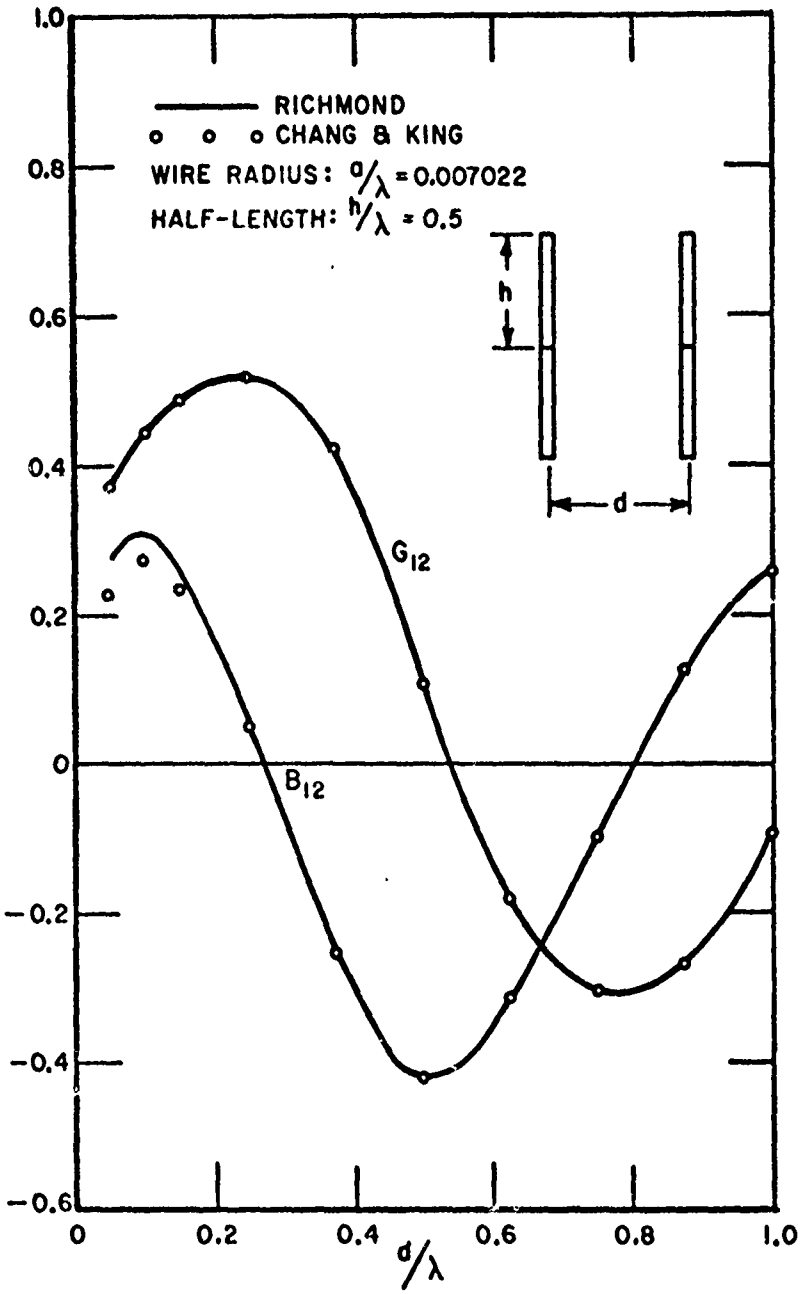

Fig. 4. Mutual admittance vs. spacing for parallel one-wave antennas.

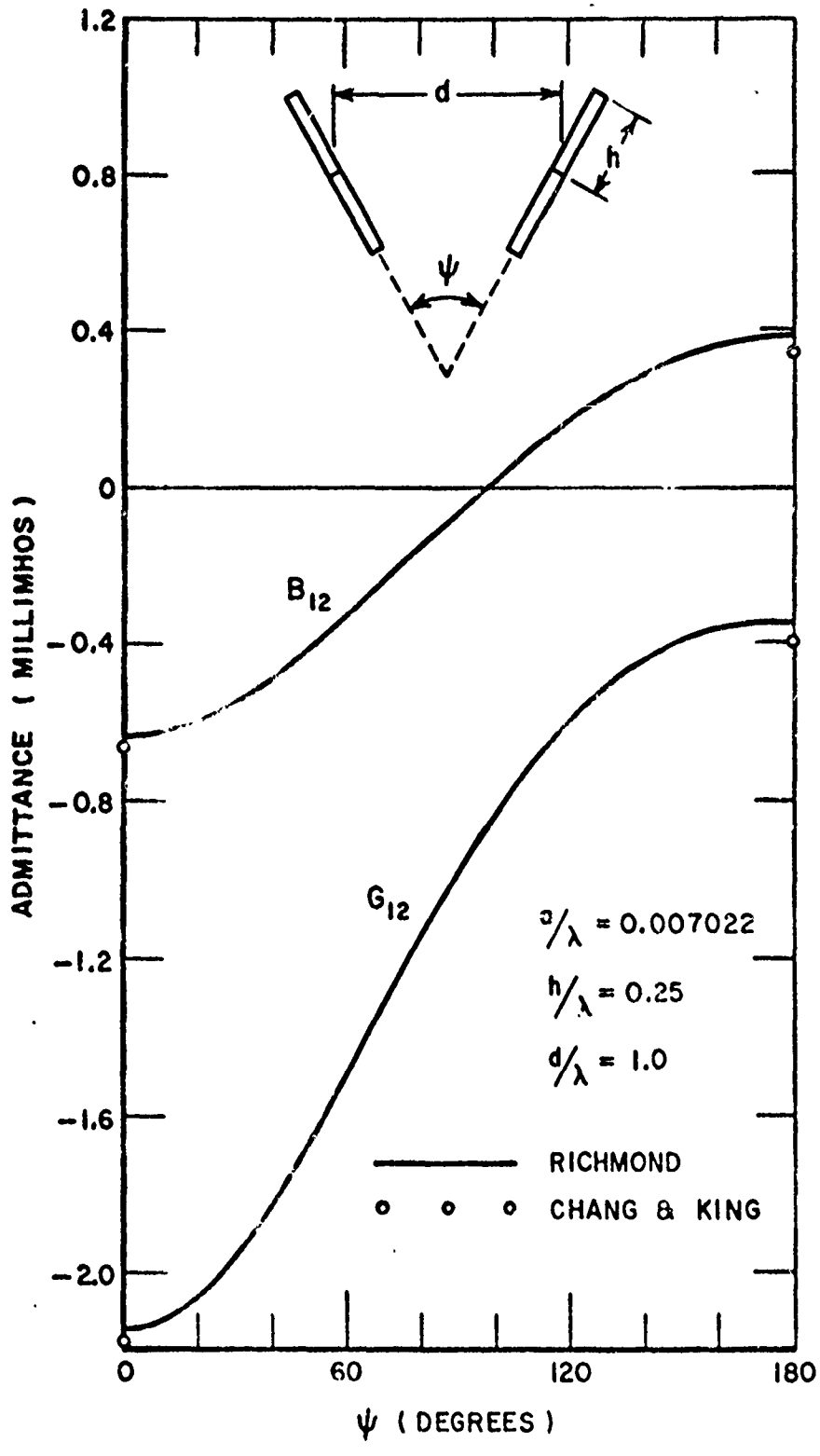

Fig. 5. Mutual admittance vs. rotation angle for half-wave coplanar-skew antennas.

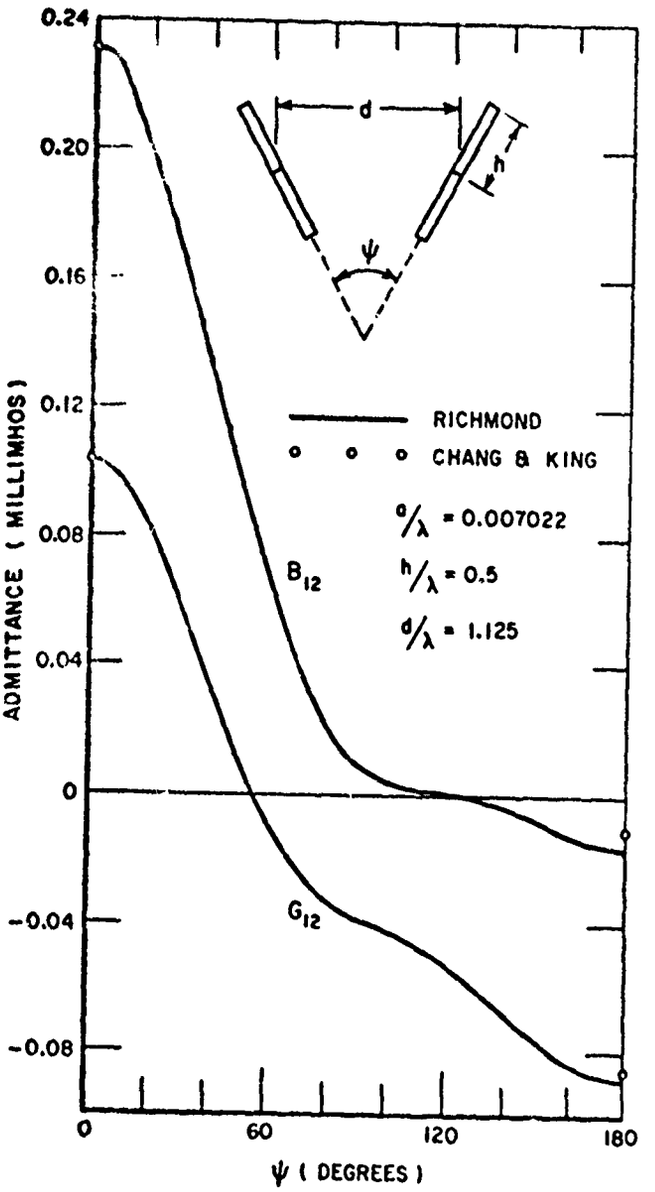

Fig. 6. Mutual admittance vs. rotation angle for one-wave coplanar-skew antennas.

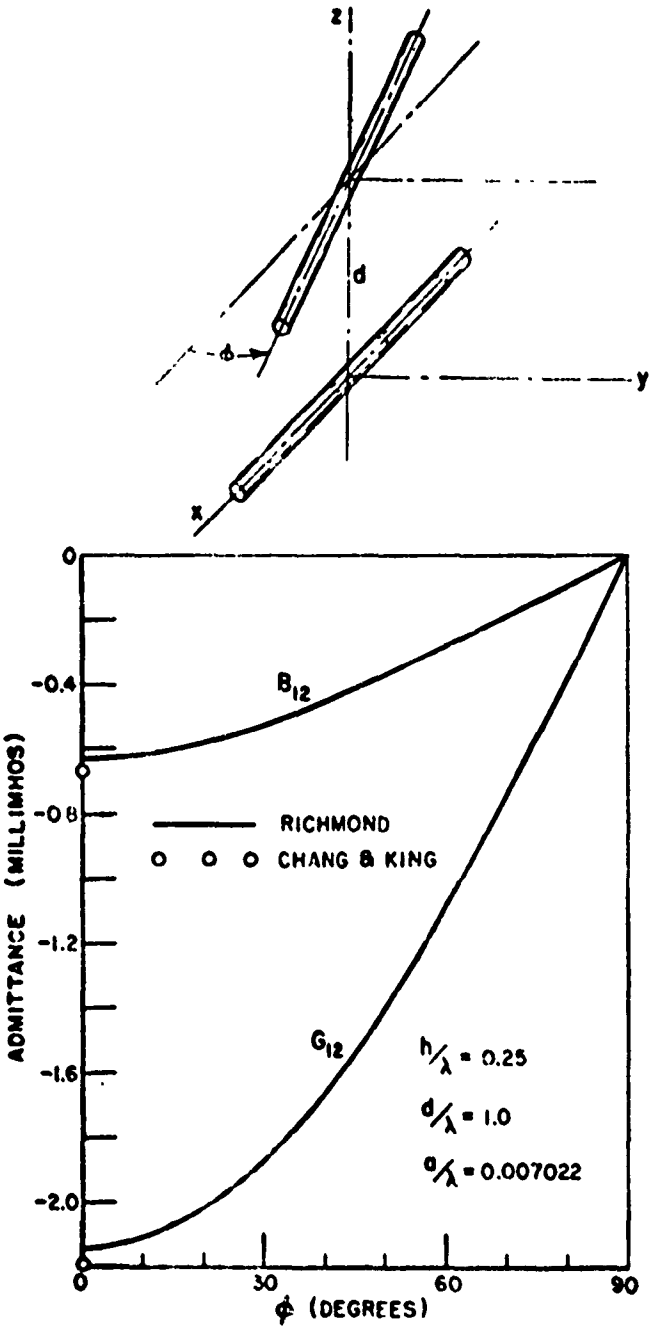

Fig. 7. Mutual admittance vs. rotation angle for half-wave nonplanar-skew antennas.

REFERENCES

1. Chang, V.W. H. and R.W.P, King, "On Two Arbitrarily Located Identical Parallel Antennas," IEEE Trans. Vol. AP-16, (May 1968), pp. 309-317.

2. Schelkunoff, S.A., "On Diffraction and Radiation of Electromagnetic Waves," Physical Review, Vol. 56, (August 15, 1939).

3. King, H.E., "Mutual Impedance of Unequal Length Antennas in Echelon," IRE Trans., Vol. AP-5, (July 1957), pp. 306-313.

4. Baker, H.C. and A.H. LaGrone, "Digital Computation of the Mutual Impedance Between Thin Dipoles," IRE Trans., Vol. AP-10, (March 1962), pp. 172-178.

5. Richmond, J.H. and N.H. Geary, "Mutual Impedance Between Coplanar-skew Dipoles," Report 2708-2. (Report in preparation).

APPENDIX F

COMPUTER ANALYSIS OF THREE-DIMENSIONAL WIRE ANTENNAS

J. H. Richmond

ElectroScience Laboratory
The Ohio State University
Columbus, Ohio 43212

TECHNICAL REPORT 2708-4

Contract No. DAAD 05-69-C-0031

22 December 1969

Department of the Army
Ballistic Research Laboratory
Aberdeen Proving Ground Maryland 21005

ABSTRACT

The reaction concept is employed to formulate a solution for thin-wire antennas with arbitrary shape. Based on this theory, a digital computer program has been developed to provide a complete analysis of such antennas. Calculated and measured impedances are included for several antennas to demonstrate the accuracy and versatility of the formulation and the program.

This report presents the computer program and the details of the solution for the current distribution, impedance, far-zone patterns, radiation efficiency and scattering. The analysis of wires with multiple excitation and lumped loads is considered.

The techniques can be extended to a more advanced problem of considerable current interest: A wire antenna exciting a circumferential slot on a rocket or projectile.

I. INTRODUCTION

The upper atmosphere research program of the Signature and Propagation Division of the Ballistic Research Laboratory presents severe design problems in the field of rocket mounted antennas. Space, weight, and configuration limitations impose severe restrictions on design. High radiating efficiencies and uniform field strength patterns are required to make accurate measurements of the parameters under investigation as they are affected by both natural and artificial disturbances. Because of the small physical size of the rocket vehicle the antennas are necessarily short compared to those normally used for the frequencies when space is not a problem. To prevent high voltages across the antennas and the resultant voltage breakdown and low efficiency the standing wave ratio at the antenna feed point must be kept low. The Polar Cap Absorption experiment presents a typical problem. Six antennas operating at frequencies of 9, 18, 36, 72, 144 and 576 MHz must, in effect, occupy the same limited space on a nine inch diameter rocket. At the 9 MHz frequency, for example, the maximum dimension of the effective radiating element can be only 0.068 wavelengths. This imposes very severe design and operational problems.

Novel antenna configurations which seem to provide greatly improved operational characteristics have recently been devised. However, the progress to date has been primarily by the application of intuitive "cut and try" techniques rather than the more reliable methods of analysis based on an understanding of the radiating mechanism and the relations between radiation pattern, polarization, impedance, bandwidth, and other parameters which can be derived from a study of computerized mathematical models of these novel antennas.

To analyze and optimize various antennas, The ElectroScience Laboratory has developed a computer program for thin-wire antennas mounted on a ground plane or in free space. This program will handle a wide variety of antenna configurations including the linear dipole, V-dipole, zig-zag and three-dimensional antennas such as the halo and multiturn loop. The output data include the current distribution, impedance, radiation efficiency, directivity and far-zone field patterns.

The theory is developed in the following sections, followed by a comparison of calculated and measured results for several antenna configurations. Appendices present the computer program and an analysis of the scattering problem.

II. NEAR-ZONE FIELD OF SINUSOIDAL LINE SOURCE

Our formulation for three-dimensional wire antennas uses a

piecewise-sinusoidal expansion for the current distribution. Consider a typical straight segment of the antenna to be located on the z axis with endpoints at z_1 and z_2 as shown in Fig. 1. The assumed current distribution on this segment is

$$(1) \quad I(z) = Ae^{jkz} + Be^{-jkz}$$

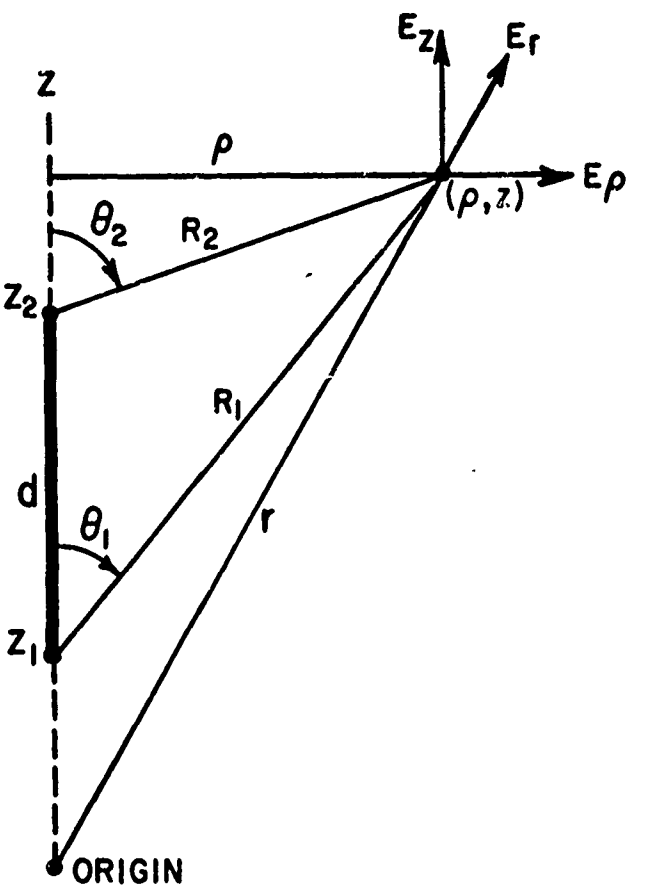

Fig. 1. An electric line source on the z axis and the observation point at (ρ,z).

where A and B are complex constants, $k = 2\pi/\lambda$ and the time dependence $e^{j\omega t}$ is understood. The field of this sinusoidal line source is given by Schelkunoff[1] as follows

$$(2) \quad 4\pi j\omega\varepsilon E_z = \frac{I_1' e^{-jkR_1}}{R_1} - \frac{I_2' e^{-jkR_2}}{R_2}$$

(3) $4\pi j\omega\varepsilon\rho \quad E_\rho = [I_2' \cos\theta_2 - jkI_2]\, e^{-jkR_2} - [I_1' \cos\theta_1 - jkI_1]\, e^{-jkR_1}$

where I_1 and I_2 denote $I(z_1)$ and $I(z_2)$, and I_1' and I_2' denote the derivative of $I(z)$ at z_1 and z_2. The remaining quantities are defined in Fig. 1.

The constants A and B in Eq. 1 can be eliminated to express the current distribution in terms of the endpoint currents I_1 and I_2 as follows:

(4) $I(z) = [I_1 \sin k(z_2-z) + I_2 \sin k(z-z_1)\,] / \sin kd$

where d is the length of the segment. From Eq. 4,

(5) $I_1' = k(I_2 - I_1 \cos kd)/\sin kd$

(6) $I_2' = k(I_2 \cos kd - I_1)/\sin kd$

from Eqs. 2-6, the electric field intensity is

(7) $$E_z = \frac{j30}{\sin kd}\left[(I_1 \cos kd - I_2)\,\frac{e^{-jkR_1}}{R_1} + (I_2 \cos kd - I_1)\,\frac{e^{-jkR_2}}{R_2}\right]$$

(8) $$E_\rho = \frac{j30}{\rho \sin kd}\left[(I_2 - I_1 \cos kd)(z-z_1)\frac{e^{-jkR_1}}{R_1} - j\, I_1 \sin kd\, e^{-jkR_1}\right.$$

$$\left. + (I_1 - I_2 \cos kd)(z-z_2)\,\frac{e^{-jkR_2}}{R_2} + j\, I_2 \sin kd\, e^{-jkR_2}\,\right]$$

Now consider the radial field E_r as shown in Fig. 1. From Eqs. 7 and 8

(9) $$E_r = \frac{j30}{r \sin kd}\left[(I_1 \cos kd - I_2)\, z_1\,\frac{e^{-jkR_1}}{R_1} - j\, I_1 \sin kd\, e^{-jkR_1}\right.$$

$$\left. + (I_2 \cos kd - I_1)\, z_2\,\frac{e^{-jkR_2}}{R_2} + j\, I_2 \sin kd\, e^{-jkR_2}\right]$$

Eqs. 7-9 are useful in calculating the mutual impedances among the various portions of a wire antenna.

The next section shows how the three-dimensional wire antenna problem is reduced to a simpler one: the mutual impedance between elementary (two-segment) V-dipoles.

III. THEORY OF THE THREE-DIMENSIONAL WIRE ANTENNA

As indicated in Fig. 2, the wire antenna is assumed to have straight segments with lengths d_1, d_2, $\cdots d_{N+1}$. Starting from one end, the distance along the antenna is measured by the coordinate ℓ. The current distribution $I(\ell)$ is unknown. However, a series of

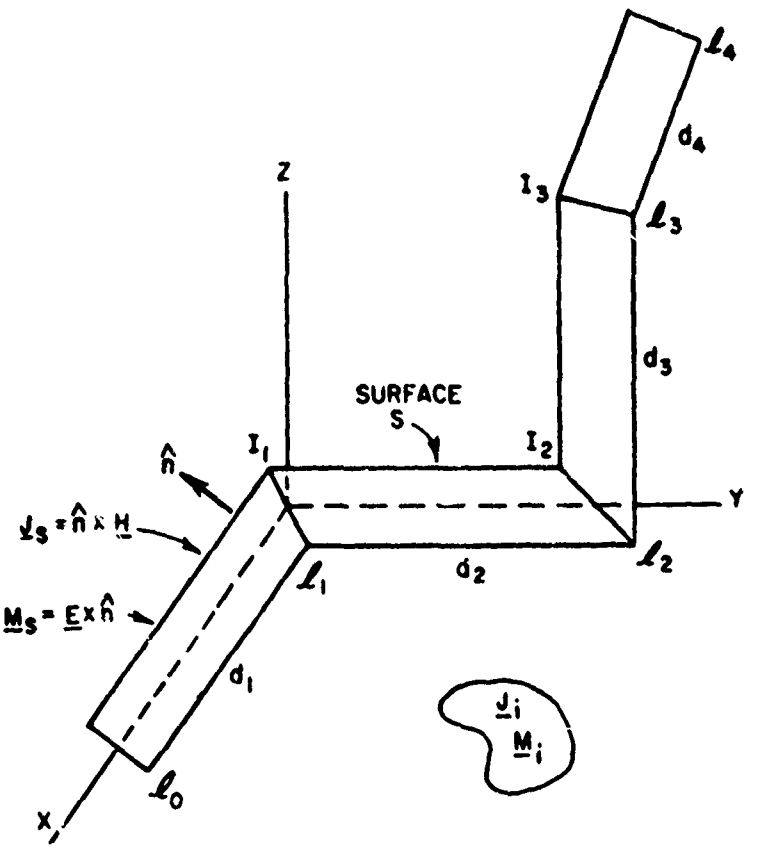

Fig. 2. A three-dimensional thin-wire antenna with straight segments.

complex constants I_1, I_2, $\cdots I_N$ are defined to denote consecutive samples of the current at the points ℓ_1, ℓ_2, $\cdots \ell_N$. For example, $I_1 = I(\ell_1)$ and $I_2 = I(\ell_2)$ as shown in Fig. 2. The current is assumed to vanish at both ends of the antenna.

For accurate results, the segment length should be about $\lambda/4$ or smaller. If any straight segment of the antenna has a length greater than this, it is subdivided.

Using the piecewise-sinusoidal approximation, the current distribution on the antenna is given by

$$(10) \quad \underline{I}(\ell) = \sum_{n=1}^{N} I_n \left[\hat{s}_n P_n(\ell) \frac{\sin k(\ell - \ell_{n-1})}{\sin k d_n} + \hat{s}_{n+1} P_{n+1}(\ell) \frac{\sin k(\ell_{n+1} - \ell)}{\sin k d_{n+1}} \right]$$

where $I_n = I(\ell_n)$ and d_n is the length of segment n. The unit vector $\hat{s}_n$ is parallel with segment n and is directed from the point ℓ_{n-1} toward the point ℓ_n. $P_n(\ell)$ is a pulse function which has unit value on segment n and vanishes elsewhere. Eqs. 10 represents a current distribution which is continuous and vanishes at the ends of the antenna. Furthermore, this expression allows for a slope discontinuity in the current function at each generator. Our objective is to determine the complex constants I_n.

Let S denote the composite circular-cylindrical surface of the antenna. To make S a closed surface, we include the flat ends. As indicated in Fig. 2, consider the antenna to be excited by a source with electric and magnetic current densities $\underline{J}_i$ and $\underline{M}_i$ located in an exterior region V. The incident field $(\underline{E}_i, \underline{H}_i)$ is generated by $(\underline{J}_i, \underline{M}_i)$ when radiating in free space. The total field $(\underline{E}, \underline{H})$ is generated by $(\underline{J}_i, \underline{M}_i)$ when radiating in the presence of the wire. The equivalent surface-current densities on S are $\underline{J}_s = \hat{n} \times \underline{H}$ and $\underline{M}_s = \underline{E} \times \hat{n}$, where $\hat{n}$ is the outward unit normal vector on S. Consider the field generated in free space when the primary source $(\underline{J}_i, \underline{M}_i)$ and the surface currents $(\underline{J}_s, \underline{M}_s)$ are both turned on. According to the surface equivalence principle of Schelkunoff,[2] the total field $(\underline{E}, \underline{H})$ will exist in the exterior region and a null field in the interior region of S.

Since these sources generated a null field in the interior region, they have no coupling or reaction with any source located in the interior. The reaction with an interior source is given by

$$(11)\quad \oint\!\!\!\!\!\!\diagup_S (\underline{J}_s\cdot\underline{E}'-\underline{M}_s\cdot\underline{H}')ds + \iiint_V (\underline{J}_i\cdot\underline{E}'-\underline{M}_i\cdot\underline{H}')\,dv = 0$$

where $(\underline{E}',\underline{H}')$ denotes the free-space field of the interior test source. Eq. 11 follows from the reciprocity theorem of Carson.[3] The volume integral in Eq. 11 may reduce to a surface or line integral depending on the nature of the source $(\underline{J}_i,M_i)$.

To simplify the first integral in Eq. 11, we assume the wire antenna has perfect conductivity so that $\underline{M}_s$ vanishes. Furthermore, we neglect the integration over the flat ends of the antenna. To simplify the last integral, let $\underline{J}_i = 0$ and assume the antenna is driven by a series of voltage generators $V_1,V_2,\cdots V_N$ located at $\ell_1, \ell_2, \cdots \ell_N$. (A generator voltage is considered positive if it tends to force a current flow in the direction of increasing ℓ.) For an interior test source we choose an electric line source $I'(\ell)$ located on the antenna axis and radiating in free space. Now Eq. 11 reduces to

$$(12)\quad -\iint_S \underline{J}_s\cdot\underline{E}'ds = \sum_{n=1}^{N} V_n\, I'(\ell_n)$$

In deriving Eq. 12, the wire radius "a" is assumed to be small and a "delta-gap" model is employed for the voltage generators. Thus, each generator is represented by a magnetic current loop encircling the wire. Furthermore, we may use Ampere's law:

$$(13)\quad a\int_0^{2\pi} H_\phi'(a,\ell)\,d\phi = I'(\ell)$$

Eq. 13 neglects the displacement current. (Although it is easy to treat the gap problem in a more satisfactory manner, this subject is reserved for a future report.)

The current density $\underline{J}_s$ is related to the current $\underline{I}$ as follows

$$(14)\quad \underline{J}_s = \frac{\underline{I}(\ell)}{2\pi a}$$

From Eqs. 12 and 14,

$$(15)\quad -\int_0^L \underline{I}(\ell)\cdot\underline{E}'d\ell = \sum_{n=1}^{N} V_n\, I'(\ell_n)$$

where L is the overall length of the antenna.

We shall enforce the reaction test (Eq. 15) with several different test sources. In test m, the interior test source is an electric dipole with a sinusoidal current distribution given by

$$(16)\quad \underline{I}'_m(\ell) = \hat{s}_m P_m(\ell)\,\frac{\sin k(\ell-\ell_{m-1})}{\sin kd_m} + \hat{s}_{m+1}\,P_{m+1}(\ell)\,\frac{\sin k(\ell_{m+1}-\ell)}{\sin kd_{m+1}}$$

This test source is generally a V dipole (rather than a linear dipole), and it may be noted in Eq. 16 that it has unit terminal current. The test dipole is located on the antenna axis and extends from ℓ_{m-1} to ℓ_{m+1}. When radiating in free space, it generates the field $\underline{E}'_m$. From Eqs. 15 and 16,

$$(17)\quad -\int_0^L \underline{I}(\ell)\cdot\underline{E}'_m\,d\ell = V_m$$

since $I'(\ell_n) = 0$ and $I'(\ell_m) = 1$. From Eqs. 10 and 17,

$$(18)\quad \sum_{n=1}^{N} I_n Z_{mn} = V_m$$

where Z_{mn} is the mutual impedance between the axial test dipole m and the surface dipole mode n. Specifically,

$$(19)\quad Z_{mn} = -\int_{\ell_{n-1}}^{\ell_n} \frac{\hat{s}_n\cdot\underline{E}'_m \sin k(\ell-\ell_{n-1})\,d\ell}{\sin kd_n} - \int_{\ell_n}^{\ell_{n+1}} \frac{\hat{s}_{n+1}\cdot\underline{E}_m \sin k(\ell_{n+1}-\ell)\,d\ell}{\sin kd_{n+1}}$$

The axial test dipole m is a filamentary electric line source. In many cases the surface dipole n can also be regarded as a filamentary V dipole located on the composite cylindrical surface S. In this event Eq. 19 applies, and the elements in our mutual-impedance matrix are given by classical induced emf theory. The field $\underline{E}'_m$ is obtained from Eqs. 7-9, and the integrations in Eq. 19 are usually performed by Gaussian quadrature on a digital computer. When dipoles m and n are close together, however, a closed-form integration (in terms of exponential integrals) is employed for Z_{mn}.

In using Eq. 19 it is noted that the numerical results depend

to some extent on the circumferential position of dipole n on surface S. This dependence is greatest when the angle of intersection of segments n and n+1 is acute. When the intersection angle is small it may be necessary to average the values obtained for Z_{mn} for several circumferential positions of the surface dipole n. Strictly speaking, Z_{mn} should be regarded as the mutual impedance between a filamentary axial dipole m and a tubular surface-current dipole n.

Letting N represent the number of unknown current samples, we enforce N reaction tests by letting m = 1,2,···N in Eq. 18. This yields a system of simultaneous linear equations. This system is solved numerically to determine the current samples I_n. The impedance matrix Z_{mn} is, of course, symmetric. In most problems the antenna is driven by a single one-volt generator (V_g=1) located at ℓ_g, and the antenna impedance is $Z = 1/I_g$.

After the current samples I_n have been calculated, the far-zone antenna field patterns can be obtained in a straightforward manner as shown in the next section.

IV. THE FAR-ZONE FIELD ANALYSIS

We shall develop expressions for the far-zone field of one straight segment of the antenna. By superposition, the antenna field can then be obtained by summing the contributions from all the segments.

Let (x_1,y_1,z_1) and (x_2,y_2,z_2) denote the coordinates of the endpoints of the segment. The current distribution on the segment is represented by $\underline{I}(\ell) = \hat{\ell} I(\ell)$ where $\hat{\ell}$ is a unit vector from (x_1,y_1,z_1) toward (x_2,y_2,z_2) and ℓ is the distance along the segment measured from the point (x_1,y_1,z_1). In the far zone, the vector potential is

$$(20) \quad \underline{A}\,(r,\theta,\phi) = \frac{\mu e^{-jkr}}{4\pi r} \int_0^d \underline{I}(\ell)\, e^{jkf}\, d\ell$$

where

$$(21) \quad f = x \sin\theta \cos\phi + y \sin\theta \sin\phi + z \cos\theta$$

and d is the length of the segment. The source coordinates are (x,y,z). The spherical coordinates (r,θ,ϕ) for the observation point are defined by the following transformation:

(22) $x = r \sin\theta \cos\phi$

(23) $y = r \sin\theta \sin\phi$

(24) $z = r \cos\theta$

The electric field intensity is $\underline{E} = -j\omega\underline{A}$, where the radial component E_r is to be suppressed. The rectangular coordinates of any point on the source are

(25) $x = x_1 + \ell \cos\alpha$

(26) $y = y_1 + \ell \cos\beta$

(27) $z = z_1 + \ell \cos\gamma$

where $(\cos\alpha, \cos\beta, \cos\gamma)$ are the direction cosines of the ℓ axis. From Eqs. 20 and 25-27,

(28) $$E_\ell(r,\theta,\phi) = -\frac{j\omega\mu}{4\pi r} e^{-jkr} e^{jkf_1} \int_0^d I(\ell)\, e^{jg\ell} d\ell$$

where

(29) $f_1 = x_1 \sin\theta \cos\phi + y_1 \sin\theta \sin\phi + z_1 \cos\theta$

(30) $g = k(\cos\alpha \sin\theta \cos\phi + \cos\beta \sin\theta \sin\phi + \cos\gamma \cos\theta)$.

Noting that

(31) $\hat{\ell} = \hat{x} \cos\alpha + \hat{y} \cos\beta + \hat{z} \cos\gamma$

(32) $\hat{\theta} = \hat{x} \cos\theta \cos\phi + \hat{y} \cos\theta \sin\phi - \hat{z} \sin\theta$

and

(33) $\hat{\phi} = -\hat{x} \sin\phi + \hat{y} \cos\phi$,

we find that

(34) $E_\theta = (\cos\alpha \cos\theta \cos\phi + \cos\beta \cos\theta \sin\phi - \cos\gamma \sin\theta)E_\ell$

and

(35) $E_\phi = (-\cos\alpha \sin\phi + \cos\beta \cos\phi)E_\ell$

Using the piecewise-sinusoidal expansion, the current distri-

bution on the segment is given by

$$(36) \quad \underline{I}(\ell) = \frac{\hat{\ell}}{\sin kd} \left[I_1 \sin k(d-\ell) + I_2 \sin k\ell \right]$$

where $I_1 = I(0)$ and $I_2 = I(d)$. From Eqs. 28 and 36,

$$(37) \quad E_\ell(r,\theta,\phi) = \frac{30 \; e^{-jkr}}{(1 - g^2/k^2) \; r \sin kd} \left(C \; I_1 \; e^{jkf_1} - C^* \; I_2 \; e^{jkf_2} \right)$$

where

$$(38) \quad C = \sin gd - g \sin kd + j(\cos kd - \cos gd)$$

$$(39) \quad f_2 = x_2 \sin\theta \cos\phi + y_2 \sin\theta \sin\phi + z_2 \cos\theta$$

After calculating E_ℓ from Eq. 37, the theta- and phi-polarized components of the far-zone field are obtained from Eqs. 34 and 35.

After summing the field contributions from all the segments of the antenna, one has the far-zone fields $E_\theta(r,\theta,\phi)$ and $E_\phi(r,\theta,\phi)$. Finally, the power gain is determined as follows

$$(40) \quad G_p(\theta,\phi) = \frac{\left(|E_\theta|^2 + |E_\phi|^2 \right) r^2}{30 \; |I_g|^2 \; R}$$

where I_g is the terminal current and R is the real part of the antenna impedance Z. The directive gain G_d is obtained from Eq. 40 by replacing R with R_r. The radiation resistance R_r is discussed in section VII. As shown in the next section, the effects of lumped impedance loading are readily analyzed with the reaction formulation.

V. LUMPED LOADS

Suppose a lumped load impedance Z_m is inserted in the wire antenna at each of the current sampling points ℓ_m. These impedances may be active or passive, identical or assorted. The current through the load Z_m is denoted by I_m, and the total voltage acting at the point ℓ_m is

(41) $V_m = V_m^g - I_m Z_m$

where V_m^g represents a voltage generator that may be located at ℓ_m in series with the load Z_m. From Eqs. 18 and 41, the system of linear equations is

42) $$\sum_{n=1}^{N} I_n Z_{mn} = V_m^g - I_m Z_m$$

Transposing the last term, we find

(43) $$\sum_{n=1}^{N} I_n Z'_{mn} = V_m^g$$

Except for the diagonal elements, the new impedance matrix is the same as the original: $Z'_{mn} = Z_{mn}$. The diagonal elements are given by

(44) $Z'_{mm} = Z_{mm} + Z_m$.

Thus, the effect of lumped loading is accounted for simply by adding the load impedances Z_m to the corresponding diagonal elements in the impedance matrix.

The effects of the finite conductivity of the antenna wire are considered in the next section.

VI. FINITE CONDUCTIVITY

After Eq. 11, we assumed for simplicity that the wire antenna has perfect or infinite conductivity. However, it is not difficult to account for the finite conductivity σ of the metal actually used in constructing a practical antenna. Although the tangential component of $\underline{E}$ vanishes at the surface of a perfectly conducting wire, it does not vanish with finite conductivity. Instead,

(45) $E_\ell = Z_s H_\phi$

where the electric and magnetic field intensities E_ℓ and H_ϕ are evaluated at the surface of the wire and Z_s denotes the surface impedance of the wire. E_ℓ represents the longitudinal electric field component (parallel with the axis of the wire), and H_ϕ is the circumferential magnetic field component (encircling the wire).

If each segment of the antenna has the same radius and conductivity, we may consider the surface impedance to be a constant.

From Eq. 14 and $\underline{J}_s = \hat{n} \times \underline{H}$,

$$(46) \quad H_\phi = J_s = \frac{I(\ell)}{2\pi a}$$

where $I(\ell)$ is the total (conduction and displacement) current. From Eq. 45 and $\underline{M}_s = \underline{E} \times \hat{n}$,

$$(47) \quad \underline{M}_s = \hat{\phi} E_\ell = \frac{\hat{\phi} Z_s I(\ell)}{2\pi a} .$$

From Eq. 11,

$$(48) \quad -\iint_s \underline{J}_s \cdot \underline{E}' ds + \iint_s \underline{M}_s \cdot \underline{H}' \, ds = \sum_{n=1}^{N} V_n \, I'(\ell_n)$$

From Eqs. 14, 47 and 48,

$$(49) \quad -\int_0^L \underline{I}(\ell) \cdot \underline{E}' \, d\ell + Z_s \int_0^L I(\ell) H_\phi' \, d\ell = \sum_{n=1}^{N} V_n \, I'(\ell_n)$$

In Eq. 49, it is to be noted that E_ℓ' and H_ϕ' represent the free-space fields of the axial test source, evaluated on the surface S. If the wire radius is small, Eq. 13 yields

$$(50) \quad H_\phi' = \frac{I'(\ell)}{2\pi a}$$

From Eqs. 49 and 50,

$$(51) \quad -\int_0^L \underline{I}(\ell) \cdot \underline{E}' d\ell + \frac{Z_s}{2\pi a} \int_0^L I(\ell) I'(\ell) d\ell = \sum_{n=1}^{N} V_n \, I'(\ell_n)$$

In reaction test m the current function $I'(\ell)$ is given by Eq. 16, and Eq. 51 reduces to

$$(52) \quad -\int_0^L \underline{I}(\ell) \cdot \underline{E}_m' + \frac{Z_s}{2\pi a} \int_{\ell_{m-1}}^{\ell_{m+1}} I(\ell) I_m'(\ell) d\ell = V_m$$

Using Eqs. 10 and 16, we readily evaluate the last integral in Eq. 52 to obtain the simultaneous linear equations:

$$(53)\quad \sum_{n=1}^{N} I_n \bar{Z}_{mn} = V_m$$

where

$$(54)\quad \bar{Z}_{mm} = Z_{mm} + \frac{Z_s}{8\pi ka}\left[\frac{2\,kd_m - \sin 2\,kd_m}{\sin^2 kd_m} + \frac{2\,kd_{m+1} - \sin 2\,kd_{m+1}}{\sin^2 kd_{m+1}}\right]$$

$$(55)\quad \bar{Z}_{m,m+1} = Z_{m,m+1} + \frac{Z_s}{4\pi ka}\,\frac{\sin kd_{m+1} - kd_{m+1}\cos kd_{m+1}}{\sin^2 kd_{m+1}}$$

$$(56)\quad \bar{Z}_{m,m-1} = Z_{m,m-1} + \frac{Z_s}{4\pi ka}\,\frac{\sin kd_m - kd_m \cos kd_m}{\sin^2 kd_m}$$

The mutual impedances Z_{mn} for a perfectly conducting antenna are given by Eq. 19. Eqs. 54-56 show the adjustments that must be made to obtain the mutual impedance matrix $\bar{Z}_{mn}$ for the antenna with finite conductivity. Only the diagonal elements $\bar{Z}_{mm}$ and their next-door neighbors $\bar{Z}_{m,m+1}$ and $\bar{Z}_{m,m-1}$ are affected. For the remaining elements, $\bar{Z}_{mn} = Z_{mn}$.

It has been pointed out that the matrix Z_{mn} is symmetric. From Eqs. 54-56 it can easily be shown that $\bar{Z}_{mn}$ is also symmetric: $\bar{Z}_{mn} = \bar{Z}_{nm}$.

Previous investigations of finitely conducting wires have used comparatively crude methods. In some cases the distributed effects of the conductivity have been approximated with equivalent lumped loads. In a widely used perturbation method, the current distribution is assumed to be the same as that on a perfectly conducting antenna. Since our new analysis avoids the usual approximations, it is believed to be accurate for a wider range of conductivities.

VII. RADIATION EFFICIENCY

If the antenna has only one voltage generator V_g, the time-average power input is

$$(57)\quad P_{in} = |I_g|^2 R$$

where R is the real part of the antenna impedance at the terminal point ℓ_g. The radiated power is

$$(58) \quad P_r = |I_g|^2 R_r$$

where R_r is the radiation resistance. The power loss is

$$(59) \quad P_\ell = |I_g|^2 R_\ell$$

where R_ℓ Is the loss resistance. From conservation of energy,

$$(60) \quad R = R_r + R_\ell$$

The radiation efficiency is defined by

$$(61) \quad P_r/P_{in} = \frac{R_r}{R} = \frac{R-R_\ell}{R}$$

With finite conductivity and lumped loads, the antenna impedance (and the resistance R) can be calculated with the techniques developed in the preceding sections. It is assumed that the antenna is situated in free space or located over a perfectly conducting ground plane. Therefore, power loss occurs only in the lumped loads and the antenna wire itself. The power loss in the lumped loads is given by

$$(62) \quad P_{\ell\ell} = \sum_{m=1}^{N} |I_m|^2 R_m$$

where R_m is the real part of the load impedance Z_m.

Now let us consider the power P_d dissipated in the antenna wire with finite conductivity. If $\underline{E}$ and $\underline{H}$ denote the rms field intensities, the time-average dissipated power is

$$(63) \quad P_d = - \text{Real} \oint\!\!\!\oint_S (\underline{E} \times \underline{H}^*) \cdot \underline{ds}$$

where S denotes the antenna surface. In view of Eqs. 45 and 46, Eq. 63 reduces to

$$(64)\quad P_d = \frac{R_s}{2\pi a} \int_0^L I\, I^*\, d\ell$$

where the surface resistance R_s is the real part of Z_s. Eq. 64 can be written as follows:

$$(65)\quad P_d = \frac{R_s}{2\pi a} \sum_{n=1}^{N+1} \int_{\ell_{n-1}}^{\ell_n} I(\ell)\, I^*(\ell)\, d\ell$$

where the current on segment n is

$$(66)\quad I(\ell) = \frac{I_{n-1} \sin k(\ell_n - \ell) + I_n \sin k(\ell - \ell_{n-1})}{\sin k\, d_n}$$

From Eqs. 65 and 66, the dissipated power is

$$(67)\quad P_d = \frac{R_s}{8\pi ka} \sum_{n=1}^{N+1} \frac{1}{\sin^2 kd_n} \Big[(I_{n-1} I_{n-1}^* + I_n I_n^*)(2kd_n - \sin 2kd_n) + 2(I_{n-1}\, I_n^* + I_{n-1}^* I_n)(\sin kd_n - kd_n \cos kd_n) \Big]$$

The total power loss is

$$(68)\quad P_\ell = P_{\ell\ell} + P_d$$

From Eq. 59, the loss resistance is

$$(69)\quad R_\ell = P_\ell / |I_g|^2$$

Finally, the radiation efficiency is calculated as shown in Eq. 61.

An alternative method is to determine the radiated power by integrating the power density in the far-zone field. However, the technique developed above is much faster.

When R and R_ℓ have been computed, the radiation resistance R_r is obtained from Eq. 60. The directive gain G_d of the antenna can then be calculated from Eq. 40 with R replaced by R_r.

VIII. COMPARISON OF CALCULATED AND MEASURED RESULTS

The Smith charts in Figures 3, 4 and 5 compare the calculated and measured impedances for three different antenna configurations. Although these antennas are reasonably simple, no adequate theory or computational method has heretofore been available.

The antennas were constructed of brass rod with a diameter of 1/8 inch. Each antenna has straight segments with a right-angle bend every 5 cm. The antenna was mounted at the center of a large aluminum ground plane and fed with a 50-ohm coaxial cable. A General Radio UHF Admittance Meter was used for the measurements.

It may be noted in Figures 3-5 that the calculated and measured impedances show good agreement.

Figure 6 shows the impedance versus frequency for a 16-sided polygon-loop antenna. These data were calculated with the technique described earlier in this report, except that the current function $I(\ell)$ is not assumed to vanish at any points on a loop antenna. For comparison, Figure 6 also shows Storer's[4] calculations for a circular loop with a circumference equal to the perimeter of the polygon-loop. The close agreement between our calculations and Storer's is a further indication of the accuracy of the new formulation.

Figure 7 shows measured and calculated impedance versus frequency for a square halo antenna driven from a 50 ohm coaxial cable through a ground plane. The good agreement indicates that our technique is accurate for three-dimensional loops as well as dipoles.

Figure 8 shows the radiation efficiency versus frequency for the antenna in Figure 4, calculated with the techniques developed in Section VI. The antenna in Figure 3 has a slightly higher efficiency, and the antenna in Figure 5 has a slightly lower efficiency.

IX. CONCLUSIONS

The experimental approach to antenna measurement and optimization is a time-consuming cut-and-try affair even with modern swept-frequency equipment. To augment the experimental approach, we have developed an accurate and efficient digital computer program for a wide variety of wire antenna configurations. This program provides a complete analysis of the antenna characteristics including the impedance, current distribution, radiation efficiency, field patterns and gain.

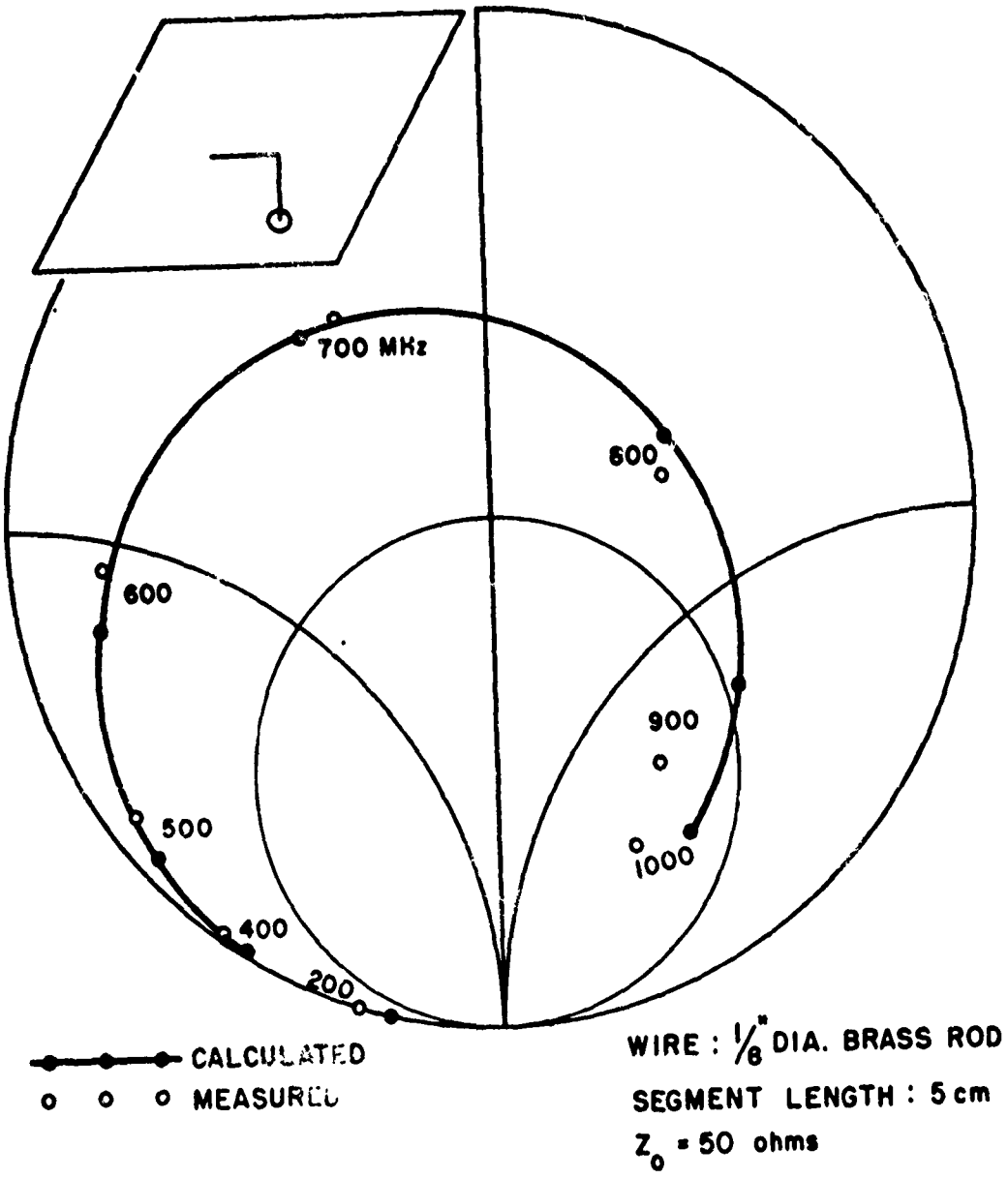

Fig. 3. Impedance vs. frequency for top-loaded dipole.

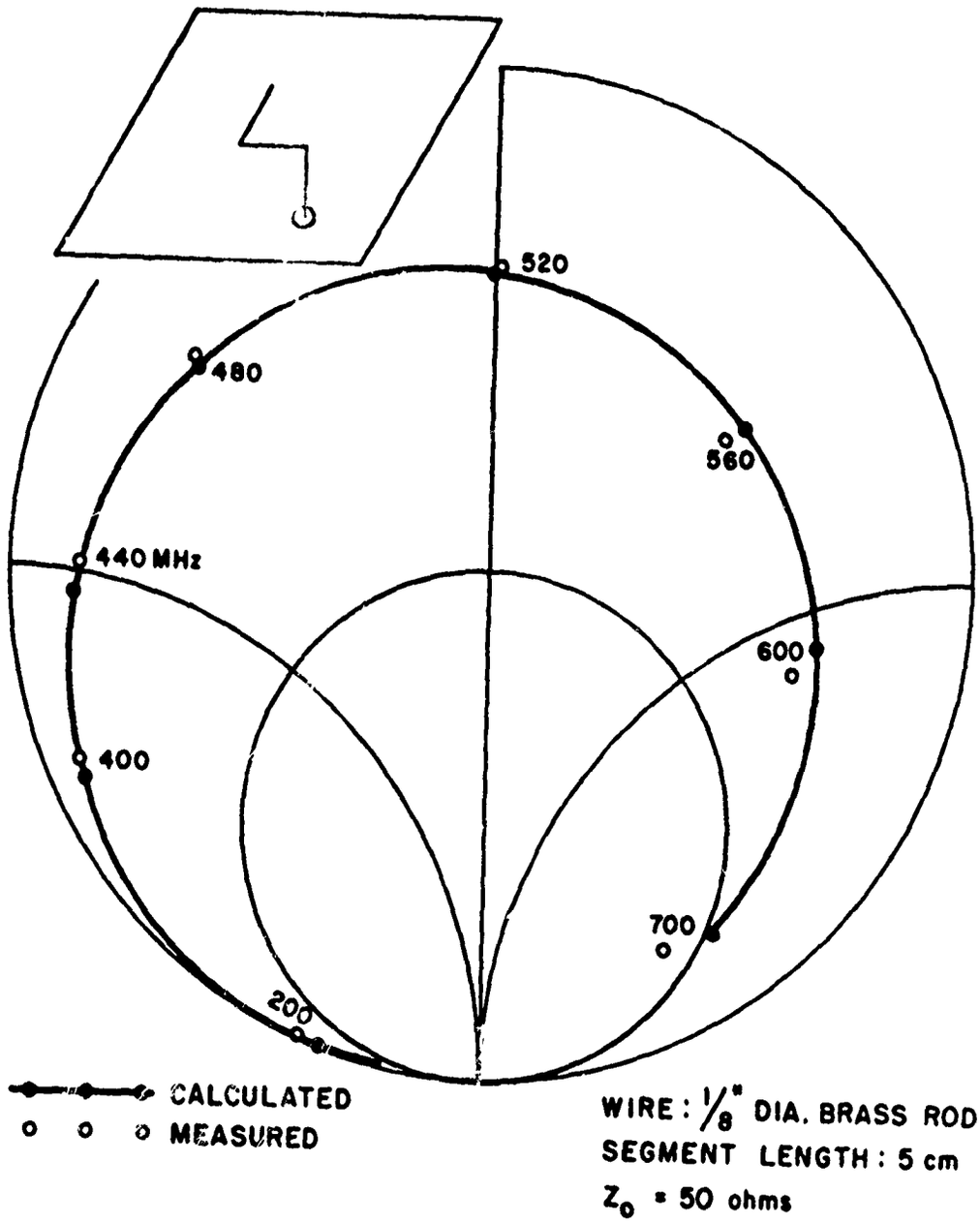

Fig. 4. Impedance vs. frequency for three-dimensional dipole.

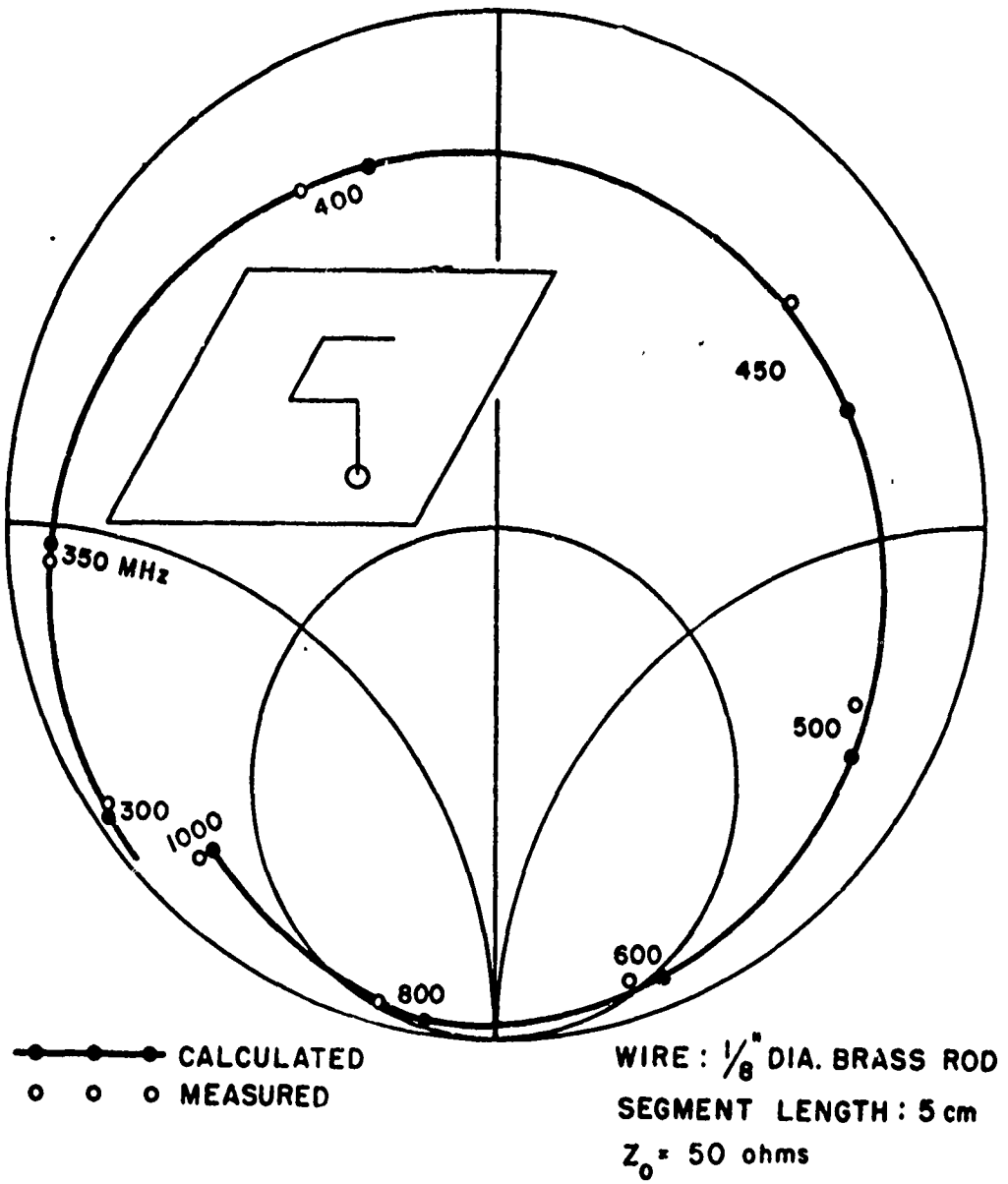

Fig. 5. Impedance vs. frequency for three-dimensional dipole.

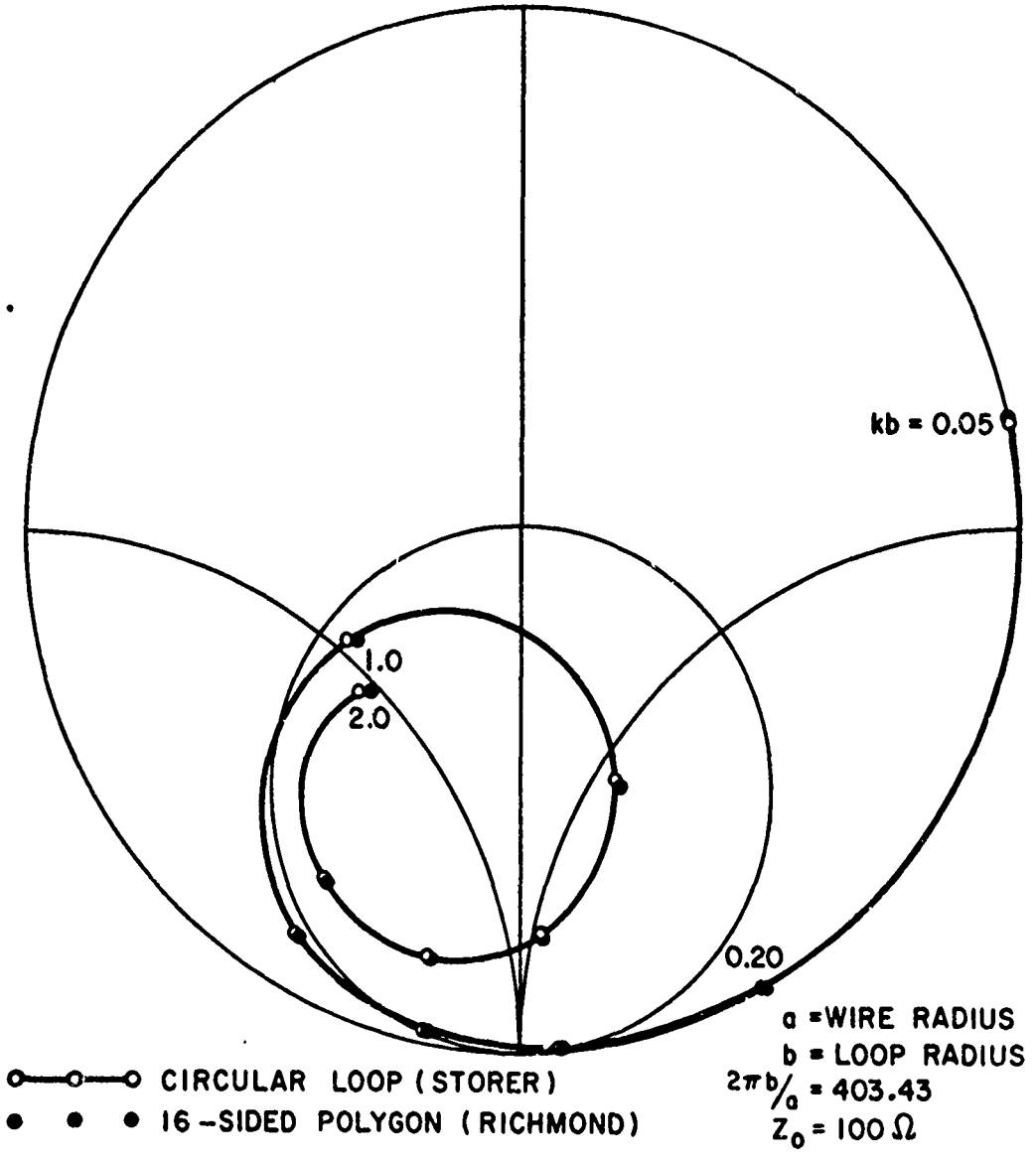

Fig. 6. Impedance vs. frequency for circular loop and corner-driven sixteen-sided polygon with same perimeter.

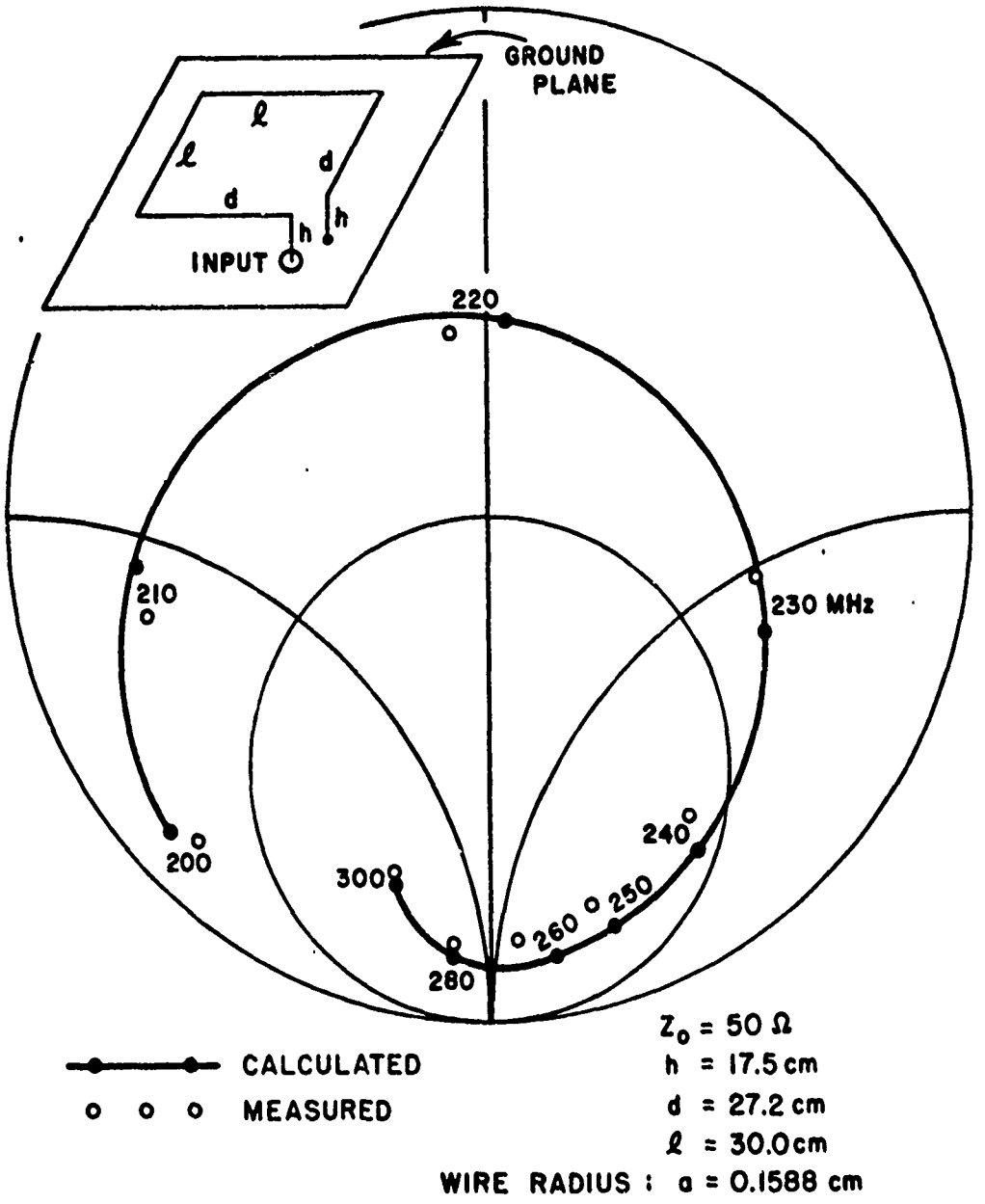

Fig. 7. Impedance vs. frequency for square halo antenna.

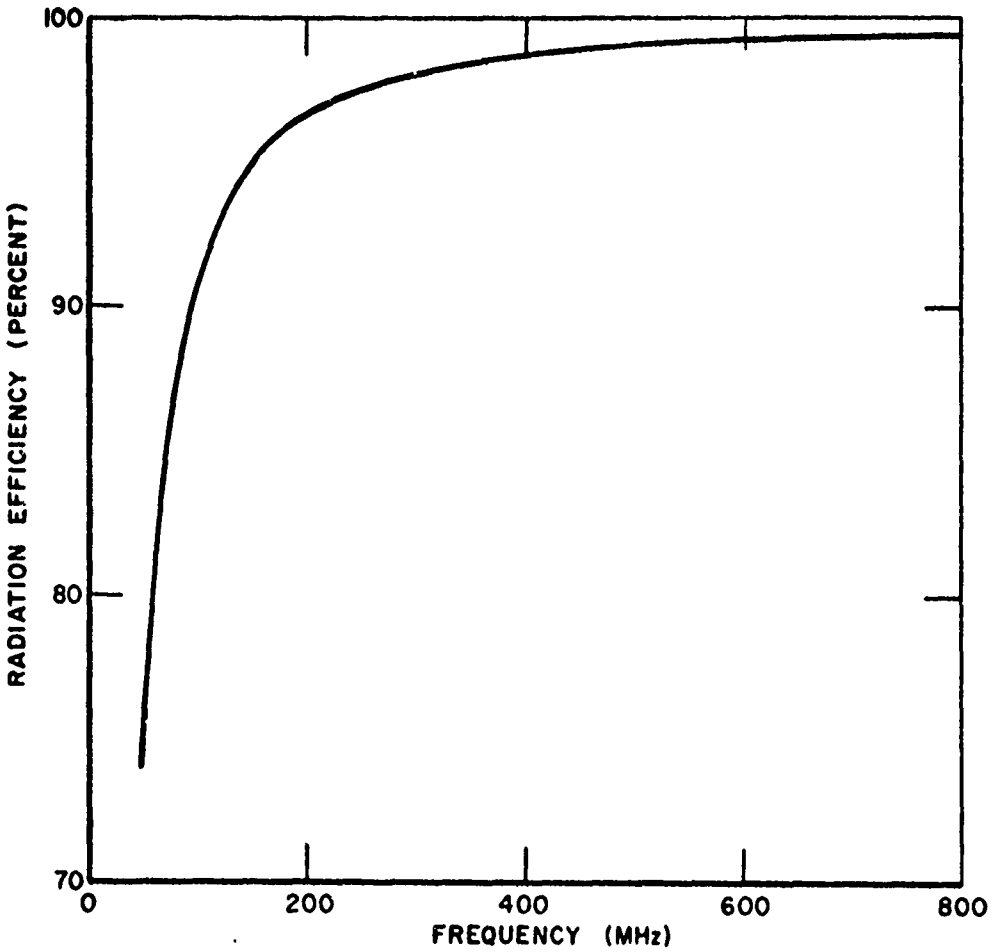

Fig. 8. Radiation efficiency vs. frequency for antenna in Fig. 4.

This report develops the theoretical basis for our new formulation, including the effects of multiple excitation, lumped loading and finite conductivity. Experimental impedance data are included for several three-dimensional antennas to verify the accuracy of the calculations. Appendices present the computer program and an analysis of scattering by three-dimensional thin-wire antennas.

The computer program is convenient to use. One merely gives input data to specify the antenna shape, wire radius, conductivity, frequency, lumped loads and generators.

The program is quite efficient. With an IBM 7094 computer, an analysis of the antenna in Figure 3 requires only 0.5 seconds for each frequency. The antennas in Figures 4 and 5 require 1.0 and 1.5 seconds respectively.

We have found that these techniques for wire antennas in free space can be applied also to a more advanced problem of considerable current interest: A wire antenna exciting a circumferential slot on a rocket or projectile. Continuing investigation in this direction is recommended.

ACKNOWLEDGEMENTS

The experimental results reported herein on antenna impedance were measured by Danai Lekhyananda and George A. Richards. Their assistance is sincerely appreciated.

REFERENCES

1. Schelkunoff, S. A. and Friis, H. T., Antennas, Theory and Practice, New York: Wiley, 1952, p. 401.

2. Schelkunoff, S. A., "On Diffraction and Radiation of Electromagnetic Waves", Physical Review, Vol. 56, August 15, 1939.

3. Carson, J. R., "Reciprocal Theorems in Radio Communication", IRE. Proc., Vol, 17, June 1929, p. 952.

4. Storer, J. E., "Impedance of Thin-Wire Loop Antennas", Trans. A.I.E.E., Part I, Vol. 75, Nov. 1956, pp. 606-619.

APPENDIX I
Scattering

In the scattering problem, we assume the antenna has perfect conductivity, no voltage generators and no lumped loads. Let the incident field ($\underline{E}_i$,$\underline{H}_i$) be generated by an electric current source $\underline{J}_i$. Then $\underline{M}_i = 0$ and Eq. 11 reduces to

$$(70) \quad -\iint_S \underline{J}_s \cdot \underline{E}' \, ds = \iiint_V \underline{J}_i \cdot \underline{E}' \, dv$$

As in Section III, Eq. 70 leads to a system of simultaneous linear equations:

$$(71) \quad \sum_{n=1}^{N} I_n Z_{mn} = \iiint_V \underline{J}_i \cdot \underline{E}_m' \, dv = V_m$$

where the mutual impedances Z_{mn} are given by Eq. 19.

The simplest case, and one of considerable interest, is that in which the primary source $\underline{J}_i$ is at a great distance r from the antenna. In this case the field $\underline{E}_m'$ of test dipole m is given by Eqs. 34,35 and 37 in Section IV.

To analyze the plane-wave scattering properties of a three-dimensional thin-wire antenna, we let the source $\underline{J}_i$ be remote and infinitesinal in extent. Then the right-hand side of Eq. 71 reduces to

$$(72) \quad V_m = \underline{E}_m' \cdot \iiint_V \underline{J}_i dv = \frac{j\lambda r e^{jkr}}{60\pi} \underline{E}_m' \cdot \underline{E}_i$$

where the incident field $\underline{E}_i$ is evaluated at the coordinate origin which is at or near the wire antenna. To illuminate the antenna with a plane wave arriving from direction (θ_i,ϕ_i), we locate the source $\underline{J}_i$ at the position (r,θ_i,ϕ_i) and evaluate $\underline{E}_m'$ in Eq. 72 at (r,θ_i,ϕ_i). Likewise, we orient $\underline{E}_i$ in the $\hat{\theta}$ or $\hat{\phi}$ direction to investigate the scattering for a theta-polarized or a phi-polarized incident plane wave.

It may be noted from Eqs. 71 and 72 that the solution for the scattering problem proceeds in precisely the same manner as in the antenna radiation problem. Indeed, the currents I_n induced on the antenna in the scattering problem are the same as those excited by a series of equivalent voltage generators V_m inserted at the current sampling points ℓ_m. The voltages of these equivalent generators are given by Eq. 72.

When the solution has been completed for the simultaneous equations (Eq. 71), Eqs. 34, 35 and 37 may be employed to calculate the scattered field $\underline{E}_s$ at any distant observation point (r,θ_s,ϕ_s). The monostatic or bistatic echo area of the wire is then given by

$$(73) \quad \sigma = \lim_{r\to\infty} \left[\frac{4\pi r^2 \underline{E}_s \cdot \underline{E}_s^*}{\underline{E}_i \cdot \underline{E}_i^*} \right]$$

If the wire has lumped loads and finite conductivity, the effects are readily treated in the scattering problem with the techniques developed in Sections V and VI.

APPENDIX II
The Computer Program

Figure 9 presents the main computer program (in Fortran IV) for three-dimensional dipole antennas in free space. A similar program is available for three-dimensional loop antennas.

The symbols for the input data are defined as follows:

IND	1 if patterns are desired, or 0 if not desired.
NCAS	Number of frequencies to be analyzed.
NG	Index number of antenna driving-point terminal.
NP	Number of points on the antenna.
ACM	Outer radius of wire in centimeters
BCM	Inner radius of wire in centimeters
CMM	Conductivity of wire in megamhos/m (-1. for perfect conductivity).
EPSIR	Relative permittivity of the internal medium.
FMC	Initial frequency is MHz.
DFMC	Frequency increment in MHz.
XC(I), YC(I), ZC(I)	The coordinates in centimeters of point i on the antenna axis.
VG(I)	The complex voltage of the generator V_i^g.
ZLD(I)	The complex lumped load impedance Z_i.

Typical input data are shown in Fig. 8 at the end of the program listing. These data apply to the antenna shown in Fig. 3. In this example, far-zone pattern calculations are not desired. The impedance is to be calculated at 19 frequencies starting at 100 MHz with increments of 50 MHz. The antenna has no lumped loads. There is just one voltage generator and it is located at the center of the antenna. The antenna shape is defined by an ordered list of the coordinates (x_i, y_i, z_i) of five points (NP=5) on the antenna axis, where $i = 1,2,3,4,5$. There are three current samples I_1, I_2 and I_3 to be calculated. The unit voltage generator is located at the point where the current I_2 is defined, and therefore, NG = 2. The wire radius is 0.1588 cm and the conductivity is 10.4 megamhos per meter. Since the wire is solid, the inner radius BCM is zero.

In the program, WAVE represents the wavelength in centimeters, AK = ka and TPL = k. The surface impedance ZS is calculated in the subroutine ZHOLOW. Subroutine TDD calculates the mutual impedances Z_{mn} (Eq. 19) and $\bar{Z}_{mn}$ (Eqs. 54-56). In the program $\bar{Z}_{mn}$ is denoted by C(I,J). Just above statement 100 the lumped loads are accounted for in accordance with Eq. 44, and the impedance matrix is made symmetric.

```
$EXECUTE        IBJOB
$IBJOB          GO
$IBFTC MAIN     NODECK
  1    FORMAT(1X,8F15.7)
  2    FORMAT(1X,8F15.7)
  5    FORMAT(1H0)
  7    FORMAT(7F10.5)
  8    FORMAT(7I10)
 11    FORMAT(1H1)
 12    FORMAT(1X,8F15.1)
       COMPLEX CN,CL
       COMPLEX CJ,ZLD(50),VG(50)
       COMPLEX ET1,ET2,EP1,EP2
       COMPLEX ETH,EPH,ETT(50),EPP(50)
       COMPLEX Z11,Z12,Y11,Y12
       COMPLEX C(50,50),CJ(50)
       COMPLEX CP11,CP12,CP21,CP22
       COMPLEX ZHOLOW,ZS,ZH
       DIMENSION X(50),Y(50),Z(50)
       DIMENSION U(50),V(50),W(50),CPS(50),SPS(50)
       DIMENSION XC(50),YC(50),ZC(50)
       DIMENSION CDK(50),SDK(50),STDK(50)
       TP=6.28318853
       READ(5,8)IND,NCAS,NG,NP
       WRITE(6,8)IND,NG,NP
       WRITE(6,5)
       READ(5,7)ACM,BCM,CMM,EPSIR,FMC,DFMC
       WRITE(6,2)ACM,BCM,CMM,EPSIR,FMC
       WRITE(6,5)
       NM=NP-1
       N=NP-2
       DO 20 I=1,NP
       READ(5,7)XC(I),YC(I),ZC(I)
       FI=I
  20   WRITE(6,2)FI,XC(I),YC(I),ZC(I)
       WRITE(6,5)
       DO 25 I=1,N
       READ(5,7)VG(I),ZLD(I)
       FI=I
  25   WRITE(6,2)FI,VG(I),ZLD(I)
       WRITE(6,5)
       DO 400 NCASE=1,NCAS
       WAVE=30000./FMC
       AL=ACM/WAVE
       AK=TP*AL
       TPL=TP/WAVE
       DO 28 I=1,NP
       X(I)=XC(I)*TPL
       Y(I)=YC(I)*TPL
  28   Z(I)=ZC(I)*TPL
       BL=BCM/WAVE
       BK=TP*BL
       FCPS=FMC*1.E6
       SIGMA=CMM*1.E6
       ZS=(.0,.0)
       IF(CMM.GT.0.)ZS=ZHOLOW(AK,BK,FCPS,SIGMA,EPSIR)
       WRITE(6,2)ZS
       WRITE(6,5)
       ZH=ZS/4./TP/AK
       CALL TDO(AK,C,CMM,D,X,Y,Z,ZH,NM)
       DO 100 I=1,N
       C(I,I)=C(I,I)+ZLD(I)
       DO 100 J=1,N
       FI=I
```

Fig. 9. Computer program for three-dimensional antennas.

```
      FJ=J
      C(J,I)=C(I,J)
  100 CONTINUE
      WRITE(6,5)
C     CROUT METHOD FOR SYMMETRIC MATRIX
C     N REPRESENTS THE NUMBER OF SIMULTANEOUS LINEAR EQUATIONS
C     SET UP THE SQUARE MATRIX C(I,J) BEFORE ENTERING CROUT PROGRAM
      NN=N+1
      DO 120 L=1,N
      LLL=L-1
      DO 120 I=L,N
      IF(L.EQ.1)GO TO 118
      DO 117 K=1,LLL
  117 C(L,I)=C(L,I)-C(L,K)*C(K,I)
  118 CONTINUE
      IF(L.EQ.1)GO TO 120
      C(I,L)=C(L,I)
      C(L,I)=C(L,I)/C(L,L)
  120 CONTINUE
C     AT THIS POINT CALCULATE OR READ THE RIGHT-HAND COLUMN C(I,NN)
      DO 124 I=1,N
  124 C(I,NN)=VG(I)
      DO 130 L=1,N
      LLL=L-1
      IF(L.EQ.1)GO TO 128
      DO 127 K=1,LLL
  127 C(L,NN)=C(L,NN)-C(L,K)*C(K,NN)
  128 CONTINUE
  130 C(L,NN)=C(L,NN)/C(L,L)
      IF(N.EQ.1)GO TO 138
      DO 136 L=2,N
      I=NN-L
      II=I+1
      DO 136 K=II,N
  136 C(I,NN)=C(I,NN)-C(I,K)*C(K,NN)
  138 CONTINUE
C     NOW THE SOLUTION IS STORED IN THE RIGHT-HAND COLUMN C(I,NN)
      DO 140 I=1,N
      CJ(I)=C(I,NN)
      CMAG=CABS(CJ(I))
      CREAL=REAL(CJ(I))
      CIMAG=AIMAG(CJ(I))
      PHASE=.0
      IF(CMAG.EQ.0.)GO TO 139
      PHASE=57.29578*ATAN2(CIMAG,CREAL)
  139 WRITE(6,2)CMAG,PHASE
  140 CONTINUE
      WRITE(6,5)
      Z11=1./CJ(NG)
      R=REAL(Z11)
      RL=.0
      IF(CMM.LT.0.)GO TO 160
      PD=.0
      DO 150 I=1,NM
      DK=D(I)
      SDK=SIN(DK)
      CDK=COS(DK)
      STDK=SIN(2.*DK)
      CN=(.0,.0)
      CL=(.0,.0)
      IF(I.GT.1)CL=CJ(I-1)
      IF(I.LT.NM)CN=CJ(I)
      PA=(2.*DK-STDK)*(CABS(CL)**2+CABS(CN)**2)
      PB=4.*(SDK-DK*CDK)*(REAL(CL)*REAL(CN)+AIMAG(CL)*AIMAG(CN))
```


Fig. 9. Continued

```
150 PD=PD+(PA+PB)/SDK/SDK
    RS=REAL(ZS)
    PD=RS*PD/(4.*TP*AK)
    RL=PD/(CABS(CJ(NG))**2)
160 EFFIC=100.*(R-RL)/R
    WRITE(6,2)FMC,EFFIC,Z11
    IF(IND.EQ.0)GO TO 350
    WRITE(6,11)
    CJG=CJ(NG)
    DO 206 I=1,N
206 CJ(I)=CJ(I)/CJG
    DO 340 NPR=1,3
    TH=90.
    PH=.0
    IF(NPR.EQ.3)PH=90.
    DO 300 NT=1,19
    THR=.01745329*TH
    PHR=.01745329*PH
    CTH=COS(THR)
    STH=SIN(THR)
    CPH=COS(PHR)
    SPH=SIN(PHR)
    DO 221 I=1,N
    ETT(I)=(.0,.0)
    EPP(I)=(.0,.0)
221 CONTINUE
    DO 225 K=1,NM
    XA=X(K)
    YA=Y(K)
    ZA=Z(K)
    KP=K+1
    XB=X(KP)
    YB=Y(KP)
    ZB=Z(KP)
    DD=D(K)
    CALL ZFF(XA,YA,ZA,XB,YB,ZB,DD,CTH,STH,CPH,SPH,ET1,ET2,EP1,EP2)
    ETT(K)=ETT(K)+ET2
    EPP(K)=EPP(K)+EP2
    IF(K.EQ.1)GO TO 225
    KM=K-1
    ETT(KM)=ETT(KM)+ET1
    EPP(KM)=EPP(KM)+EP1
225 CONTINUE
    ETH=(.0,.0)
    EPH=(.0,.0)
    DO 250 I=1,N
    ETH=ETH+CJ(I)*ETT(I)
    EPH=EPH+CJ(I)*EPP(I)
250 CONTINUE
    GPT=(CABS(ETH)**2)/R/30.
    GPP=(CABS(EPH)**2)/R/30.
    GP=GPT+GPP
    WRITE(6,2)TH,PH,GP,GPT,GPP
    IF(NPR.EQ.1)PH=PH+20.
    IF(NPR.EQ.1)GO TO 300
    TH=TH-10.
    IF(NT.LT.10)GO TO 300
    TH=10*(NT-9)
    PH=180.
    IF(NPR.EQ.3)PH=-90.
300 CONTINUE
340 WRITE(6,5)
350 CONTINUE
    WRITE(6,5)
```


Fig. 9. Continued

```
      IF(IND.NE.0)WRITE(6,11)
      TIME=CLOCK(0.016667)
      WRITE(6,2)TIME
  400 FMC=FMC+DFM
      STOP
      END
$DATA
         0          19          2           5
   .15880          .0        10.4         1.0       100.0        50.0
      5.0          .0          -5.0
       .0          .0          -5.0
       .0          .0            .0
       .0          .0           5.0
      5.0          .0           5.0
       .0          .0            .0          .0
      1.0          .0            .0          .0
       .0          .0            .0          .0
```

Fig. 9. Continued

The simultaneous linear equations (Eq. 18) are solved between statements 100 and 138. The voltage generators are accounted for in statement 124. Statement 130 writes out the magnitudes and phases of the complex current samples I_i = CJ(I). The dissipated power is calculated between statements 140 and 160 using Eq. 67. The radiation efficiency EFFIC calculated in statement 160 neglects the power loss $P_{\ell\ell}$ in the lumped loads and assumes there is just one voltage generator. The antenna impedance Z11 is calculated under the assumption that there is just one generator and that it has unit voltage. The frequency, efficiency and impedance are written out after statement 160.

The far-field patterns are calculated between statements 206 and 340. Specifically, the power gain GP(Eq. 40) is calculated in the three principal planes with 10-degree increments in θ and 20-degree increments in ϕ. In addition, the theta-polarized and phi-polarized power patterns GPT and GPP are calculated. These calculations use subroutine ZFF which is based on Eqs.34, 35 and 37.